WASM: Minerals, Energy and Chemical Engineering

Integrated Reservoir Characterization of the Goldwyer Formation, Canning Basin

Lukman Mobolaji Johnson

This thesis is presented for the Degree of

Doctor of Philosophy

of

Curtin University

June 2019

Declaration

I hereby declare that this thesis entitled "*Integrated Reservoir Characterization of the Goldwyer Formation, Canning Basin"* has not been submitted for the award of a higher degree at any other university or institution other than Curtin University. I also certify that this thesis is an original piece of research that has been written by me and that all sources used have been appropriately acknowledged.

Four chapters are in the form of a series of either published, submitted or "in-preparation" papers, of which I am the primary author. Information on author and co-authors contribution for the published papers are clearly stated on the attached attribution form.

This thesis was carried out under the supervision of Professor Reza Rezaee (WASM -Department of Petroleum Engineering), A. Prof. Gregory Smith (WASM – Department of Geology) and Dr. Ali Kadkhodaie (WASM -Petroleum Engineering, currently Department of Geology, University of Tabriz, Iran).

Experimental work was carried out in both the Department of Petroleum Engineering (Curtin University) and the Helmholtz Centre Potsdam, GFZ – German Research Centre for Geosciences, under the supervision of Nicolaj Mahlstedt.

Parts of this thesis have been published in the following journals and conference articles:

- Johnson, L. M., Rezaee, R., Kadkhodaie, A., Smith, G., & Yu, H. (2017): A new approach for estimating the amount of eroded sediments, a case study from the Canning Basin, Western Australia. *Journal of Petroleum Science and Engineering*. 156; 19-28.
- Johnson, L. M., Rezaee, R., Kadkhodaie, A., Smith, G., & Yu, H. (2017): Integrated Reservoir Characterization of Goldwyer Formation, Canning Basin. One Curtin International Postgraduate Conference (OCPC) 2017, Miri, Sarawak, Malaysia.
- Johnson, L. M., Rezaee, R., Kadkhodaie, A., Smith, G. and Yu, H. (2018) Geochemical property modelling of a potential shale reservoir in the Canning Basin (Western Australia), using Artificial Neural Network and Geostatistical tools. *Computers and Geosciences.* doi: 10.1016/j.cageo.2018.08.004.

At the time of this submission, the following manuscripts are in draft form or have been submitted to the mentioned journal outlets.

- Johnson, L. M., Rezaee, R., Smith, G., Unconventional oil potential of the Goldwyer III shale unit in the Theia 1 well, Central Broome Platform, Canning Basin *submitted to* Energies.
- Johnson, L. M., Rezaee, R., Smith, G., Mahlstedt, N., Kadkhodaie, A., and Yu, H. Source rock properties and kerogen kinetics of Ordovician Goldwyer shales in Canning Basin, Western Australia *To be submitted to* Energy and Fuels.
- Johnson, L. M., Rezaee, R., Smith, G., Kadkhodaie, A, Ondrak, R., and Yu, H. Source rock characterization and burial history reconstruction for selected wells in North West Canning Basin *To be submitted to* Journal of Petroleum Geology.

Lukman Mobolaji Johnson

12/06/2019

Abstract

In underexplored sedimentary basins such as the Canning Basin, understanding the geochemical property distribution is critical for successful hydrocarbon exploration. This study utilizes an integrated approach to characterize the organic-rich sections of the Ordovician Goldwyer Formation, in terms of their potential as an unconventional shale play, in the Broome Platform and adjacent sub-basins of the Canning Basin. Core and cuttings samples from a large number of wells were analysed by pyrolysis of the organic matter (Rock-Eval 6 and kinetic studies) and integrated with existing organic geochemical data from the Western Australia Department of Mines and Petroleum (WAPIMS) online database. A Machine Learning method was used to predict continuous geochemical logs in wells with limited or no geochemical information from the wells that had good downhole geochemical data and logs in the Goldwyer Formation. The optimised geochemical logs in all wells were then used to create 3D petrophysical property models using Kriging in Petrel (Schlumberger software) to predict the geochemical property distribution in 3D across the study area. Burial and thermal history models were constructed in Petromod (Schlumberger software) for six selected well locations to assess the evolution through time of the kerogen maturity and transformation in the Goldwyer Formation. This modelling was constrained by the kinetic data and compared with the standard default values based on previous studies in basins overseas that are not necessarily transferrable to the Canning Basin.

The pyrolysis and kinetic results indicate that the Goldwyer III shale unit is mostly in the early to peak mature stage of hydrocarbon generation, with generally fair to good generative potential across the study area. The average geochemical property distribution maps showed that the distribution of kerogen type (HI), total organic carbon (TOC), free hydrocarbons (S_1) and yield potential (S_2) are higher in the central to south-eastern part of the study area, while relatively lower values occur in the north-western part of the study area. The burial history models indicate that kerogen transformation in the Goldwyer III

shale unit increases gradually from the north-western part of the study area to the south-eastern area where the kerogen transformation is highest. However, the maturation history is complicated because the region has experienced at least two episodes of burial and uplift with exposure to higher temperatures and pressures.

The best organic-rich shales in the Goldwyer III unit for unconventional exploration occur in the central to the south-eastern part of the study area. This conclusion is based on an integrated study of their organic geochemical properties, kerogen transformation kinetics and thermal maturity. The timing of the generative episodes relative to trap formation remains an issue for successful conventional petroleum exploration. However, this is not such a major impediment to economic production for unconventional prospects.

Acknowledgements

Table of Contents

List of Tables

List of Figures

CHAPTER 1. Integrated Reservoir Characterization of Goldwyer Formation, Canning Basin

1.1 Introduction

Successful hydrocarbon exploration in sedimentary basins relies on the interpretation of the data available with respect to geologic processes that might have taken place in the basin's history, as well as their interactions. This can be achieved only by careful integration of available data from different sources to arrive at a unified and consistent story (Poelchau *et al.*, 1997).

Recent advances in directional drilling and hydraulic fracturing have led to the emergence of exploration for oil and gas trapped within the pores of low permeability fine-grained rocks. In this case, the fine-grained rocks (mostly shales) act as both the source and the reservoir rock (Jarvie *et al.*, 2007; Passey *et al.*, 2012) and are known as unconventional reservoirs. Successful exploration for shale oil or gas resources in these reservoirs usually requires conjunction of various geochemical parameters which include that the shale is thermally mature ($\sim$0.6%-1.3 R_o%), organic rich (TOC >1.0-2 wt %; thickness >20m), and has an oil saturation index >100 mg oil/g TOC (Jarvie, 2012; Jiang *et al.*, 2016). The burial/uplift history must be considered because timing is also important (Andrews, 2014). Other factors such as mineralogy, adsorption capacity, fracture networks, fluid properties (density, viscosity, water saturation, phase behaviour) and expulsion efficiency all play roles in unlocking these resources (Jarvie, 2012). Approximate criteria and benchmarks have been developed using the relatively well-known property interplay for the shale oil/gas production in North America, although the precise controlling processes seem to vary from basin to basin. In addition, the absence/ insufficiency of a property cannot be compensated for by another property (Raji *et al.*, 2015); for example, lack of sufficient organic content cannot be compensated by high thermal maturity for a shale unit.

Rapid geochemical screening tools, such as Rock-Eval pyrolysis, maceral analysis scans and vitrinite reflectance measurements can be used to map the presence and maturation rank of organic rich shale intervals. Geostatistical tools and burial history modelling may be employed to model the occurrence and distribution of these properties across a basin, sub-basin or an area.

Typically, pyrolysis involves artificial decomposition of organic matter by heating in the absence of oxygen. Data obtained from pyrolysis provides information on the type, quality and quantity of disseminated organic matter (kerogen) in shales. In addition to estimates of the level of thermal maturity, the amount of hydrocarbon generated, and the remaining hydrocarbon generation potential of these shales as unconventional shale reservoirs can also be determined. Jarvie (2015) provided a detailed description of organic geochemical techniques as employed for unconventional shale resource systems. A good understanding of these shale properties is important in the reconstruction of the timing of kerogen maturation and amounts of hydrocarbon that can be generated in well locations across a sedimentary basin.

Burial history modelling is an approach that aims to reconstruct the geological processes that have taken place in a sedimentary basin over geologic time. The results help provide a good understanding of the geological history of the basin and the processes involved in hydrocarbon maturation. Commonly, the model results are verified against measured data like vitrinite reflectance, borehole temperatures and kerogen kinetics in order to accurately calibrate and constrain the simulated thermal histories (Grobe *et al.*, 2015). Detailed information on theories and principles behind various aspects of the burial history modelling is discussed in Hantschel and Kauerauf (2009).

Exploration of shale reservoir systems has proven successful in North America, resulting in the US becoming essentially self-sufficient in petroleum production. Based on the North American experience, the potential for unconventional petroleum resources to be tapped elsewhere is significant and this could provide comparable energy benefit to consumers globally.

In this study, the Ordovician Goldwyer Shale in the Broome Platform of the Canning Basin, Western Australia (Figure 1.1) has been studied as an example of an unconventional shale. The research has assessed its organic geochemical characteristics, the maturation history, and the kerogen kinetics to better understand its potential for hydrocarbon generation.
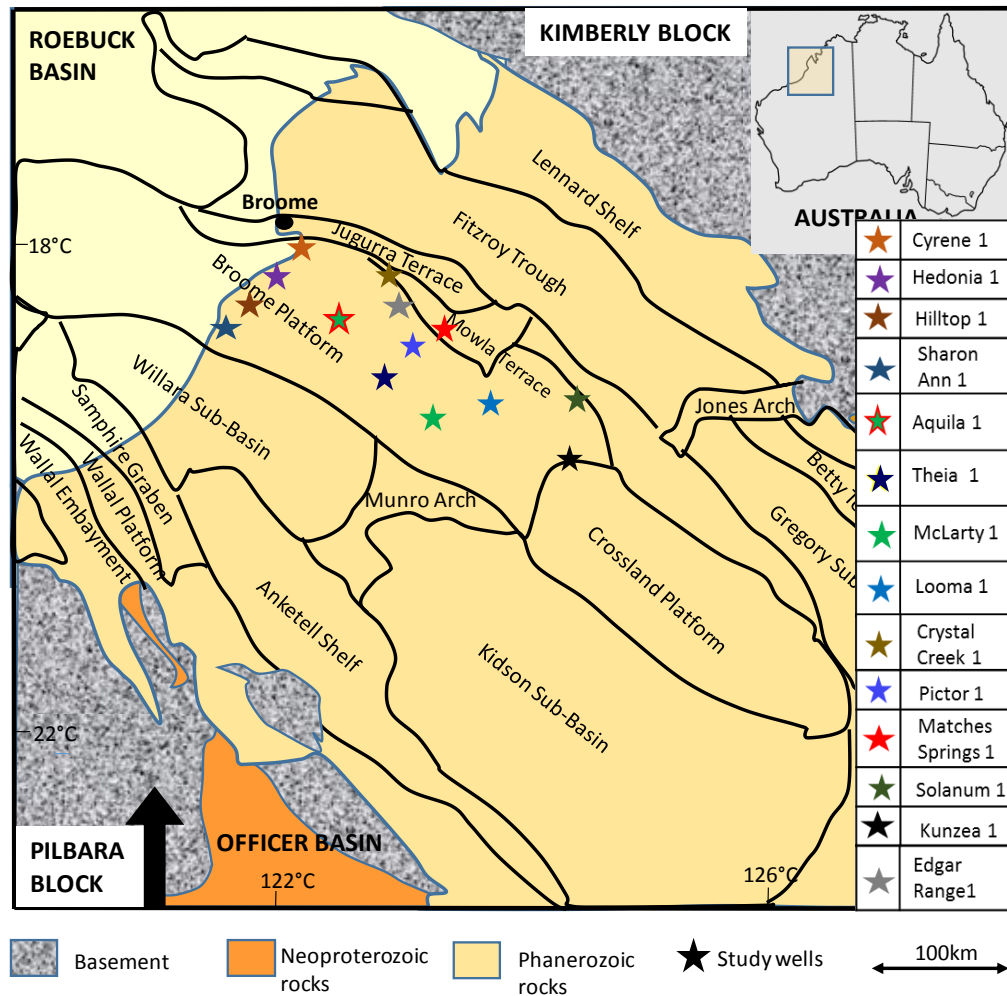
Figure 1.1Structural elements of the Canning Basin, showing the different sub-basins. Modified from Haines (2004). Coloured stars represent the wells used in this study.

1.2   Exploration history in the Canning Basin

Hydrocarbon exploration in the Canning Basin commenced in the 1920's when oil shows were encountered in shallow drill holes on the Lennard Shelf. Sparse and episodic exploration continued until the 1970's, when the Bureau of Mineral

Resources (now Geoscience Australia) and Western Australia Petroleum Pty. Ltd. conducted a series of gravity, magnetic and seismic surveys. Since then, almost 300 wells have been drilled in the Canning Basin, complemented with almost 90,000 square km of 2D seismic data acquisition (DMP, 2014).

Exploration focused mainly in the northern and central parts of the basin from the 1970's until the mid-1980's (Figure 1.1), primarily targeting the Devonian reefs on the Broome Platform, Lennard Shelf and the Fitzroy Trough; with gas flows in most of the exploration wells, but only a few yielded commercial quantities (DMP, 2014). In 1981, commercial oil was finally discovered by Home Energy on the edge of the Lennard Shelf in the Fairfield Group sediments. Subsequently, the Sundown, Lloyd, Boundary, West Terrace, West Kora and Point Torment fields were discovered. In the early 1990's, the subsalt Ordovician sediments were targeted by larger companies. Oil associated with the Goldwyer Formation has been recovered in wells drilled on the: Barbwire Terrace (Dodonea 1, Percival 1, and Solanum 1); Dampier Terrace (Edgar Range 1 and Pictor 1); Broome and Crossland platforms (Looma 1); and Admiral Bay Fault Zone (Cudalgarra 1, Great Sandy 1, and Leo 1) (GSWA, 2014). In 2009, Buru Energy completed the first 3D seismic survey in the Canning Basin, and later (in 2011) discovered oil in the Unguani oil field.

Kuuskraa *et al.* (2013) estimated that the Goldwyer Formation, could contain up to 70.7 Tm^3 (2496 Tcf) gas in-place and a risked recoverable shale gas resource estimated at 3.18 Tm^3 (112.3 Tcf), using a 30% risk factor and 15% recovery factor. These numbers are based on the entire Goldwyer Formation and are believed to be highly uncertain (DMP, 2014). Also, Triche and Bahar (2013) examined the Goldwyer III Formation, where initial gas in-place was estimated to be 24.5 Tm^3 (867 Tcf). The estimate of recoverable gas for the Goldwyer III shale Member was 1.1 Tm^3 (39 Tcf), which was also based on a 30% risk factor and a 15% recovery factor.

The Goldwyer Formation lies at an average present day depth of 1300 m, with an average thickness of 350 m in the terraces and platforms; and TOC values up to

6.4% (GWA, 2014). Brown *et al.* (1984) suggested that the Goldwyer Formation is within the oil generating window in the Broome Platform and some of the southern sub-basins. The prospectivity of the Goldwyer shales varies across the Canning Basin, with varied organic matter quality, and with varying maturation history across the basin. Recent work by New Standard Energy, Buru Energy and Finder Exploration have focused on the unconventional shale exploration potential of the Goldwyer shale, with over five new exploration wells drilled since 2010.

In terms of production from this unconventional resource, there has been a ban on Hydraulic Fracturing in Western Australia for the past several years, therefore Hydraulic Fracturing and drill stem tests (DST's) have not been carried out to test the Goldwyer Formation. In July 2018, an inquiry, led by Environmental Protection Authority (EPA) Chairman made 44 recommendations to the Western Australia Government, which included

- No fracking to be allowed within 2 kilometres of public drinking water sources;
- All projects to include EPA assessment;
- An enforceable code of practice; and
- No fracking to be allowed within 2 kilometres of towns and dwellings, which includes national parks (Laschon and Shine, 2018)

However, recent news articles (from 10th September 2019) mentions that the WA Government has lifted the hydraulic fracturing moratorium on petroleum titles, following the 6 September publication of the Petroleum and Geothermal Energy Resources (Hydraulic Fracturing) Amendment Regulations 2019 (Day, 2019).

1.3   Geological settings

The Canning Basin, Western Australia covers an approximate area of 506,000km² with 400,000km² onshore and has been divided into a number of structural elements and sub-basins (Figure 1.1). A summary of the basin stratigraphy is shown in Fig. 1.2.

Detailed accounts of the geological evolution of the Canning Basin can be found in several studies including Seymour (1972); Forman and Wales (1982); Yeates *et al.* (1984); Brown *et al.* (1984); King (1998); Ghori and Haines (2006); Mory and Hocking (2011); Parra-Garcia *et al.* (2014) amongst others. A brief summary is presented here.

The basin development began in the Late Cambrian as an inferred intracratonic sag between the Precambrian Pilbara and Kimberley Basins. The evolution of the Canning Basin is divided into four main tectono-stratigraphic megasequences, spanning the Ordovician – Silurian, Devonian – Early Carboniferous, Late Carboniferous – Permian and the Jurassic – Cretaceous.

Deposition in the Ordovician commenced in fault controlled sub-basins with marginal marine, coarse siliclastic sediments and shallow marine sediments of the Nambeet Formation. It is a transgressive unit containing graptolites, trilobites, brachiopods, conodonts and grastropods (King, 1998). Increasing marine transgression led to the deposition of the carbonate-dominated Willara Formation across most of the Canning Basin, which conformably overly the Nambeet Formation (King, 1998). The maximum flooding is marked by the widespread deposition of the Ordovician Goldwyer Formation, including over the Broome Platform, with major depocenters in the Kidson and Willara sub-basins (Romine *et al.*, 1994). This formation comprises mostly shales with interbedded limestones, deposited in subtidal / restricted marine environments, and also contains graptolites, trilobites, brachiopods, conodonts and grastropods (King, 1998). The Goldwyer Formation has been documented to have excellent source potential (Brown *et al.*, 1984), in parts, being dominated by the fossil green alga *Gleocapsamorpha prisca* (*G. prisca*). This was followed by the accumulation of platform carbonates of the Nita Formation that have been dolomitised as a result of the subsequent marine regression and exposure that occurred at the end of the Late Ordovician (Brown *et al.*, 1984).

The Nita Formation is overlain by the Ordovician to early Silurian Carribuddy Group, which represents a regressive phase in the basin development.

Sedimentation was largely dominated by marginal marine facies and restricted circulation, leading to widespread evaporite deposition in the centre of the basin (Parra-Garcia *et al.*, 2014). On the Broome Platform, the Carribuddy Group is missing from the northwestern parts of the sub-basin, probably as a result of reduced sedimentation and widespread pre-Permian erosion over this part of the sub-basin (Karajas and Kernick, 1984; Haines, 2010; Johnson *et al.*, 2017) associated with the early Devonian Rodingen Orogeny.

Major down faulting of the Fitzroy Trough and adjacent terraces occurred in the Devonian, with deposition of thick carbonate and clastic sediments, but these are not preserved over most of the study area on the Broome Platform, being removed by a period of localised uplift and erosion associated with the Alice Springs orogeny.

Hence, the older sediments are unconformably overlain by regional deposition of the Permian Grant Group, dominately comprising non–marine sediments, and succeeding Permian sediments (Brown *et al.*, 1984). The Triassic to late Jurassic was a period of non deposition on the Broome Platform, however, sedimentation continued in the adjacent Fitzroy Trough. The Jurassic to Cretaceous sediments consist mostly of marine sandstones and regressive continental sands respectively. Cretaceous to Recent sediments in the Canning Basin are dominated by thin lateritic and alluvial sediments.
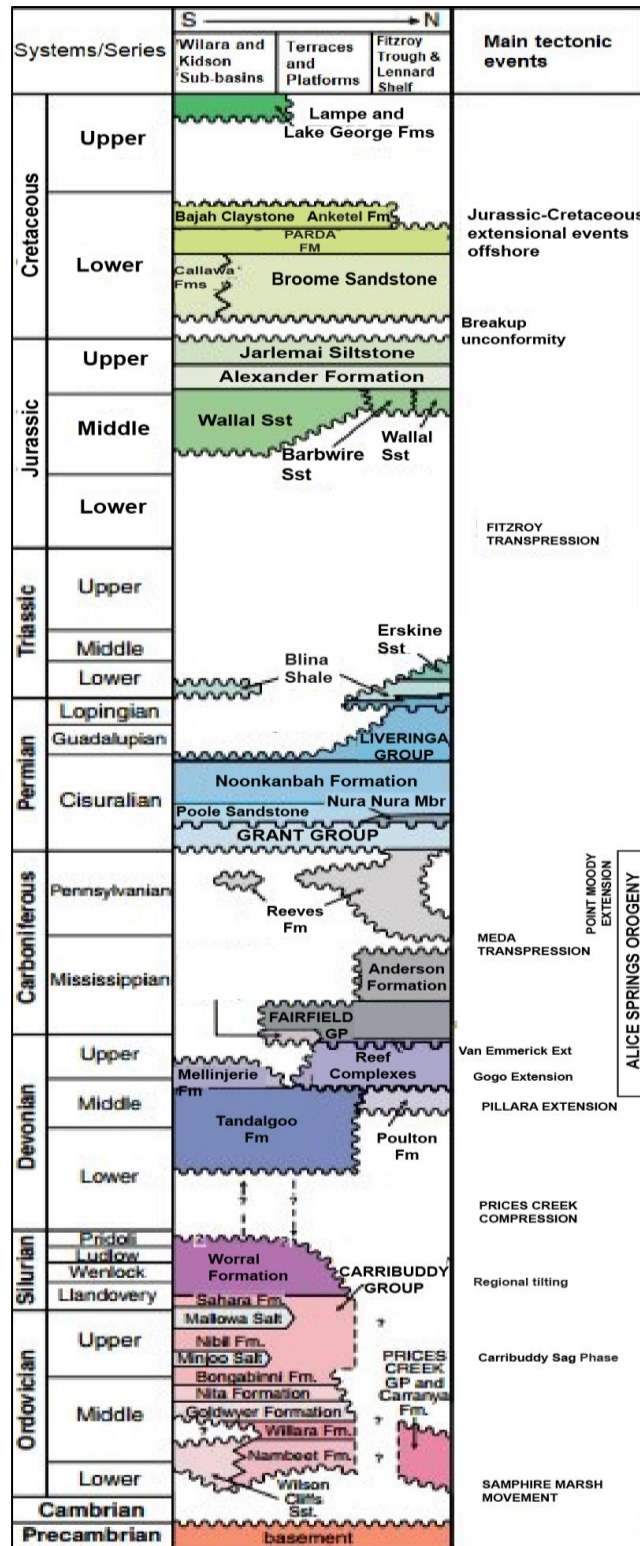
Figure 1.2 General stratigraphy of the Canning Basin, modified from GSWA (2014)

The Western Mining Corporation (WMC) carried out early petrophysical studies on wells in the Canning Basin and described the Goldwyer shales in terms of its sequence stratigraphic framework. Four units were identified in the Goldwyer, labelled WMC units 1 to 4 (Haines, 2004). The lower Goldwyer shale, recognised as Units 1 + 2, represents a major transgression that affected most of the Canning Basin, which subsequently deposited up to 700 m of thick open marine mudstones in the basinal areas, with more condensed sections on the platforms and terraces. This was followed by more localised regression in some parts of the basin, which resulted in the deposition of a carbonate-dominated succession, recognised as Unit 3. Renewed transgression led to the deposition of the upper Goldwyer Formation (Unit 4), which consists predominantly of subtidal-lagoonal shales, with abundance of the green alga *Gleocapsamorpha prisca* (*G. prisca*).

This nomenclature has been adopted by the Geological Survey of Western Australia (GSWA). However, in many well completions reports from the Broome Platform, the Goldwyer Shale is simply subdivided into 3 units; the lower shale member (WMC units 1 and 2), the middle calcareous unit (WMC unit 3) and the upper shale member (WMC unit 4). In this study, these units are referred to as Goldwyer III, Goldwyer II and Goldwyer I shale units respectively and are easily observed on the Gamma Ray and Sonic logs (Fig 1.3). These Goldwyer units have been associated with different redox conditions in the Middle Ordovician Darriwilian Period that is important for the organic matter occurrence and preservation (Spaak *et al.*, 2017).
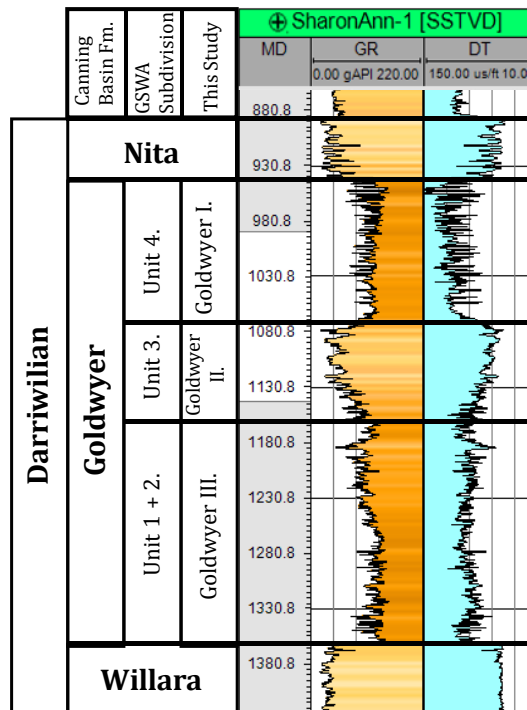
Figure 1.3 Subdivision of the Middle Ordovician Period, showing the GSWA and adopted Nomenclature for describing different units of the Goldwyer shale in the Sharon Ann 1 well.

1.3   Aims and objectives

The Ordovician Goldwyer Formation represents one of the best organic-rich shale intervals in the Canning Basin (Brown *et al.*, 1984; Ghori and Haines, 2006; Kuuskraa *et al.*, 2013; GWA, 2014; DMP, 2014) and this study aims to assess its source and reservoir properties using integrated geological and geochemical techniques over the Broome Platform. The characterisation assesses the significant parameters of organic matter quality, quantity, thermal maturity and hydrocarbon generative potential for these shales. The results have been incorporated in a 3D model using Petrel (Schlumberger software) to provide a geochemical property model in a stratigraphic and geographic context for the Goldwyer Formation within the Broome Platform. Furthermore, the burial and thermal history of the Goldwyer Formation across the Broome platform is carried out in order to understand the maturity evolution across the study area.

Some specific objectives of this study include undertaking:

- Rock Eval – TOC analysis of shale samples from the Goldwyer Formation to identify organic rich zones.
- Derivation of relationships between the geochemical results and the well logs via Neural Network techniques, to generate continuous geochemical logs for wells with no available core or drill cuttings, and thereby predict the geochemical properties in those wells.
- Identification, correlation and mapping of Goldwyer Formation organofacies within the Broome Platform wells and seismic data to provide a structural framework for the sub-basin assessment.
- 3D geochemical property modelling over the Broome Platform to identify potential geochemical sweetspots.
- Measuring the transformation kinetics of the kerogen in the Goldwyer shales to constrain and calibrate the thermal modelling.
- Thermal and burial history modelling over the Broome Platform, the adjacent Mowla Terrace and Crossland Platform, including estimation of missing section using sonic log analysis.

1.4   Data availability

The wells and seismic data used in this study are shown in Figure 1.4.

The open file data available for each well are given in Table 1.1 and were mostly derived via the DMP website downloaded from the WAPIMS database. The data were augmented by geochemical analyses obtained by the author as part of this study. The data include:

- 2D Seismic Data of various vintages
- Downhole petrophysical well logs
  - Gamma Ray, Resistivity, Sonic, Neutron, Density logs are available in most of the drilled wells

- The geochemical analyses were done on samples of core and cuttings that were available for many of the wells in the WA Geological Survey core library.
- Rock Eval/ TOC data from WAPIMS, the literature plus analyses by the author using the Curtin Petroleum Engineering Rock-Eval VI equipment
- Kinetic analyses performed in GFZ-Potsdam, Germany by the author
- Miscellaneous data for some wells via WAPIMS, including measured vitrinite reflectance data, Apatite Fission Track Analyses (AFTA) and bottom hole temperature data
- Open file report data from WAPIMS including
    - Well Completion Reports,
    - Formation tops,
    - Biostratigraphic zones
    - Geochemical reports.
- Previous publications and company report as listed in the references
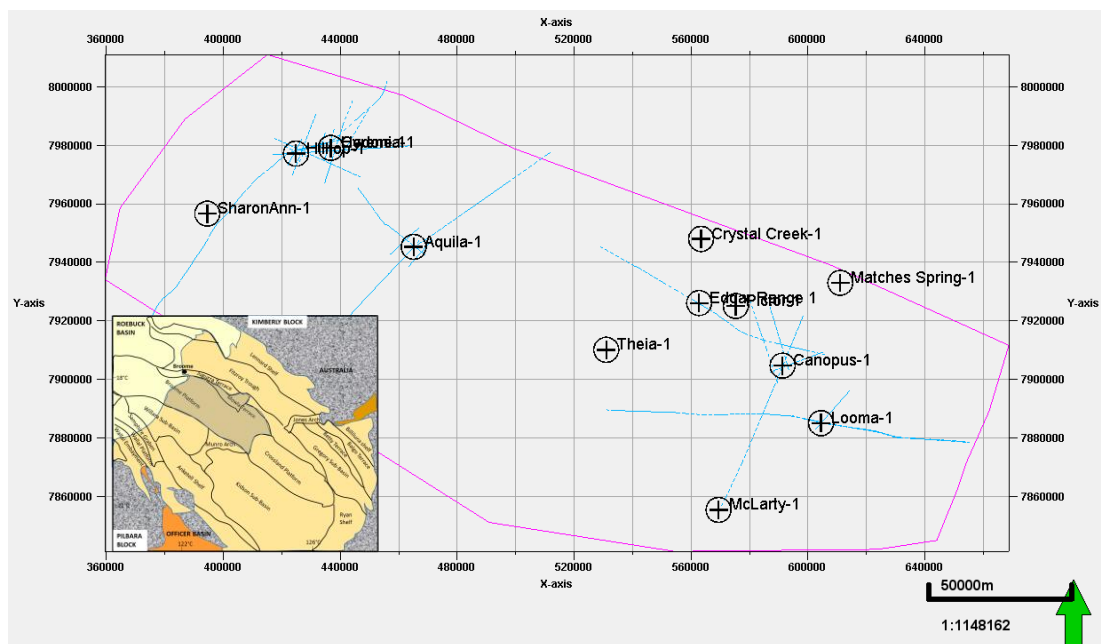
Figure 1.4 Drilled wells and seismic data used from the Broome Platform, Canning Basin. See Fig. 1.1 for inset.

Table 1.1 Data used for this study

	Well Name	Petrophysical Well Logs				Rock Eval Data (WAPIMS)	Core/Chips/Cuttings	Formation Tops
		Gamma Ray Log (API)	Deep Resistivity Log (OHMM)	Sonic Log (US/F)	Density Log			
1	Sharon Ann 1	✓	✓	✓	✓	X	X	✓
2	Hilltop 1	✓	✓	✓	✓	✓	X	✓
3	Cyrene 1	✓	X	✓	X	✓	✓	X
4	Hedonia 1	✓	✓	✓	✓	✓	X	✓
5	Aquila 1	✓	✓	✓	✓	✓	X	✓
6	McLarty 1	✓	X	✓	X	✓	✓	✓
7	Theia 1	✓	✓	✓	✓	✓	✓	X
8	Canopus 1	✓	✓	✓	✓	✓	X	✓
9	Pictor 1	✓	✓	✓	✓	✓	X	✓
10	Looma 1	✓	✓	✓	✓	X	X	✓
11	Solanum 1	✓	X	✓	✓	✓	✓	✓
12	Santalum 1	✓	X	✓	✓	✓	X	✓
13	Kunzea 1	✓	X	✓	✓	X	X	✓
14	Crystal Creek 1	✓	✓	✓	✓	✓	X	✓
15	Matches Springs 1	✓	✓	✓	✓	✓	✓	✓
16	Edgar Range 1	✓	X	✓	X	✓	✓	✓

1.5   Thesis structure

This thesis is structured such that individual chapters may stand-alone as an aspect in this integrated study. The thesis is broken into a short background to the study and an introduction to the Canning Basin in chapter 1, while chapter 2 describes the geochemical character of the Goldwyer III shale, and its distribution away from drilled wells as modelled across the Broome Platform. 3D models were constructed to interpolate data on the organic matter quality, quantity and maturity away from the well locations across the Broome Platform.

Chapter 3 covers the accurate delineation of the maximum burial depths and estimation of the thickness of eroded sections in the basin. This is one of the key uncertainties that is addressed in order to accurately reconstruct the burial and thermal history of the sub-basin.

Chapter 4 assesses the kinetics of kerogen transformation to define the activation energy distribution for hydrocarbon generation in the Goldwyer shales, which is another critical input for the thermal history modelling.

Chapter 5 discusses the 1D burial history models constructed for five wells in a northwest-southeast transect across the Broome Platform to understand maturity evolution and kerogen transformation ratios across the studied sub-basins.

Each of the above chapters include separate discussions and conclusions, while chapter 6 integrates all these results, to arrive at a unified and consistent story.

Specific wells across the Broome Platform have been used for different aspects of the study in each chapter to meet their varying objectives and the available data.

CHAPTER 2. Reservoir characterisation and geochemical property modelling of the Goldwyer III Shale Member

In this chapter, the overall geochemical character of the Goldwyer III shale member is presented for the Broome Platform. In particular, the distribution of these properties across the sub-basin has been modelled using sophisticated geostatistical tools. A summary background is given first to put the geochemical results in context.

2.1 Background

Shale systems are highly variable in terms of mineralogy, organic content, kerogen quality and quantity, thermal maturity, rock fabric and porosity amongst other attributes. Geochemical assessment of shale reservoirs is important for unconventional petroleum systems evaluation because "without the source of petroleum, all other components and processes needed to exploit a play become irrelevant" (McCarthy *et al.*, 2011). Some of the factors affecting deposition and preservation of organic matter within shale reservoirs are discussed below.

2.1.1 Depositional environment

The control of depositional environments on organic matter accumulation and preservation has long been established, as discussed in Pettijohn (1975); Pedersen and Calvert (1990); Walker (1992); Tucker (2009). The depositional environment model for the Goldwyer Formation is shown in Figure 2.1.
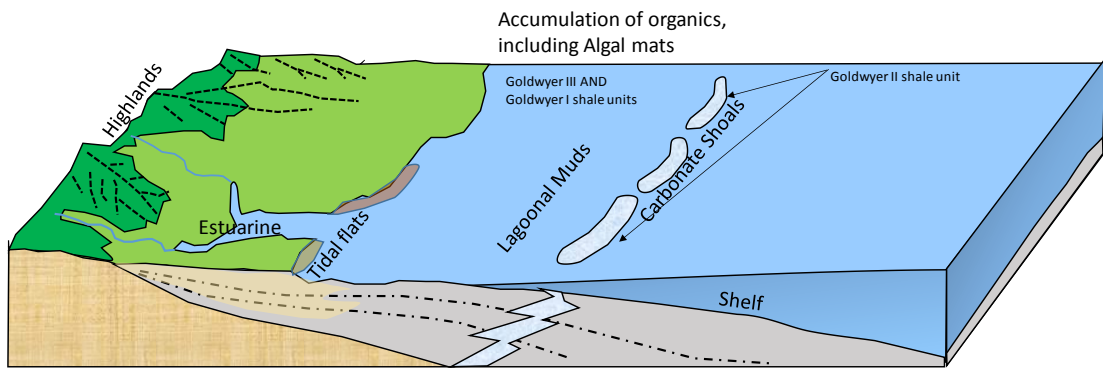
Figure 2.1 Schematic depositional environments for the Middle Ordovician – Darriwilian Goldwyer Formation in the Canning Basin.

The Goldwyer Formation comprises shale units deposited in marine environments varying from open marine to restricted marine. Copp (2015) developed a depositional model for the Goldwyer III unit and identified eight lithofacies, deposited in predominantly outer-ramp – mid-ramp environments (Fig. 2.2).
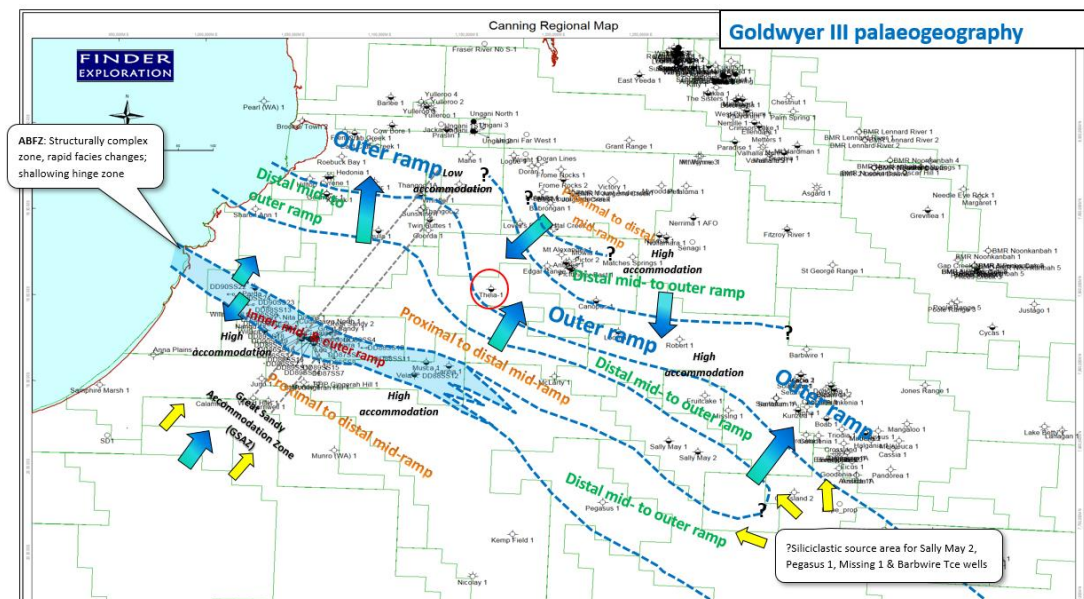
Figure 2.2 Regional depositional model for the Goldwyer III shale unit in the Canning Basin (Copp, 2015).

The organic matter in the Goldwyer Formation includes algae (*G. prisca*) and fine grained dispersed or detrital organic matter, which can yield petroleum products on exposure to bacterial degradation (biogenic generation) or increasing heat

and pressure (thermal generation). Different organic matter types can be described in terms of their elemental composition – atomic O/C and H/C ratios in a van Krevelen diagram (Fig 2.3) or by the hydrogen index (HI) and oxygen index (OI) from the pyrolysis products.
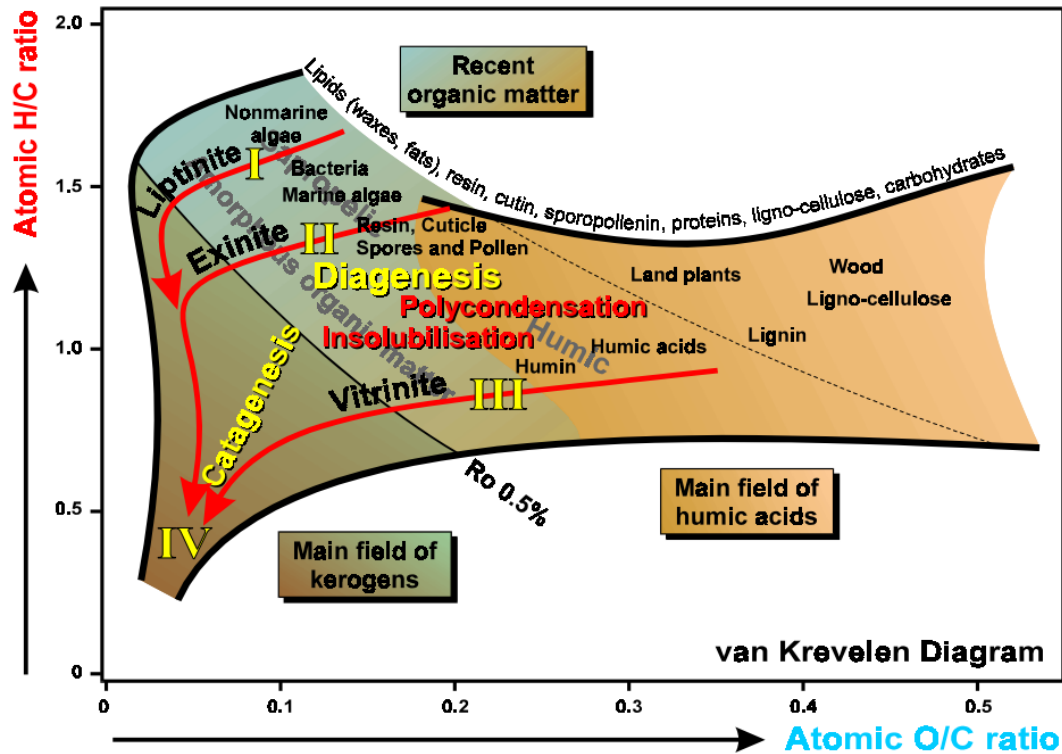
Figure 2.3 H/C and O/C ratios and the biological, biochemical and geochemical composition of organic matter (Kaye, 2006).

Type I kerogens are mostly hydrogen-rich organic matter preserved in the rock record. They mainly include algae, bacteria, archaea and microbially degraded land plant material that accumulates in stratified water columns of lakes, estuaries, and lagoons. They are perhydrous lipid-rich and generate paraffin-rich low wax oils. Type II kerogens, on the other hand, are mostly derived from marine algae, land plants and bacterially modified organic matter. They usually contain medium molecular weight aliphatic chains and generate paraffinic-naphthenic oil types in marine clastic environments. In marine carbonate environments, there is a high potential of sulphur incorporation in the kerogen network (Orr, 1986). Type III kerogen are essentially derived from woody land plant organic

17

matter and contain long chained hydrocarbon and methyl groups from plant waxes. This group mostly generate dry gas at sufficient burial depths. Type IV kerogens represent inert materials with little or no potential to generate hydrocarbons. These kerogen types can be roughly correlated to the Hydrogen Index (HI) values from pyrolysis products as shown in table 2.1.

Table 2.1 Kerogen types, composition, rock-eval HI character and depositional environment (Tissot and Welte, 1978).

Kerogen Type	Source material	Initial HC Ratio	Initial OC Ratio	HI Character	Depositional Environment
Type I	Mainly algae	~ 1.5	0.1	> 600	Stratified Lakes/Lacustrine
Type II	Mainly Planktons and algae	1.2 – 1.5	<0.1	250 – 600	Marine
Type III	Mainly higher Plants	< 1.0	0.2 – 0.3	50 – 250	Continental
Type IV	Reworked, oxidized materials	< 0.5	Varies	0 – 50	Varies

2.1.2 Organic geochemistry

This aspect of shale studies evaluates the quantity and quality of organic matter with respect to the level of maturity. The total amounts of organic matter in sediments is usually expressed as Total Organic Carbon content (TOC – wt. %). It is a gross measure of all forms of organic carbon including deposited organic matter and subsequently generated petroleum hydrocarbons (Schreier *et al.*, 1999). TOC is usually measured by laboratory pyrolysis techniques; and the other elemental ratios can be estimated from the pyrolysis results.

Visual maceral analysis and various methods of gas chromatography also provide details of organic composition in sediments and are used to infer or interpret their potential to generate hydrocarbons.

2.1.3 Maturation of organic matter & hydrocarbon generation

The structure and composition of immature kerogen changes with increase in burial depth, temperature and pressure, (maturation process) to maintain geochemical equilibrium. The process can be subdivided into three (3) main stages of diagenesis, catagenesis and metagenesis (Tissot and Welte, 1984) (Fig. 2.4). Microbial and biochemical degradation of organic matter during diagenesis takes place at relatively low temperatures and pressures, with the progressive elimination of water and functional groups containing oxygen and hydrogen changing the organic matter composition. The main released products are water and biogenic gas. Catagenesis involves the thermal degradation of organic matter to yield oil and gas (in the main oil and gas windows) when the kerogen is thermally cracked to hydrocarbons. The transformation rates depend on the organic matter type which determines the reaction kinetics, and on the time-temperature history. Metagenesis involves further thermal degradation of kerogen and the progressive orientation of highly condensed polyaromatic structures, in the process yielding mainly dry gas (CO_2 and methane) and leaving inert or residual organic matter. Detailed discussions on kerogen maturation and hydrocarbon generation are given in Tissot and Welte (1984), Kaye (2006), Hantschel and Kauerauf (2009), Mastalerz *et al.* (2013), Curiale and Curtis (2016) amongst others.

Pre-meta-morphic zones	Coal rank	R$_o$ %	Organic diagenesis phases	Hydrocarbon generation from source rocks containing kerogens type-I and type-II		
				Maturity	Types	Hydrocarbons generated
dia-genesis	peat	0.2	dia-genesis	immature	early dry gas	biogenic CH$_4$
	lignite	0.3				
	sub-bit. C B	0.38 0.4				~0.5% R$_o$
cata-genesis	high vol. bit. A C B A	0.5 0.6 0.7 0.8	cata-genesis	mature	oil	oil window
	medium vol. bit.	1.1 1.2 1.35 1.5			conden-sate and wet gas	~1.0% R$_o$
	low vol. bit.			over-mature	thermo-genic dry gas	~1.4% R$_o$
anchi-zone	semi-anthrac.	2.0 2.5	meta-genesis			
	anthra-cite	3.0 4.0 5.0				gas
	meta-anthrac.					oil biomarkers

Figure 2.4 Evolution of organic matter during sedimentation and burial (Mastalerz et al., 2013).

2.2   Sampling and Core Logging

2.2.1   Introduction

The process of sampling and core logging is of great importance to many geologic interpretations because sediments require stratified sampling to avoid bias. This entails identification of the trends, sequences and cycles, using physical characteristics seen in the well cores, cuttings and petrophysical well logs. The aim is to establish the sedimentary facies, by interpreting the detailed depositional environments and observation of grainsize trends, sedimentary structures, composition, etc. The various facies from the core logging process were then tied from the lithology log of the core to the corresponding petrophysical well logs. Representative samples were obtained from the cores (or cuttings) for further analysis.

2.2.2 Methodology

The core logging was carried out in the Western Australia Department of Mines and Petroleum (DMP) Core Repository using logging sheets following the Fugro Robertson format (Fig. 2.5). The logging was done in a methodical manner moving from one box to another to reduce the risk of omission. The length of the core was checked to accurately scale and constrain the nature of the log. Relevant details regarding the well were recorded on the log header. The parameters recorded on the core log include: lithology, grain size, sedimentary structures, bioturbation index, fossils and trace fossils, sorting, composition, oil stains, depositional energy and the depositional stacking patterns (Blackbourn, 2009). Representative shale samples were obtained from four wells in the Broome Platform (McLarty 1, Theia 1, Edgar Range 1 & Hedonia 1), one well in the Barbwire Terrace 1 (Solanum 1), one well from the Mowla Terrace (Matches Springs 1) and one well from the Crossland Platform (Kunzea 1).

Figure 2.5 Fugro-Robertson log sheet header used for recording relevant details from the cores.

2.2.3 Results

In the studied sub-basin, the lithostratigraphy established by the detailed core logging of the wells was compared, checked and correlated with the well details in the well completion reports, data from the DMP open file database and the petrophysical well log signatures. An example of well log – core relationship for the Theia 1 well (Broome Platform) is shown in Fig. 2.6.

Figure 2.6 Well log interpretation, facies summary and relationship to drill core of the Theia 1 well (Copp, 2015).

2.3   Organic geochemical analysis

2.3.1   Introduction

Pyrolysis involves artificial decomposition of organic matter by heating in the absence of oxygen, cycling the sample from ambient temperatures up to high temperatures (first 300 and then 650°C) (Jarvie and Tobey, 1999). This attempts to mimic the heating process involved in transforming natural organic matter into hydrocarbons, though it is over a much more rapid heating cycle, requires higher temperatures than in nature, and does not use similar confining pressures or formation fluids. Pyrolysis products are used to measure richness, quality and thermal maturity in sediments. In this study, pyrolysis was carried out using the Vinci Technologies "Rock Eval VI" pyrolysis instrument.

2.3.2   Methodology

The samples from the Goldwyer III shale member were crushed to powder-sized particles and weighed with approximately 60-80 mg of the shale placed into stainless steel crucibles. These crucibles have a fritted top and bottom which allows the channel of the nitrogen gas and air for oxidation through the sample (Behar *et al.*, 2001). The IFP standard sample – 16000 was analysed as the first sample and again after every 6 sample sets for calibration and reproducibility of the instrument.

The Rock-Eval pyrolysis involves a two-step-controlled heating of rock samples, first, isothermally at 300°C. This resulted in the release of free unexpelled hydrocarbons which are volatized and measured as the S_1 peak (mg HC/g rock). This was followed by an increase in temperature at 25°C/min in the pyrolysis oven to a temperature of 650°C. This process is responsible for thermal cracking of the kerogen and is recorded on the pyrogram as the S_2 peak (mg HC/g rock). The temperature corresponding to the peak of hydrocarbon generation during heating to 650°C is known as the T_{max}, which strongly depends on the type and maturity of the kerogen (Jarvie and Tobey, 1999). The relationship between

these parameters forms the basis for various indices used for geochemical property interpretation.

$S_1 + S_2$ represents the total hydrocarbon generative potential (Tissot and Welte, 1984). Standard interpretative guidelines for the hydrocarbon generative potential based on S_1+S_2 yields are given as:

- less than 2 mg HC/g rock corresponds to little or no oil potential,
- between 2 and 5 mg HC/g rock should represent fair potential,
- between 5 and 10 mg HC/g rock usually represent good potential and
- yields >10 mg HC/g rock represent excellent potential.

The TOC, which is also calculated from the pyrolysis products, provides a measure of the organic richness of the sample, expressed as a percentage of the weight of the dry rock. Bissada (1982) described organic content in rocks using the following scheme:

- 0-0.5 wt. % TOC represents poor organic richness,
- 0.5-1.0 wt. % TOC represents moderate richness,
- 1.0-2.0 wt. % TOC represents good organic content,
- 2.0-5.0 wt. % TOC represent excellent organic content.

Other ratios calculated from the Rock-Eval data include the Hydrogen Index (HI), Oxygen Index (OI), and Production Index (PI) amongst others. The kerogen type and a generalised estimation of the shale reservoir quality can be identified from the HI values (Tissot and Welte, 1978), with the classification scheme given below.

- Type I, oil-prone kerogen is usually hydrogen rich and have HI's greater than 600 mg HC/g TOC.
- Type II oil/oil and gas kerogen has HI values between 250 and 600 mg HC/g TOC

- Type III gas prone kerogen is typified with HI's between 50 and 250 mg HC/g TOC

- Type IV kerogen has HI values between 0 and 50 mg HC/g TOC, with no to very low hydrocarbon generation capacity.

Samples with T_{max} values

- less than 430 °C are immature,
- between 432°C and 442°C are in the early mature oil window
- between 442°C and 455°C are in the mid oil window
- between 455°C and 465°C are in the late oil window
- greater than 465°C are considered overmature and would generate wet or dry gas for type II kerogen (Espitalie *et al.*, 1985).

Note these temperatures are much higher than seen in hydrocarbon basins but have been approximately calibrated to actual burial temperatures.

Organic-rich (source) rock parameters and their interpretative guidelines are summarised in table 2.2.

Table 2.2 Interpretive guidelines for Rock Eval parameters (Kaye, 2006).

Parameter		Interpretation	Interpretative Guidelines	
S_1 (mg HC/g rock)	Free oil yield	Represents the amounts of free, hydrocarbon in the sample	0 – 0.5 0.5 – 1.0 1.0 – 2.0 2.0 – 3.0 > 3.0	Poor Moderate Good Very Good Excellent
S_2 (mg HC/g rock)	Source rock potential	Represents the potential of the rock to generate further hydrocarbons at higher temperatures	0 – 2.0 2.0 – 5.0 5.0 – 10.0 10.0 – 20.0 > 20.0	Poor Moderate Good Very Good Excellent
T_{max} (^{o}C)	Thermal maturity	Represents the temperature at the maximum hydrocarbon generation during the S2 cycle. Provides an indication of maturity, but can be affected by organic matter type and S1	< 430 432 – 442 442 – 455 455 – 465 465 – 530 > 530	Immature Early Mature (oil window) Mid Mature (oil window) Late Mature (oil window) Post Mature (wet and dry gas window) Post Mature (dry gas only)
S1+S2 (mg HC/g rock)	Genetic potential	Represents the potential of the source rock to generate hydrocarbon	< 2 2 - 6 < 6	Little or no potential Fair to moderate potential Good to Excellent potential
TOC (wt %)	Total Organic Carbon	Provides measure of Organic richness of a sample (%)	0 - 0.5 0.5 - 1.0 1.0 - 2.0 2.0 - 5.0 >5.0	Poor Moderate Good Very Good Excellent
HI (mg HC/g TOC)	Hydrogen Index	Used for kerogen type classification and a generalised estimation of the source rock quality	0 – 50 50 -250 250 – 600 > 600	Type IV (negligible) Type III (gas) Type II (gas/ oil & gas) Type I (oil)

2.3.3 Results and discussion

The measured TOC values (Fig 2.7, Appendix I) in the samples range between 0.1 – 4.6 wt % TOC, with 64% of the samples with TOC greater than the 0.5%wt TOC minimum threshold and 50% of the samples with TOC greater than 1%; consistent with shales that may have moderate potential to generate hydrocarbon (Bissada, 1982; Jarvie, 1991)

The analysed pyrolysis results were augmented by many more Rock-Eval values from the Western Australia Department of Mines and Petroleum (WAPIMS) online database available at (https://wapims.dmp.wa.gov.au/WAPIMS/) (Appendix I) to provide a larger and more robust dataset. Review of the well

completion reports indicated that some wells used oil based muds when drilling including the McLarty 1 well. Kennard *et al.* (1994) suggest that samples from the McLarty 1 well have significant amounts of drilling contaminants, which is evident in the unusually high Production Index (PI) values reported in the DMP open file database (Appendix I). Consequently, only the data from solvent extracted samples from Kennard *et al.* (1994) were considered here for the McLarty 1 well.
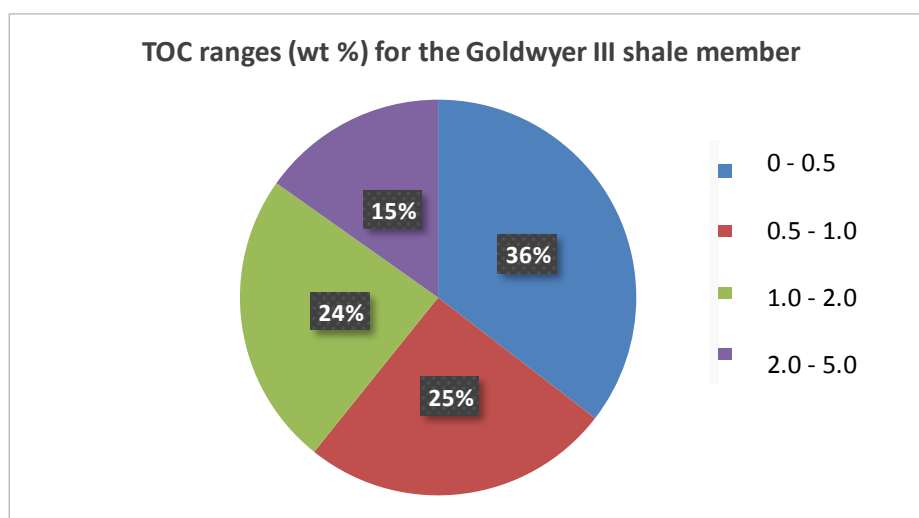
Figure 2.7 TOC distribution in the Goldwyer III shale from some Canning Basin wells.

The S_1 values range up to 3.9 mg HC/g rock in some wells and an average value of 0.7 mgHC/g rock, indicative of moderate to good amounts of free hydrocarbon in these samples. The S_2 values show that the samples have moderate to very good source rock potential with values up to 7 mgHC/g rock and an average value of 1.9 mgHC/g rock.

S_1+S_2 values represent the potential quantities of hydrocarbon a shale reservoir can generate at sufficient maturities. In the studied shales, the petroleum potential ranges up to 17.3 mg HC/g rock in the wells and averages 2.5 mg HC/g rock. This represents mostly fair to excellent generative potential in parts of the study area.

The log S$_2$ *versus* log TOC plot (Fig. 2.8) shows that the studied Goldwyer III shales generally have good to very good potential, with higher potential in most of the samples from the Aquila 1, Theia 1 and McLarty 1 wells, showing good to excellent source potential. However, the level of thermal maturity of the shales should be considered in the overall interpretation. The Tmax values in the wells that show good to excellent source potential suggest early to late mature oil generating window. The Jarvie *et al.* (2001) equation was used for the Rock Eval T$_{max}$ to vitrinite reflectance equivalent conversion. See range of values in Appendix II
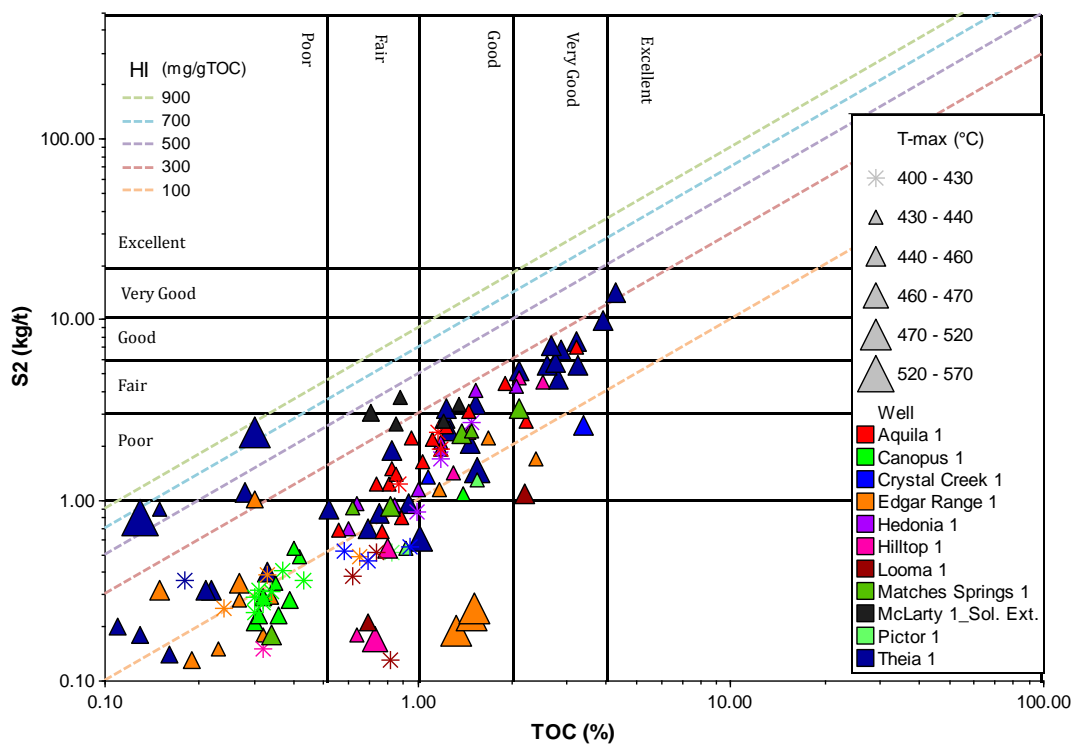
Figure 2.8 Shale reservoir characterization on a plot of log S2 versus log TOC showing the generative potential in the studied samples.

Van Krevelen Plot (Fig. 2.9) shows that the Goldwyer III shales are mostly Type II oil-prone kerogen as well as Type III gas prone kerogen; the latter, probably due to the presence of graptolites in the sediments or due to localized oxidation of some of the organic matter that is deposited in some beds.
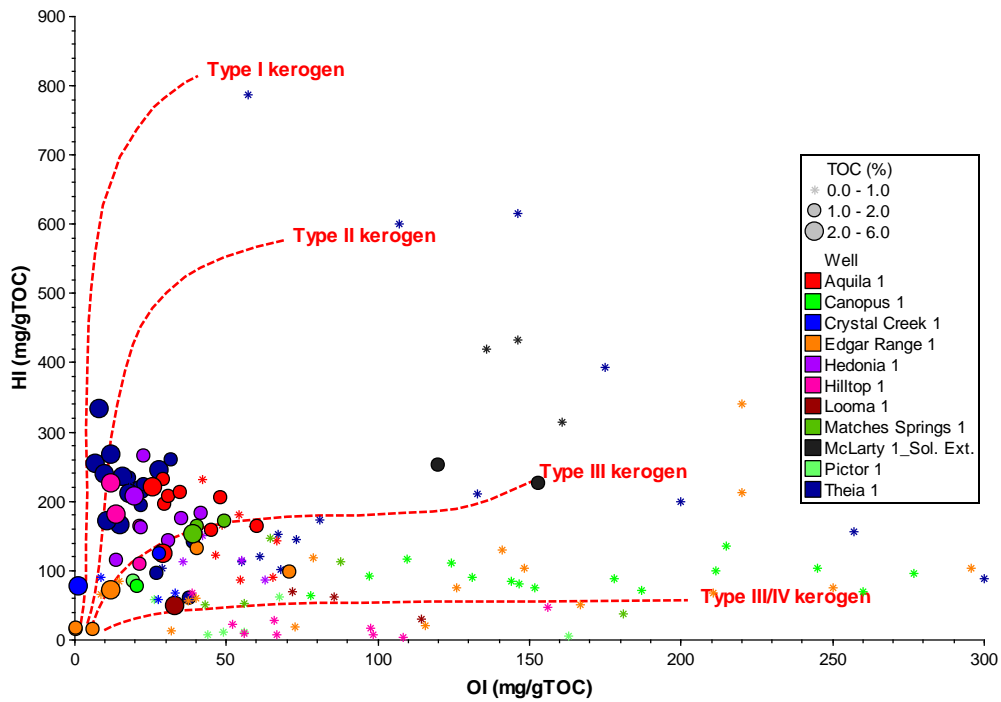
Figure 2.9 Pseudo-Van Krevelen Diagram showing kerogen type – showing predominance of Type II and Type III kerogen.

The plot of HI versus T_{max} with maturity overlay given in Fig 2.10 shows that the shales are mostly in the early mature to late mature oil window, with HI values generally between 100 and 350 (mg HC/g TOC). The horizontal spread is due to variation in kerogen type and samples with low TOC being unreliable for estimation of Tmax.

Normally, thermal maturity in sedimentary rocks is measured by vitrinite reflectance (VR). However, since the studied samples are of Ordovician age, vitrinite reflectance conversion from Tmax was used as a proxy for thermal maturity (Appendix II). In the samples with TOC's greater than 0.5 wt %, the Tmax values generally range between 430°C and 460°C, which corresponds to 0.60 -1.12 VR equivalent. In some samples from the Edgar Range 1 well, T_{max} values up to 480°C were recorded, which places them in the post mature oil window or gas generation window.
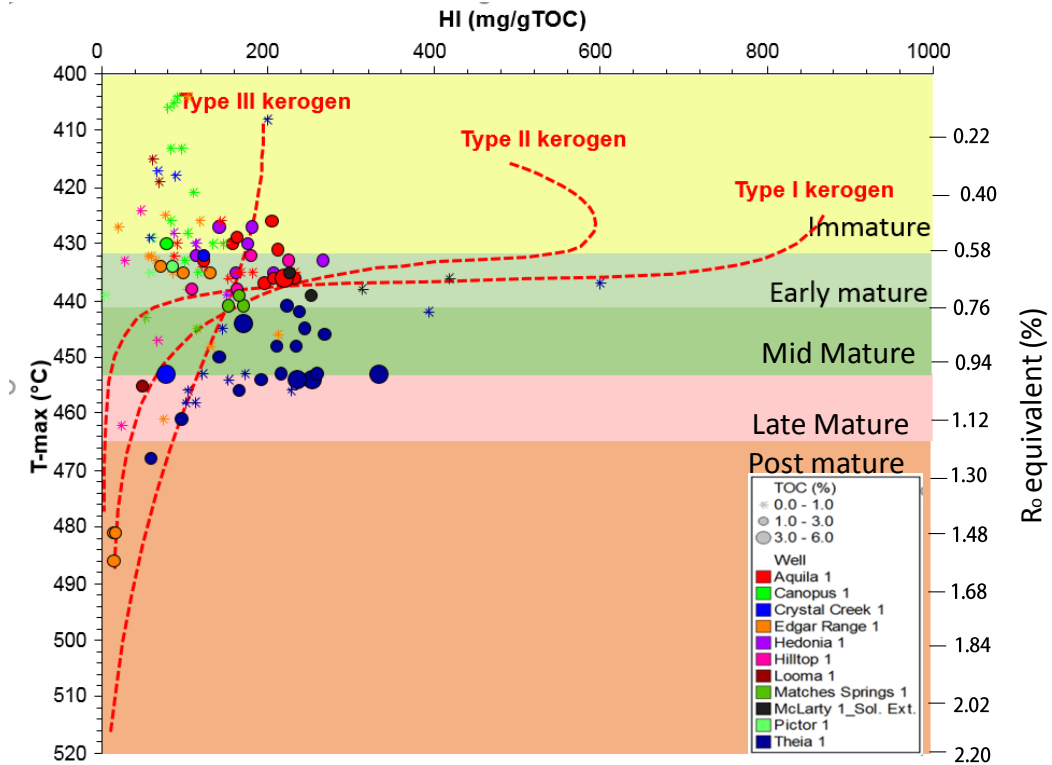
Figure 2.10 Plot of Hydrogen Index versus Tmax, showing the kerogen types and thermal maturity stages.

Overall, interpretations from the geochemical data available for this study suggest the Goldwyer III shale interval in the Theia 1 well has the best hydrocarbon source potential, in which the samples have TOC and S_2 values up to 4.28 wt % and 14.25 kg/t respectively. Also, samples from Edgar Range-1 and Theia-1 plot as predominantly oil-prone Type II kerogen suggesting they have the best overall potential as hydrocarbon source rocks compared to other wells in the study area. In the McLarty 1 well there are too few solvent extracted samples to draw any confident conclusions.

2.4 Geochemical property estimation from petrophysical well logs

The geochemical information in the Canning Basin is limited, mainly due to the limited number of wells drilled that penetrate the Ordovician Goldwyer Formation. Hence, a method to predict the geochemical properties is necessary for areas with sparse or no geochemical data. Several methods have historically been proposed to obtain some geochemical parameters from well logs, most including methods for estimating the total organic carbon (TOC) content (Schmoker, 1983); (Meyer and Nederlof, 1984) and (Passey *et al.*, 1990). More recently, several authors have utilised artificial intelligent systems such as Neural Networks and Neuro-Fuzzy Logic to estimate TOC content from petrophysical well logs, including Huang and Williamson (1996), Kamali and Allah Mirshady (2004), Rezaee *et al.* (2007) and Kadkhodaie-Ilkhchi *et al.* (2009b).

Yu *et al.* (2017) compared the TOC estimates of the Canning Basin shales, using the methods of Schmoker and Hester (1983) and Passey *et al.* (1990). The study concluded that these methods do not work well in moderate to low TOC shales – as occurs in the Canning Basin.

Two methods were considered to generate continuous geochemical logs in this study. They are

1.   The Passey *et al.* (1990) approach and

2.   Artificial Neural Networks (ANN) approach.

The results obtained from the Passey *et al.* (1990) approach do not yield satisfactory correlations between the laboratory measured TOC and modelled TOC. Therefore, Artificial Neural Networks approach was considered. Both methods and results are discussed in the subsequent sections.

2.4.1   Passey approach

The common method of assessing organic richness and maturity in organic rich rocks is through a variety of laboratory experiments such as pyrolysis (section 2.3). However, there is generally a dearth of core/cuttings samples within these source rock intervals from older wells or incomplete geochemical laboratory analysis from some cored and analysed wells (Huang and Williamson, 1996). Analysis of drill cuttings is an alternative given that they are widely available, however, accurate depth matching and contamination of the cuttings is a long-standing issue.

Passey et al. (1990) developed a practical method which uses the response of well-logs in organic-rich logs to obtain continuous TOC information in wells. The study used the overlay of sonic log and deep resistivity log on scaled track. The study suggested the logs should be overlain in the water-saturated and organic-lean intervals to define the baseline. If organic matter is present, a separation from the two curves will be observed (Fig. 2.11).
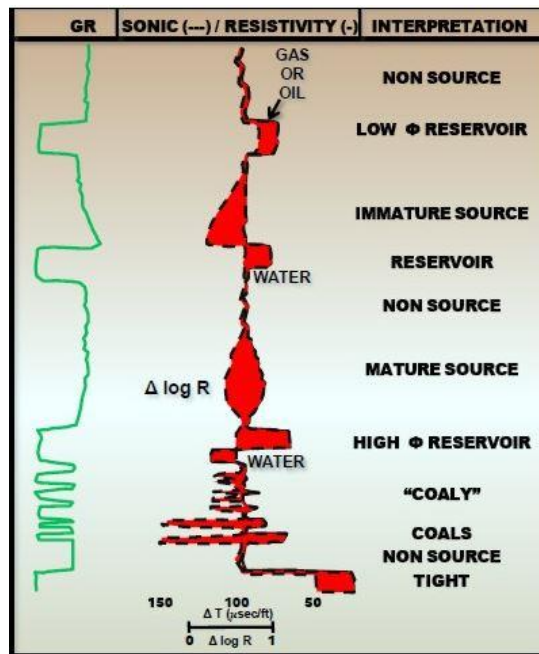
Figure 2.11 A schematic guide for the interpretation of features observed on a Δ log R overlay (Passey et al., 1990). The baseline is the point where the curves track in organic lean rocks.

The ΔlogR separation is linearly related to TOC and is a function of maturity. In this case, maturity is described in terms of Level of Organic Maturity (LOM)(Hood *et al.*, 1975). An LOM of 7 corresponds to the onset of maturity for oil-prone kerogen, while an LOM of 12 corresponds to the onset of overmaturity for oil-prone kerogen (Passey *et al.*, 1990)

The separation (ΔlogR) was calculated as follows:

$$\Delta logR = \log_{10}(R/R_{baseline}) + K (\Delta t - \Delta t_{baseline}) \qquad \text{(equation. 2.1)}$$
Where
ΔlogR: Curve Separation measured in logarithmic resistivity cycles
R: Resistivity (Ohms/m)
Δt: Measured Transit time in μs/ft
$\Delta t_{baseline}$: Value when the curves are baselined in clay-rich, non-source rocks
K: Resistivity Constant

The resultant total organic content is calculated by the equation
$$\text{TOC (wt \%)} = \Delta logR * 10^{(2.297 - 0.1688*LOM)} \qquad \text{(equation. 2.2)}$$
Where
LOM: Level of Organic Metamorphism

For any specific ΔlogR, TOC decreases as LOM increases (Cluff & Miller, 2010). LOM can be derived from maturity information, such as vitrinite reflectance R_o (Fig. 2.12).
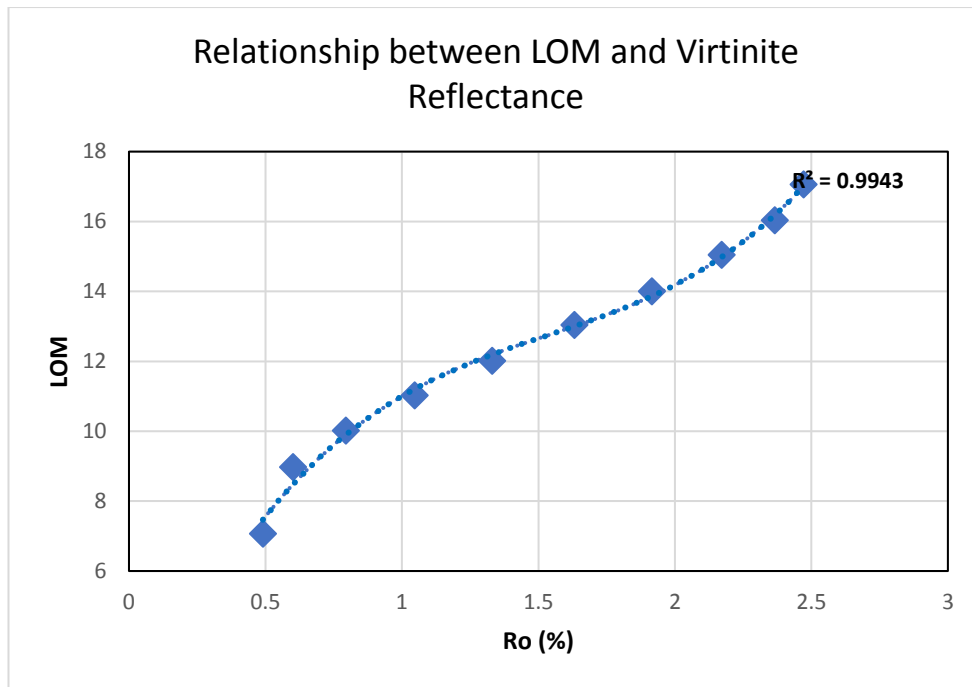
Figure 2.12 Relationship between the Level of Organic Metamorphism and Vitrinite Reflectance (Cluff and Miller, 2010).

In this study, using the Jarvie *et al.* (2001) equation to convert Tmax to R_o, an average vitrinite reflectance equivalent of 0.7-0.8 R_oe was obtained for the Goldwyer III shales in most of the studied wells. Therefore, an LOM of 8.5 – 10.0 was accordingly assumed in equation 2.2.

Substitution of the parameters in equations 2.1 and 2.2, the resultant TOC well log is shown in figure 2.13. The laboratory measured TOC data were then compared to the continuous log for validation. The results show that the calculated values have a poor correlation with the laboratory values (Fig. 2.13), with an R^2 of 0.48 and an MSE of 2.17. The plot shows that the ΔlogR method overestimates TOC in the studied wells. This is in line with the conclusions from Yu *et al.* (2017).
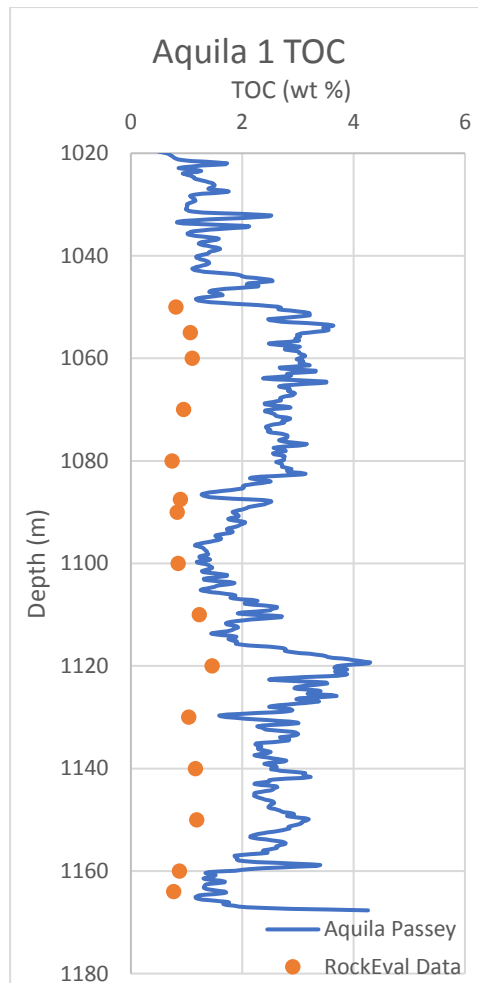
Figure 2.13 Plot of the laboratory measured TOC data on the calculated continuous geochemical TOC log for Aquila 1 using the Passey method.

The Passey *et al.* (1990) method is highly dependent on the accurate estimation of the LOM. This poses a limitation on utilizing the Passey method in this study, where a single point estimate of LOM was estimated from a single estimated Ro value (normally calibrated using vitrinite data, noting woody plants had not evolved by the Ordovician Period). The R_0 value was estimated from Tmax values, that vary with depth and here mostly represent alginite (exinite) organic matter. Hence, reliance on converted Rock-Eval Tmax or other vitrinite reflectance equivalents should have an impact on accurate LOM estimation.

2.4.2 Artificial Neural Networks Approach

The Artificial Neural Networks (ANN) method is a mathematical technique that can be used to solve nonlinear, complex problems, through pattern recognition, which model the biological processes of the human brain (Dowd and Sarac, 1994).

Several geologic studies have demonstrated the influence of organic matter on petrophysical well-log signatures, including the Passey *et al.* (1990) approach described in section 2.4.1. As a result of these relationships, recent studies have focused on using intelligent systems, such as Artificial Neural Network (ANN) to use log data to predict related geochemical property data in areas with sparse information.

Traditionally, drill cores and cuttings are obtained from selected intervals and the organic-rich sections are subjected to organic geochemical analysis to estimate the amounts of organic content (TOC), the source rock potential (S2) and the source rock quality (HI).

With ANN, logs with strong relationships to disseminated organic matter in shales are used to build the model, using a supervised method, where the user "trains" the system with the desired output. An error between the output and the desired output is computed and fed back into the system (Huang and Williamson, 1996) and the weights are adjusted until the approximate desired output value is achieved. An algorithm for the property is designed and trained for each predicted geochemical property, using petrophysical data from well logs as the input data, and the measured property values as the desired output. A detailed methodology for this is recorded in Huang and Williamson (1996); Boadu (1997); Kadkhodaie-Ilkhchi *et al.* (2009a); Alizadeh *et al.* (2012). The neural network system is particularly useful in studies such as this, due to its adaptability in learning by example and its ability to generalize.

The methods employed in this study can be subdivided into three main steps.

a. Well log to geochemical data compilation
b. Identification of the relationship between well logs and geochemical property
c. Network Training

The main objective of well log to geochemical data compilation was to establish a relationship between the suite of well logs and the corresponding measured geochemical value. Depth matching of the geochemical measurements from drill cuttings was carried out based on the TOC values and density responses, by adjusting the depths to the most probable density log response to the measured TOC value within a 1-3 m window, the standard range of error for cuttings depth (Guzman, 2003). Geochemical data from drill cores, however, did not require a further depth match. Data from the Ordovician Goldwyer Formation from other sub-basins in the Canning Basin have also been included for a more robust training dataset, starting off with 96 data points. The training data set comprises low, moderate and high TOC shales as well as calcareous shales from the Goldwyer Formation. The well logs used in this study were the gamma ray, resistivity, sonic and density logs, while geochemical inputs included TOC, S_1, S_2, and HI. Table 2.3 shows a summary of the logs over the Goldwyer section from the Hilltop 1 well and their corresponding geochemical information.

Table 2.3 Well logs and geochemical data used in this study. A total of 96 data points was used as the training dataset.

Hilltop 1

	Well log data				Laboratory Rock-Eval Data					
MD	R(D)	RHOB	Gamma	P-sonic	MD	HI	S1	S2	TMAX	TOC
1052.474	15.484	2.51	148.69	100.38	1052.5	225.71	1.68	4.74	433	2.1
1079.144	7.0857	2.53	150.13	108.39	1079.1	163.45	1.10	2.37	438	1.5
1098.042	17.6400	2.51	153.03	97.77	1098.0	180.4	2.29	4.51	432	2.5
1128.065	11.5097	2.54	154.03	103.91	1128.1	109.23	0.92	1.42	438	1.3
1170.280	14.6766	2.58	154.16	100.77	1170.0	67.5	0.42	0.54	447	0.8

The identification of the relationship between well logs and geochemical property plays an important role in the construction of the neural network model. First, simple regression plots were used to identify the logs with strong relationships with each geochemical property. The general rule is that the inputs with a stronger relationship with the output provide more accurate predictions (Kadkhodaie-Ilkhchi *et al.*, 2009b). At this stage, the cross-plots of well logs (inputs) and geochemical property (desired output response) are used to identify and eliminate noisy and potentially misleading data. The coefficient of determination (R^2) obtained from cross-plots between these relationships was used as the quality control to eliminate outliers (and their corresponding well log measurements) from the dataset. For example, the cross-plots of TOC vs gamma ray, resistivity, sonic and density logs (Fig. 2.14 a-d) shows that gamma-ray and density logs have a more direct relationship with TOC. In this example, however, the gamma-ray data was preferred as the primary input for TOC log prediction because, with the gamma-ray cross-plots, fewer outliers were observed, thereby it yielded more test and validation data points. A summary of typical well log responses to disseminated organic matter in organic rich rocks is given in Kamali and Allah Mirshady (2004), Huang and Williamson (1996) Kadkhodaie-Ilkhchi *et al.* (2009b).
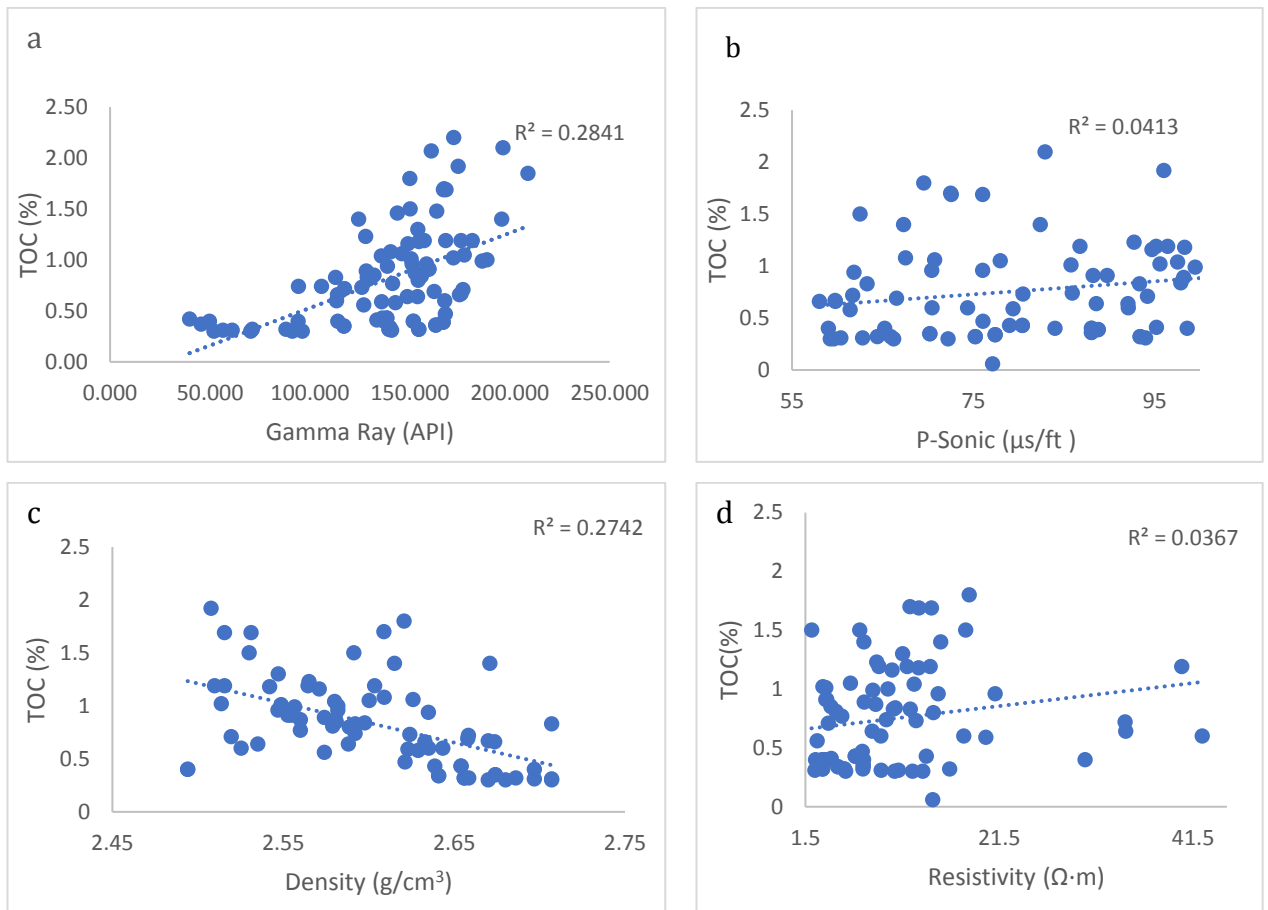
Figure 2.14 Plot of the laboratory measured TOC data on the calculated continuous geochemical TOC log for Aquila 1 using the Passey method.

This study used a supervised algorithm to train the network in wells that have both logs and geochemical data. In this case, the neural fitting tool (nftool) on MATLAB was used to train the network for the desired geochemical output. Approximately 10-15% of the data points were eliminated from the dataset as noisy data. The input dataset was divided into clusters, using 70% of the data to train the network, leaving 15% to control the model performance and 15% to test the neural network model. Networks with the four logs (neurons) as input and 6 hidden neurons (Fig. 2.15) were generated for Total organic carbon (TOC), source potential (S2) and Hydrogen Index (HI) using the Levenberg-Marquardt training algorithm on MATLAB. This algorithm aims to minimise the sum of square errors between the input and output nodes by updating the weights of the neurons in response to the errors between the actual and target output value, as detailed in (Boadu, 1997). The Mean Square Error (MSE) and the correlation

39

coefficient (R^2) between the actual and predicted property were used to validate the performance of the model. Finally, the geochemical property being modelled is calculated to best fit the resultant network and the output is generated as the continuous geochemical property.
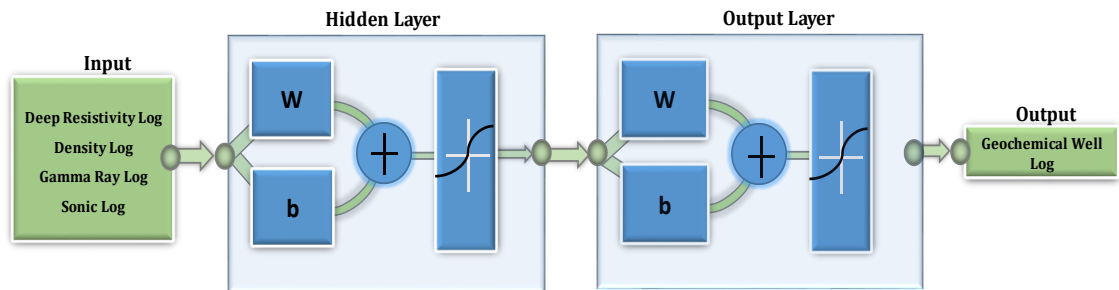
Figure 2.15 Architecture of the constructed neural network.

W = Weight, b = Bias.

2.4.2.1 ANN Results and discussion

In this study, ANN is utilized to predict organic geochemical data in wells with no laboratory measured geochemical data and in wells with limited laboratory data.

For each geochemical property, the optimum trained network was achieved by several iterations with the Levenberg-Marquardt training algorithm, with six hidden neurons. This optimum network was determined by observing the minimum deviation between the regression line and R=1 of the network between the neural network predicted value and the measured values as well as the coefficient of determination (R^2). An example from the TOC prediction gives an R^2 value of 80%, 78% and 80% for the training, validation and test data between the actual and predicted values (Fig. 2.16). The learning was stopped at these confidence estimates in order to avoid overfitting of the training dataset.
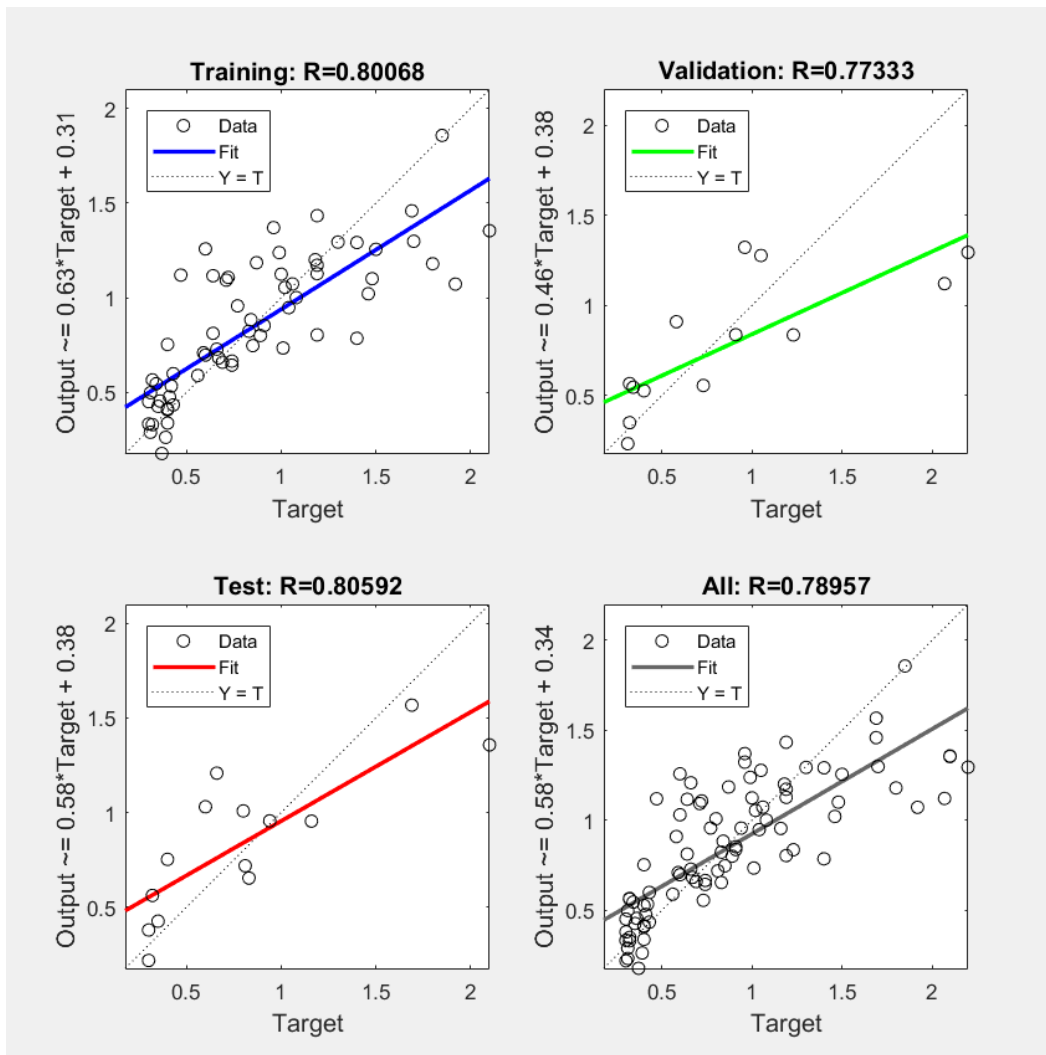
Figure 2.16 Regression plots showing the correlation coefficients between target and predicted TOC values for the training, validation and test stages.

After adjusting the weights of the neurons, the performance of the model (MSE) is 0.16631 at iteration 13 (Fig. 2.17)
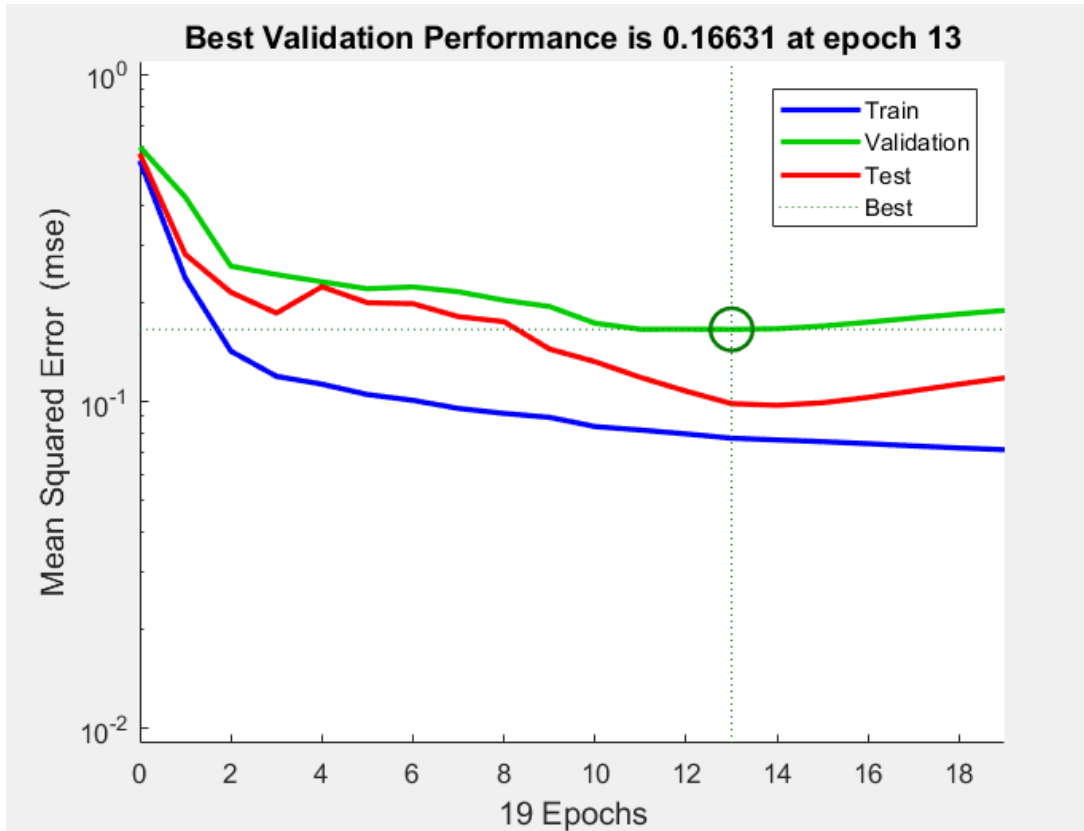
Figure 2.17 Performance diagram for Training (blue line), Validation (green line), and Test (red line) steps. The best validation performance is equal to 0.16631 at iteration 13.

The petrophysical well log data from each well was input into the optimised model to calculate the estimated geochemical data. This process was repeated for each property. Table 2.4 shows the range of values for the neural network derived geochemical data. In terms of maturity, most of the T_{max} data suggest that the shales are mostly in the immature to early mature oil window, with some data points in the mid mature oil window. This may also be due to the inclusion of the low TOC/Tmax data which has distorted the results.

Table 2.4 The network trained geochemical data from 6 Canning Basin wells.

S/No.	Well Name	HI	S1	S2	Tmax	TOC
1	Sharon Anne 1	96 – 194	0.1 – 1.06	0.3 – 8.01	393 – 457	0.3 – 1.6
2	Hedonia 1	86.8 – 266	0.3 – 1.72	0.69 – 4.07	428 – 439	0.6 – 1.53
3	Hilltop 1	4.26 – 252.7	0.06 – 1.68	0.02 – 4.74	330 – 447	0.4 – 2.01
4	Aquila 1	87.1 – 219.4	0.11 – 2.71	0.67 – 7.02	426 – 436	0.56 – 1.46
5	Canopus 1	63.8 – 135	0.08 – 0.17	0.23 – 0.54	268 – 433	0.3 – 1.4
6	Looma 1	55 – 623	0.1 – 1.01	0.1 – 8.2	395 – 457	0.2 – 2.3

The validity of the network trained data is shown here with the Aquila 1 well. This is achieved by superposition of the laboratory measured geochemical data to the network predicted data. The estimated geochemical curves fit relatively well with the measured laboratory geochemical values, particularly the TOC and S_2 logs. (Fig. 2.18). These estimated logs provide a much more complete coverage over the entire interval for the Goldwyer III shale member.
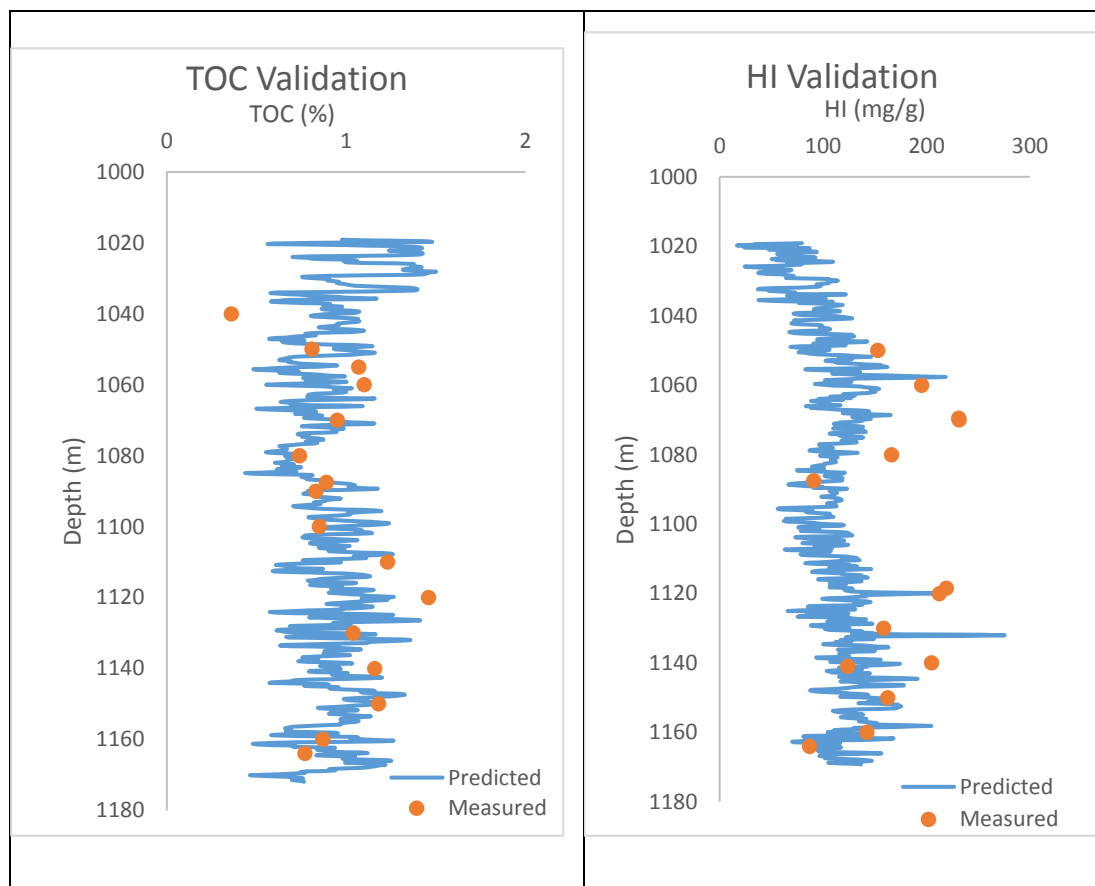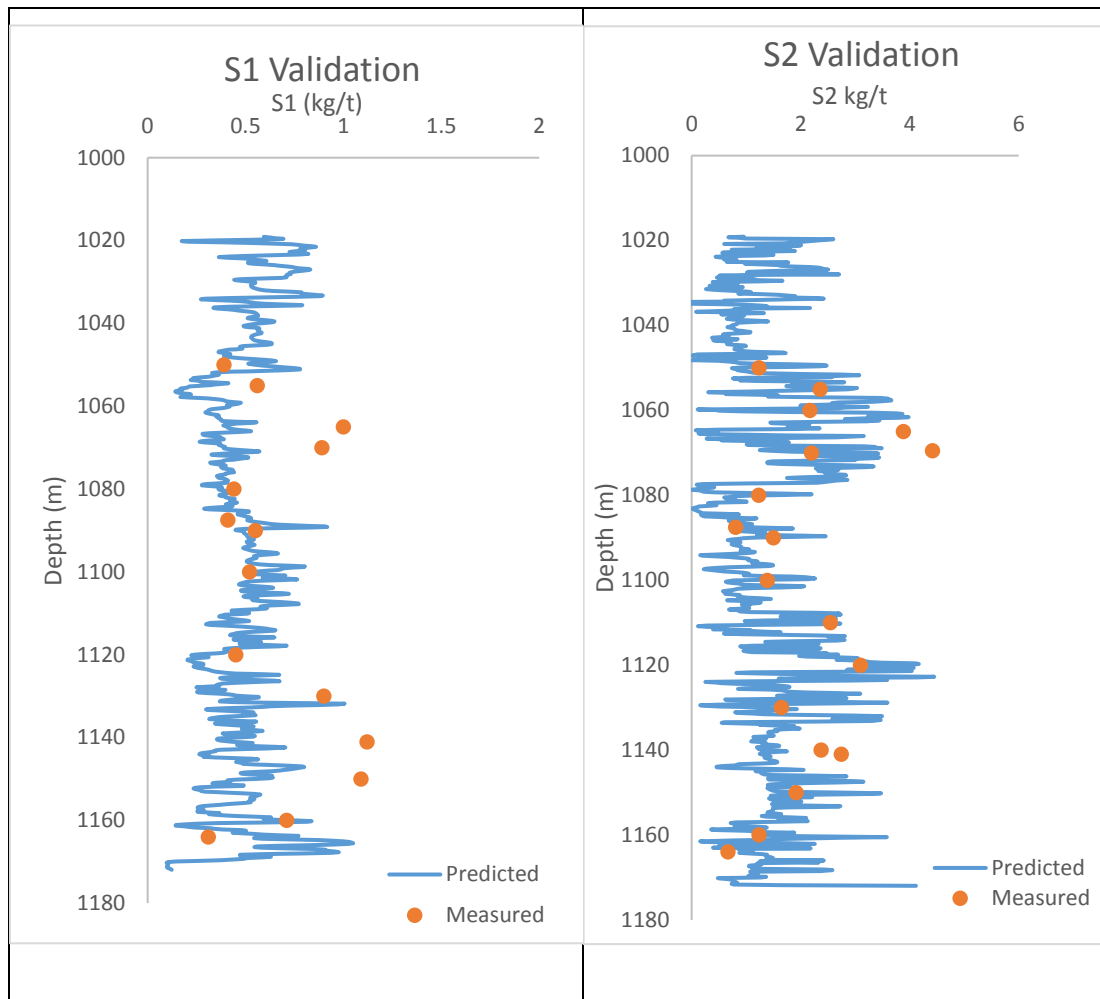
Figure 2.18 Comparison of the Artificial Neural Network predicted curves with the laboratory generated geochemical data in the Aquila 1 well.

2.5 Geochemical property modelling in Canning Basin

The distribution of some geochemical properties within the ~150m – 250m thick Goldwyer III Shale member was modelled across the Broome Platform of the Canning Basin by construction of a 3D model using the well and seismic data in Petrel (Schlumberger software) (Fig. 2.19).

The 3D modelling involved several steps before property data could be interpolated through the model, including stratigraphic correlation, horizon mapping, surface generation, structural modelling and petrophysical modelling. The workflow followed in this process is available in appendix III.

The first step in this study was the correlation of well tops in all the wells across the sub-basin using the well logs and the seismic data. Depth converted surfaces for the Canning Basin were obtained from the (WAPIMS) online database available at (https://wapims.dmp.wa.gov.au/WAPIMS/). Some discrepancies between the WAPIMS surfaces and the well tops were observed, and these were repicked to obtain a better tie between the seismic horizons and formation tops.
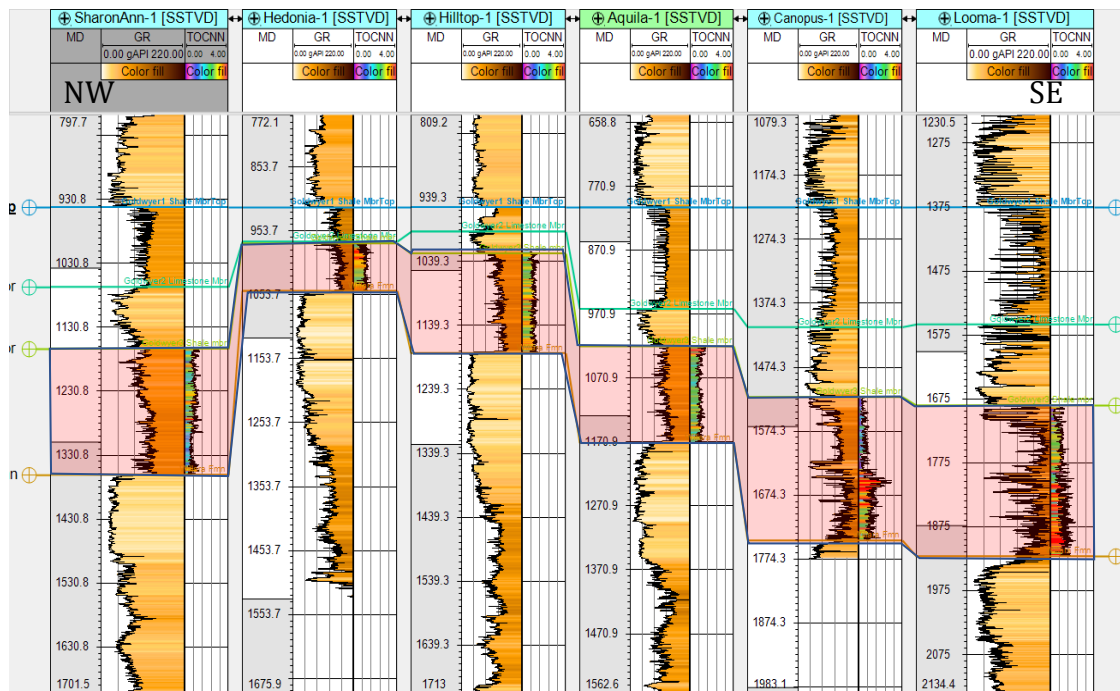
Figure 2.19 Well log correlation from northwest to southeast for some wells on the Broome Platform. The panel shows the gamma ray log and the network generated TOC logs.

The interval Goldwyer III shale is the main stratigraphic reservoir unit modelled, lying between the Goldwyer III well top and the top of the Willara Formation (Fig. 2.20 a and b). The 3D model lateral grid increment was set at 500 x 500 m and the Goldwyer III zone was divided into 10 layers, with approximately 10m of vertical resolution. The petrophysical logs and the estimated geochemical logs in each well were blocked or upscaled into the layers. The data analysis module in the Petrel software was used to obtain acceptable variogram models and estimate anisotropy, nugget and sill values. These inputs control the interpolation in 3D space of the logs and geochemical properties.

45

The 3D petrophysical modelling was done using the Sequential Gaussian Simulation (SGS) algorithm in Petrel, which is based on the open source Geostatistics Software Library (GSLIB) routines. The input included the upscaled geochemical logs at each well for control and the derived variograms to control the uncertainty. SGS is a stochastic method of interpolation based on kriging that will honour the input well data, their distributions and derived variograms and maintain trends. There are options that can use the global or local mean to estimate the overall trend. The interpolation visits the grid nodes in a random order and kriges using the variogram model to estimate the variance from the mean at that node, after which it selects a value from the input distribution to match the variance. Other related data can be used (e.g. cokriging) to guide the output using the covariance matrix. Therefore, each simulated value at a point is dependent on the original data and nearby previously simulated data points. This process is repeated until all the points are estimated at every grid value. The entire interpolation can be repeated to produce a suite of simulations that cover the range of possible outcomes given the uncertainty of the data. A detailed explanation of the procedures for reservoir property modelling are available in the Petrel Help manual and in Ringrose and Bentley (2015) as well as Cannon (2018).

The workflow employed in the property model is given in appendix III.
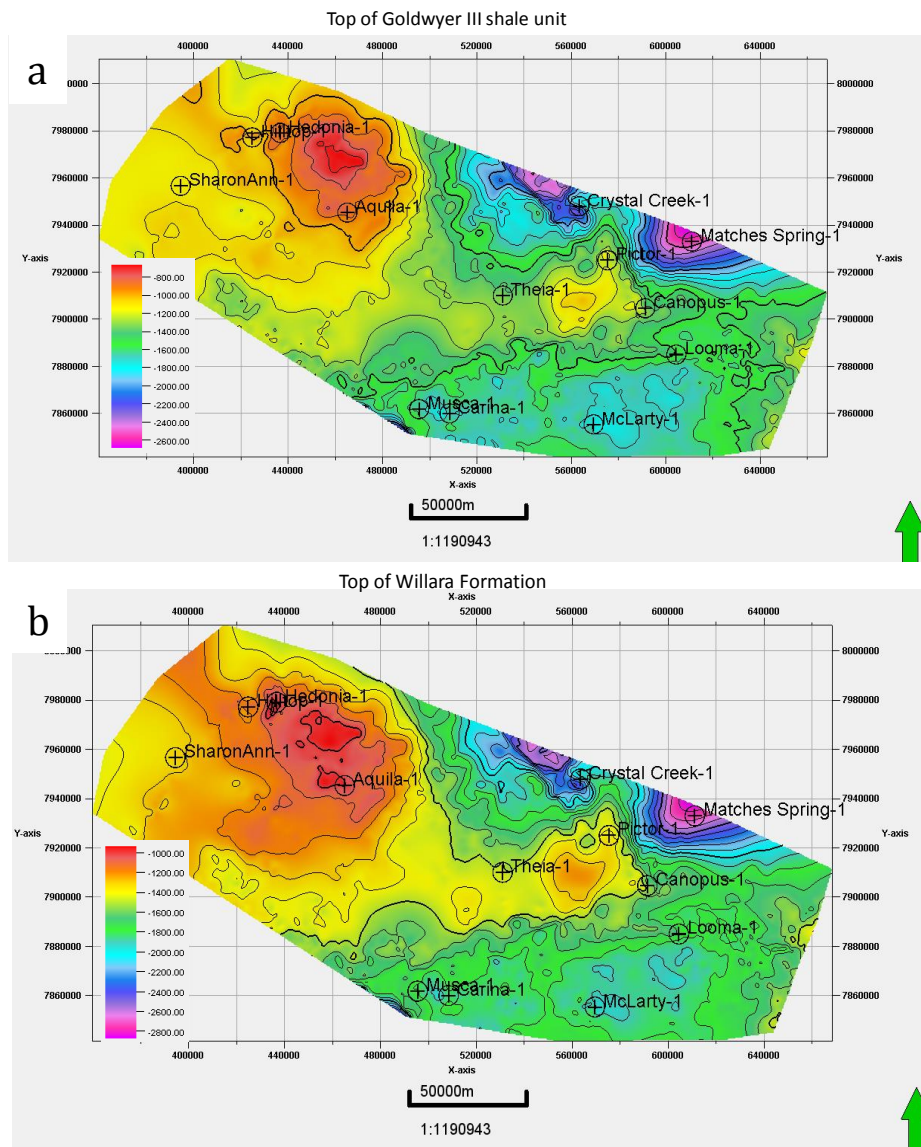
Figure 2.20 Well tied surface for the top of (a) Goldwyer III shale unit; and (b) Willara Formation.

2.5.1 Results

The predicted geochemical well logs from the neural network were upscaled and the geochemical property values were populated throughout the 3D model in the Goldwyer Formation reservoir by the SGS algorithm. Thirty reservoir model realizations were obtained for each property (i.e. TOC, HI, S_1 and S_2) and an example of the 3D model is shown in Figure 2.21 a and b.

Top of the Goldwyer III shale unit, showing TOC property distribution in the Broome Platform

Cross-section of the modelled TOC property distribution for the Goldwyer III shale unit in the Broome Platform
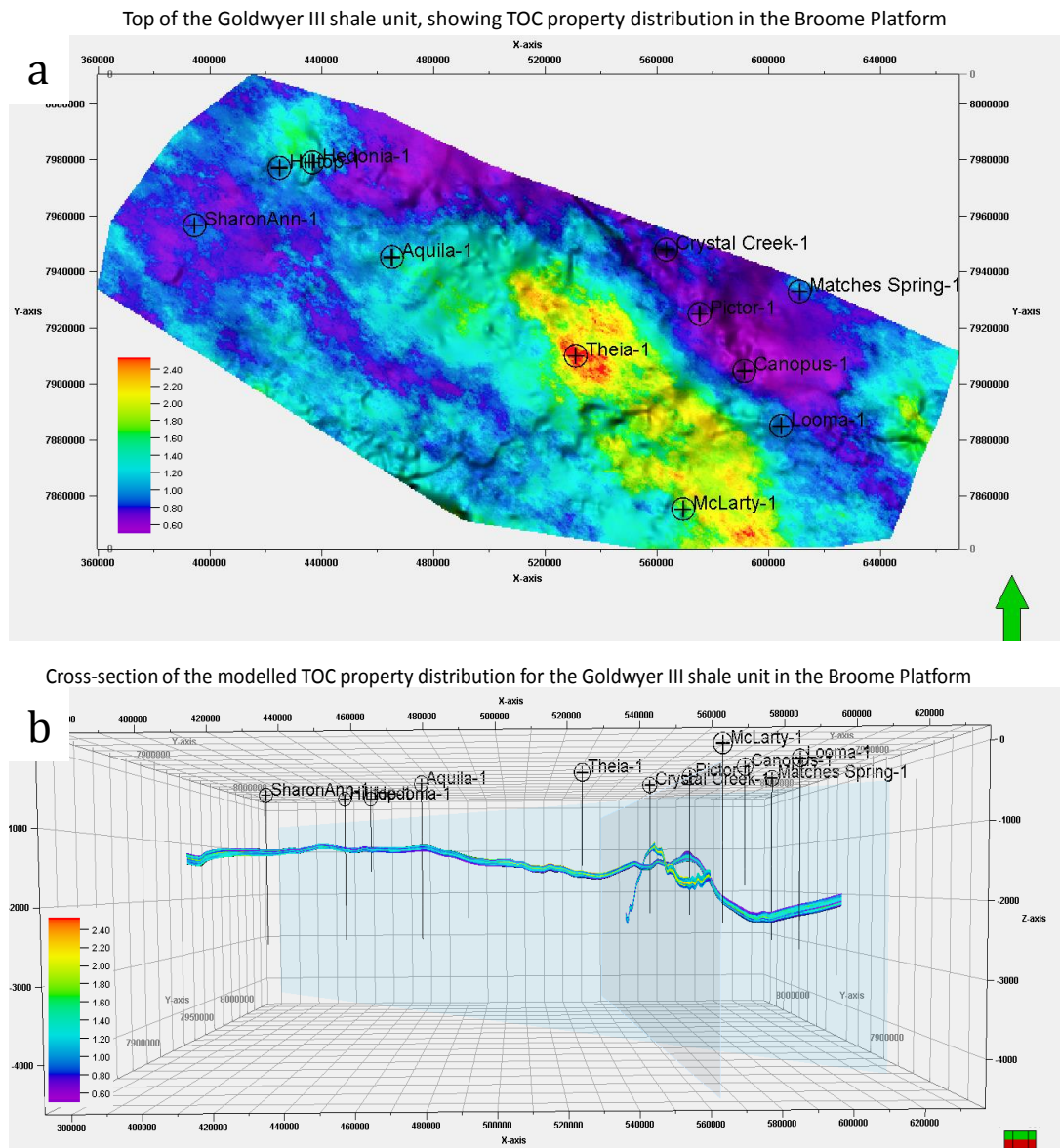
Figure 2.21 An example of the 3D model showing (a) the distribution of TOC property in the study area; (b) the cross-section distribution of TOC property in the study area (Viewed from the south).

Average property maps were calculated through each of the 3D property models realizations to produce a single map for each property to show the most likely areal distribution. Figure 2.22 a-d shows the mapped distribution of the geochemical properties within the sub-basin. The generated average maps suggest that organic matter richness/ preservation is higher in the central to south-eastern parts of the sub-basin. Note these are averaged over the full Goldwyer III section and much greater variability occurs in the vertical sections

48

between the thin beds. For higher resolution average TOC property distribution map, see appendix IV
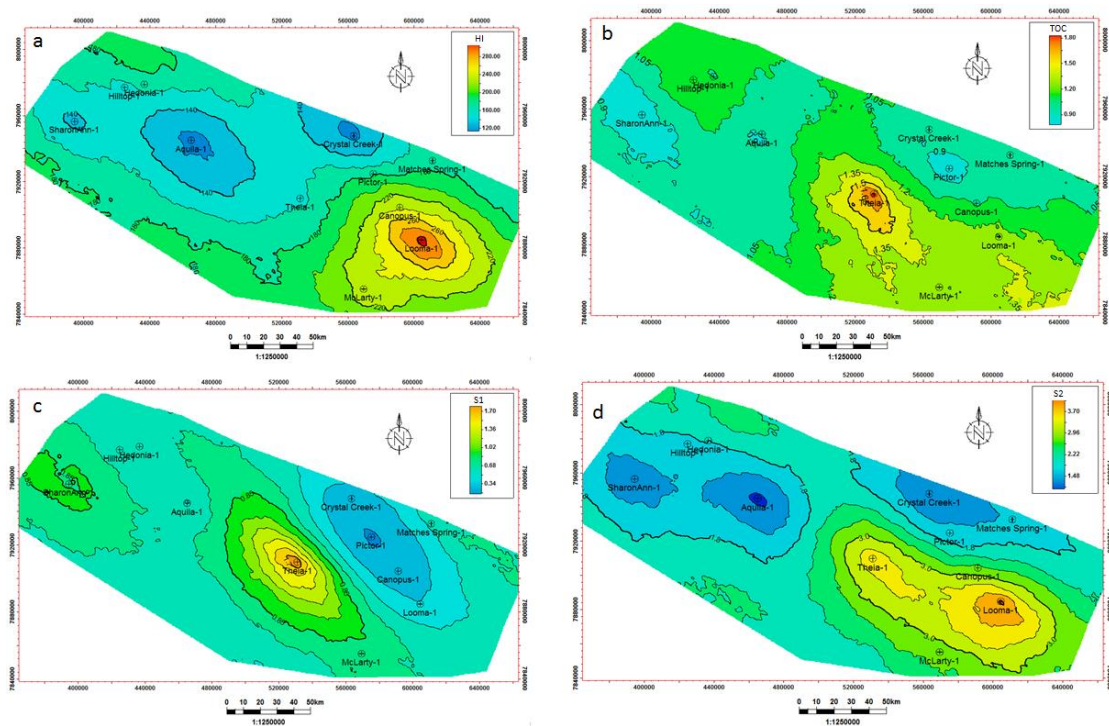
Figure 2.22 Geochemical property average distribution maps for the Goldwyer III shale in the Broome Platform, Canning Basin. The maps represent (a) Source rock quality (HI). (b) Total Organic Content (TOC) (c) Free Oil Yield (S1) and (d) Source rock potential (S2).

2.5.2 Statistical evaluation and model validation

Further statistical validations were carried out in Petrel on the modelled properties to quantitatively assess the uncertainty. The TOC model, for example, has a mean of 0.81 and standard deviation of 0.19, the data distribution is approximately normal and is statistically significant with 99.7 percent of the points occurring within three standard deviations ($\mu \pm 3\sigma$).

Where
M = Mean, σ = Standard deviation. Therefore,
Data distribution =
0.81- 3(0.19). = 0.24
0.81+ 3(0.19), = 1.71

Hence, the modelled average TOC in the Goldwyer across the study area occurs between 0.24 and 1.71 wt % TOC (Figure 2.23a).

The low value of the calculated RMSE: 0.034 and an R^2 of 0.78 in the Aquila 1 well indicates that the predicted log in this well has a relatively good fit. Also, Fig. 2.23b provides a comparison of the modelled error between the measured, modelled and upscaled TOC.
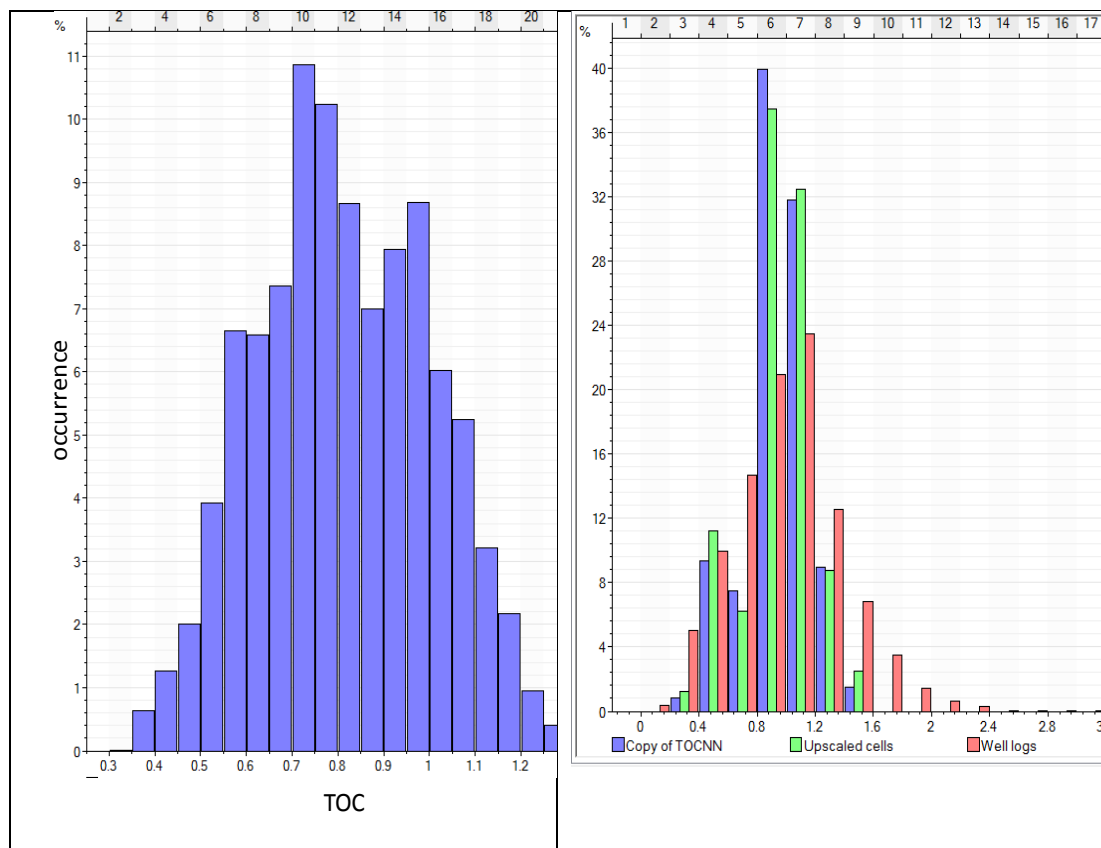
Figure 2.23 (a) A plot of Goldwyer III shale average TOC distribution in the study area; (b) Comparison of the modelled error between the measured, modelled and upscaled TOC.

2.6   Discussion and conclusion

The Ordovician Goldwyer shale is an important Formation in the Canning Basin, WA (Ghori and Haines, 2006). Core samples were investigated by organic geochemical analysis and the results indicate that this shale contains mostly Type II and Type III oil prone and gas prone kerogen. Organic richness values range between 0.1-4.6 wt % TOCs, with source rock generative potential (S_2) mostly varying from poor potential to moderate/good potential. The T_{max} *versus* HI values show that the studied shales have reached thermal maturities analogous to the early to peak stages of oil generation.

Generally, the presence of organic matter can be identified from well logs. This has been well studied, with the most popular approach for TOC calculation being the Schmoker and Hester (1983) and the Passey et al. (1990). Schmoker and Hester calculated TOC as a function of the reciprocal of bulk density. This method has its limitations as bulk density is usually affected by several reservoir properties. The Passey approach, on the other hand, utilizes the porosity logs (e.g. sonic, neutron and density) and resistivity log to define a baseline – which may vary from one well to another. A good knowledge of the shale mineralogy should also be taken into account when using this method as the presence of expandable clay minerals can lead to significant underestimation of TOC's (Gonzalez *et al.*, 2013). The Passey et al. (1990) method was considered in this study and the results obtained was similar to the results from Yu *et al.* (2017), which suggested that these methods do not work well in moderate to low TOC shales – as occurs in the Canning Basin*.*

In this study, an artificial intelligence machine learning approach has been used to overcome some of the aforementioned limitations through pattern recognition. An Artificial Neural Network was used to generate continuous geochemical logs, which relies on the distinct response of logging tools to disseminated organic matter in sediments. In consequence, well logs with more direct relationships with geochemical data have been used to generate the input to train the network model.

51

The density logs, for example, have an inverse linear relationship with TOC as shown in Figure 2.14c. This is attributed to the low density of organic matter relative to other solid components in the rock, given a similar degree of matrix compaction, fluid density and water saturation (Kamali and Allah Mirshady, 2004). Gamma-ray logs, on the other hand, have a linear positive relationship with TOC as a result of the uranium enrichment in organic matter (Huang and Williamson, 1996). The correlation between sonic logs and resistivity logs with TOC, however, is not a direct one. Thermal maturity of sediments affects resistivity more than the organic richness for sediments with low to moderate TOC (Kamali and Allah Mirshady, 2004), while the sonic log is a function of lithology, porosity and fluid content. Passey *et al.* (1990) combined gamma-ray and sonic log combinations to provide a parameter that linearly relates to the organic richness in sediments.

The accuracy of the network was tested visually by overlay of the laboratory measured data on the network generated logs as well as cross plots of the data. In this study, the best fit is observed on the TOC and S_2 logs. The S_1 represents the free thermally extractible hydrocarbon that vaporize at temperatures of approximately 300°C (Espitalie *et al.*, 1977). Heavier free hydrocarbons that vaporize at higher temperatures are included in the S_2 peak, thereby, affecting the reliance solely on the S_1 values to estimate free hydrocarbons. Commonly, further detailed geochemical tests are required on extracted samples to determine the total extractable hydrocarbon content in a sample (Clementz *et al.*, 1979). Nonetheless, in the example well, only a few laboratory measured S1 data points fall short of the neural network predicted logs.

The geochemical property model shows the potential geochemical sweet spots. The kerogen type distribution (HI), organic content (TOC), higher free oil yield (S_1) and source potential (S_2) are higher in the central to south-eastern part of the sub-basin and relatively lower values occur in the north-western part of the sub-basin. This may result from better organic matter accumulation and

preservation in more restricted, shallow marine lagoonal parts of the basin or in deeper starved areas where *G. prisca* can accumulate preferentially.

The north-western parts of the basin represent marginal marine and shallow marine depositional environments where clastic input and bioturbation are higher meaning *G. prisca* is unlikely to accumulate. The organic matter in these areas is more likely to be oxidised and degraded. The influence of significant land plants can be discounted in the Ordovician shales, although recent studies such as Rubinstein *et al.* (2010); Spaak *et al.* (2017) have identified the possibility of some land plant input in global Ordovician sediments. Hence, the predominance of gas-prone kerogen (HI >250 mg HC/g TOC) in the north-western part of the study area can be attributed mostly to the depositional environment, possibly enhanced by localized oxidation of some of the organic matter present, which would increase bacterial degradation of the organic matter in the sediment. Bohacs *et al.* (2005) provides further reading on the factors that may influence the organic development and richness of shale units.

The neural network model has produced satisfactory matches to the geochemical proxies. The 3D property model interpolations using kriging techniques and Gaussian Simulation uncertainty analysis has allowed extension of the geochemical data across the Broome Platform in-spite of the sparse number of wells. These new geostatistical techniques are invaluable aids to help geoscientists in underexplored but potentially productive areas of basins such as the Broome Platform and the whole Canning Basin. These machine learning methods should be encouraged during early exploration studies.

CHAPTER 3. Erosion Estimation in the Broome Platform, Canning Basin

3.1   Introduction

A key step in the determination of hydrocarbon prospectivity in a sedimentary basin is accurate estimation of the amount of exhumed sections. This is important in terms of defining the burial history, maturation and hydrocarbon generation potential of source rocks or shale reservoirs. In the conventional realm, this is important in constraining the time of trap formation relative to the time of hydrocarbon expulsion from source rocks, while in unconventional reservoirs, deep burial and subsequent exhumation stops the kerogen reactions in the shales reservoir and brings the thermally mature source rocks closer to the surface.

The Canning Basin has undergone at least three major events of uplift and erosion during its geologic history. Triche and Bahar (2013) as well as Kuuskraa *et al.* (2013) suggested that this basin holds the largest amounts of unconventional shale gas resource in Australia, although, information from the Ordovician shales from this basin is limited. Carlsen and Ghori (2005) suggested that the Canning Basin is one of the least explored Palaeozoic systems in the world, and a detailed understanding of some of the systems has been a long-standing issue due to limited outcrop exposure (Eyles *et al.*, 2001). A major exploration risk in the Canning Basin that is also associated with global Palaeozoic systems (e.g., the North Caspian Basin, Kazakhstan; the Alberta Basin, Canada; and the Shetland Basin, UK) is the timing of hydrocarbon charge and subsequent preservation within the complex stratigraphic and tectonic history (Ghori and Haines, 2006).

Despite the significance of exhumation estimation for conventional and unconventional hydrocarbon recovery, there is very limited literature that discusses this in detail for the Canning Basin. However, Duddy *et al.* (2006) presented a report using Apatite Fission Track Analysis (AFTA) to quantify the

amounts of the removed sections from the Triassic-Jurassic and Eocene-Present day erosions respectively. This method works by providing information on the maximum paleotemperatures and subsequent cooling that sediments have been exposed to over geologic time, using information that is stored in the Apatite grains. While this method is valid and in general use in the industry, it is often desirable to obtain exhumation magnitudes from log data irrespective of burial temperatures, given the susceptibility of thermal methods of estimation to occasional transient heating and anomalously hot hydrothermal fluids from igneous events in a basin. Although, pervasive igneous intrusives haven't been reported in the Canning Basin, it is always a good approach to utilize a number of independent, yet complementary approaches to constrain the thickness of exhumed sections in sedimentary basins (Corcoran and Doré, 2005). Furthermore, the exposure of poorly age constrained old formations to high temperatures as a result of deep burial, leads to total annealing of the Apatite Fission tracks at about 120°C, making use of the results difficult for accurate estimation of paleotemperature and exhumation.

The aim of this chapter is to document exhumation magnitudes from the Broome Platform of the Canning Basin, based on the irreversible effect of burial on the physical properties of shales. This effect can be estimated from the sonic logs by plotting the sonic transit time of compacted shales against depth. Sonic logs are usually acquired for formation evaluation and seismic well tie which makes them available in most drilled wells. The log typically measures the present-day transit time, which is a measure of lithology and the total compaction the sedimentary succession has been exposed to from burial and tectonic uplift. This approach provides a complementary estimate of exhumation in the Canning Basin, as well as an improved spread of data across the sub-basin relative to the more restricted AFTA data.

Four wells in the Broome Platform were studied and the results from these wells were applied to other wells within the sub-basin.

This method was first proposed by Athy (1930), and has been applied to several global basins and has proved to be effective in the study areas. Jankowsky (1962); Magara (1976) used the shale compaction trends to document exhumation estimates for the north-western German Basin and the southwestern part of Western Canada Basin respectively.

The exhumation values obtained from this study are compared with exhumation values obtained from the thermal history dependent approach (R_o and AFTA) in order to validate or accurately constrain the obtained values.

3.2   Previous work from Apatite Fission Track Analysis

Duddy *et al.* (2006) analysed some Canning Basin wells for qualitative thermal histories, including the timing of thermal episodes from Apatite Fission Track Analysis (AFTA) and Vitrinite Reflectance (R_o %). That study concluded the following:

1   Present day geothermal gradients supplied from the Canning Basin wells Bottom Hole Temperatures (BHT) are too high. Generally, these BHT's were obtained from log headers, where they have been corrected using a simplified correction procedure. These were further corrected using AFTA steady state geothermal gradient.

2   AFTA and R_o data showed that pre-Jurassic sequences cooled from maximum paleo-temperatures in the Triassic, resulting in cessation of active source rock maturation in these pre-Jurassic sequences.

3   AFTA and R_o data demonstrate two regional heating and cooling episodes in the Cretaceous and Tertiary.

4   The geothermal gradient in the basin has been consistent with the present-day heat flow with no sign of elevated basal heat flow during the exhumation periods. This suggests that heating in each event was as a result of sediment loading, with associated cooling during uplift and erosion.

Duddy *et al.* (2006) estimated the removed sections in the Acacia 1 and 2 wells were approximately 1300 and 2000 metres in the Triassic and Eocene sediments respectively (Table 3.1). However, their study indicated significant variability at varying confidence limits for the magnitude of exhumation.

Table 3.1 Removed section estimates from the Acacia 1 and 2 wells, Canning Basin (Duddy et al., 2006).

	Estimates of removed section (m)	
	Triassic-Jurassic (230-170 Ma)	L. Eocene - Present Day (40-0) Ma
Maximum Likelihood Estimate	1300	1950
Lower and upper 95% confidence limits	800-2800	400->10000
Fixed paleo-geothermal gradients		
5°C/km	*not allowed*	>10000
10°C/km	*not allowed*	3050-4950
15°C/km	*not allowed*	1800-3300
20°C/km	*not allowed*	1200-2300
25°C/km	2650-2950	900-1800
30°C/km	2000-2300	700-1300
33.9°C/km -Present Day	1900±200	800±200
40°C/km	1300-1700	450-650
50°C/km	950-1250	*not allowed*
60°C/km	750-85	*not allowed*
65°C/km	*not allowed*	*not allowed*

3.3   Estimation of the amount of erosion

3.3.1   Compaction Trends from Sonic logs

Burial of sediments leads to compaction and a reduction in sedimentary volume or thickness. This results from a reduction in porosity with burial resulting from increasing effective stress. Sonic logs can be used as a proxy for compaction because sonic interval travel time depends on porosity (Hillis *et al.*, 1994). The sonic log curve inherently records the different stages of uplift and erosion for the basin's stratigraphic record.

Quantifying the amount of exhumation with sonic logs was carried out in three steps:

1   Defining a representative standard or normal compaction curve (NCT): The normal compaction curve defines the sedimentary succession in a basin at its maximum burial depth (Tassone, 2014). Magara (1976) defined the surface transit time for shales at zero depth (ΔT_o) as 200μs/ft. in a partially exhumed basin, and suggested that ΔT_o values for most basins will not exceed 210μs/ft. There is generally a decrease in porosity as well as sonic transit time with depth (Fig. 3.1). In this study, the scheme of Jankowsky (1962) and Magara (1976) was modified to obtain a standard "super-curve", by fitting a polynomial function of the sonic transit time with depth.

2   The reduction in porosity results from normal mechanical and thermochemical compaction (Japsen *et al.*, 2007). The sonic data is filtered to include only shales using the gamma ray log with a cut-off value of 130API. Data from studied wells are then compared with the standard compaction curve by plotting the filtered sonic transit data against this curve. The observed vertical displacement of the present day sonic transit time values from the standard compaction curve is measured and represents an estimate of the average exhumation thickness for a particular horizon (Ware and Turner, 2002). This is represented by the equation 3.1 below (Tassone, 2014):

$$E_T = B_{max} - B_{present\text{-}day} \tag{3.1}$$

Where

- E_T is thickness of eroded section,
- B_{max} is maximum burial depth from the compaction curve, and
- $B_{present\text{-}day}$ is the mean present day burial depth.
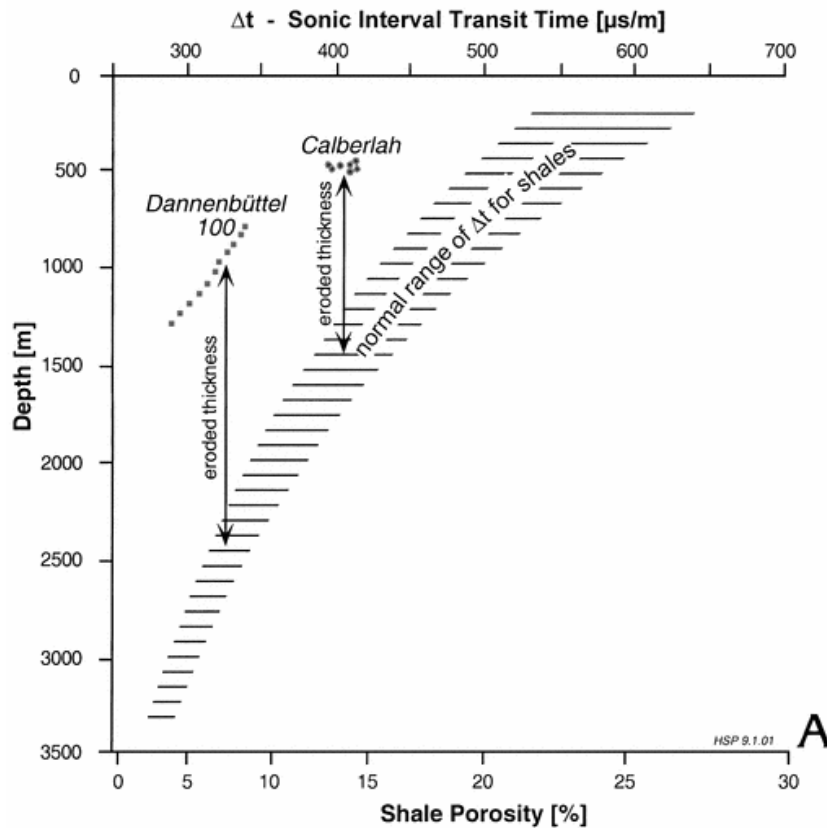
Figure 3.1 Standard compaction curve (Jankowsky, 1962).

The resultant shale interval is the representative shale at the maximum burial depth for a specific stratigraphic unit. As shown in Figure 3.1, the shale porosity-depth curves are plotted with the normal compaction curve, and the difference in depth between the well curve and the normal compaction curve represents the amount of uplift. In this study, the relative timing of exhumation was also obtained by comparing the present-day depths of the extrapolated shales with the formation tops and biostratigraphic data from each well.

Poelchau (2001) summarised some of the several assumptions associated with the sonic compaction method of exhumation this method of exhumation estimation.

3.3.2 Extrapolation from Vitrinite reflectance trends

Vitrinite reflectance (R_o) data were obtained from the WAPIMS database and from converted Rock Eval – T_{max} data. The R_o values were plotted against depth, and the offset from the normal trend was measured as the amount of exhumation using a simple approximation method after (Dow, 1977).

3.4 Results

3.4.1 Compaction Trends from Sonic logs

A normal compaction trend (NCT) was defined following the method proposed by Jankowsky (1962) and Magara (1976). The plot of sonic transit time (ΔT) against depth for each well was obtained and is shown for Hilltop-1 well, with the present-day sonic transit time superimposed on the NCT (Fig. 3.2). Utilizing equation 3.1, mean offset values (to the NCT curve) of 1600m and 1400m of exhumation in both the Carboniferous-Permian unconformity and the Jurassic-Cretaceous unconformity for the Hilltop 1 well. This value, when compared to other values within the basin is similar to the values reported from the AFTA analysis for the "Triassic-Jurassic" event. However, this has not accounted for the missing section at the Eocene unconformity as reported in Duddy *et al.* (2006). Also, the Carboniferous-Permian erosional event was not reported in the Geotrack report (Duddy *et al.*, 2006), possibly because of the exposure the older formations to higher temperatures thereby, leading to completely annealed fission tracks**.**
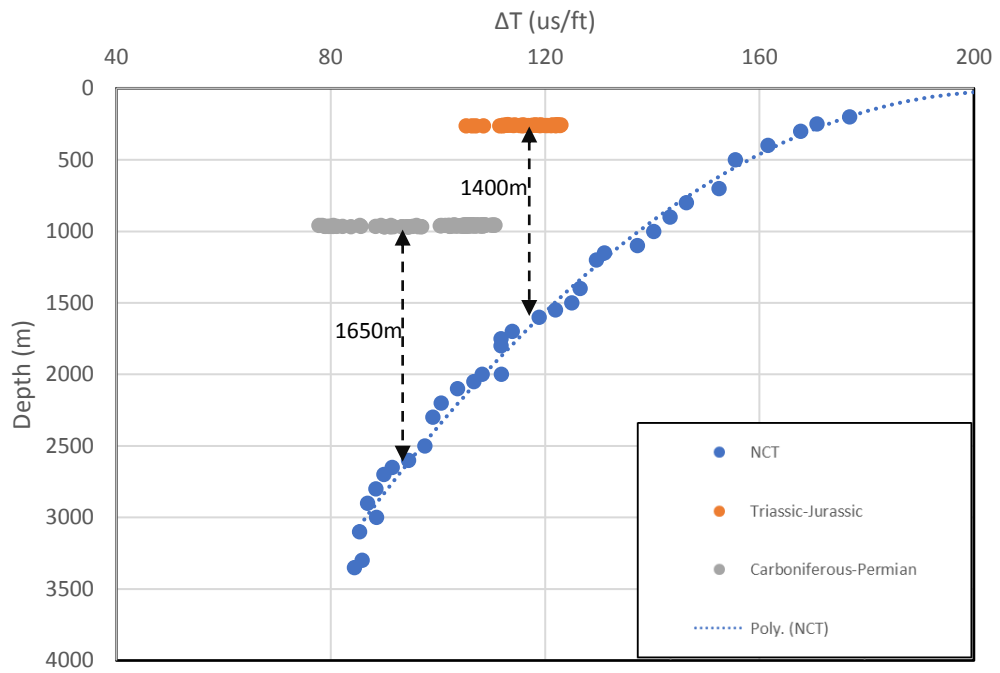
Figure 3.2 Interpolation of the sonic data from Hilltop 1 well on the normal compaction curve.

The method was repeated for three (3) other wells along a northeast-southwest transect and the results are shown in Table 3.2

Table 3.2 Erosion estimation from 4 (four) Broome Platform wells, Canning Basin.

Well Name	Sections	
	Triassic-Jurassic	Permian-Carboniferous
Hilltop 1	400-2100 (1600)	500-2000 (1400)
Aquila 1	800-1900 (1400)	500-2200 (1300)
McLarty 1	200-1200 (800)	1000-2000 (1700)
Kunzea 1	400-800 (500)	200-1800 (900)

3.4.2 Extrapolation from Vitrinite reflectance trends

The plot of Vitrinite reflectance (R_o), (and its equivalent) against depth shows a consistent increase with depth from Recent to Permian deposits. A pronounced break in the reflectance gradient occurs below the Permian into the Ordovician sediments, with a much higher reflectance gradient occurring in the Ordovician sediments. However, there is no higher plant organic matter in the Ordovician samples which rely mainly on Graptolite reflectance, which probably has a different depth – reflectance paragenesis than does Vitrinite reflectance. The samples also contain abundant telaginite (*G. prisca*) and the sediments at low ranks probably contained a groundmass of lamalginite. The deepest samples are also reported to contain minor pyrobitumen (Hilltop 1 well completion report). Hence, the sharp increase in R_o between the Permian Grant Formation and the Ordovician Goldwyer Formation may in part result from uplift, in part from maceral type variation and in part from exposure to unusually high heating that may be from local intrusives (Fig. 3.3).
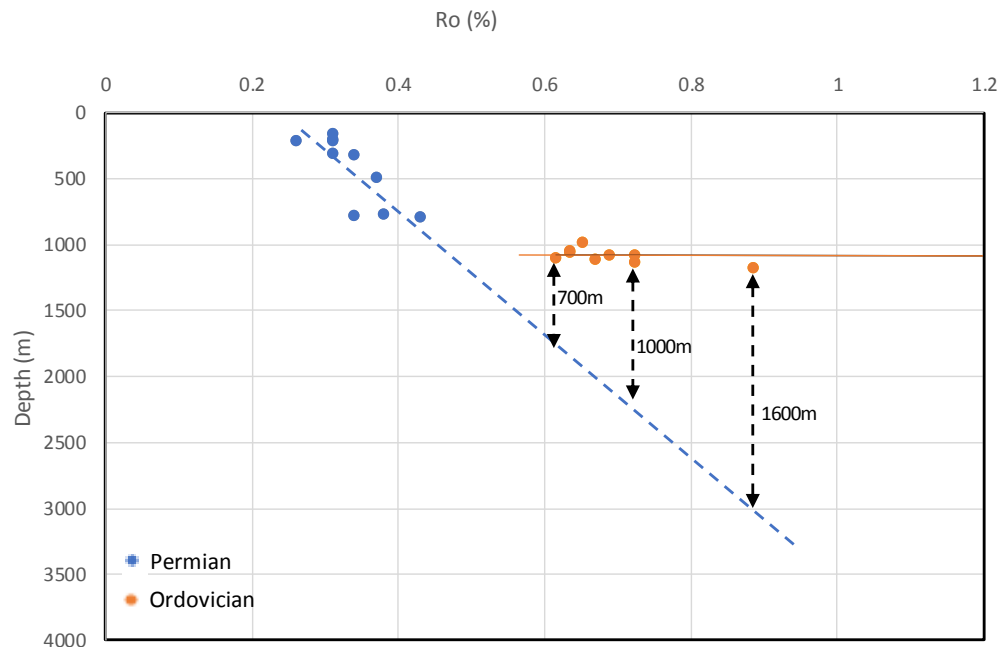
Figure 3.3 Vitrinite reflectance vs depth plot for Hilltop 1 well, showing a discontinuity in the maturation profile of the sediment, suggestive of an uplift.

3.5   The new approach

In order to establish an empirical relationship between the magnitude of erosion and ΔT with respect to present day depths for compacted shales within the Canning Basin, several ΔT and observed displacement values were computed (Appendix V) and used to derive a multi-variate regression equation, which is as follows:

Thickness of eroded section (TES) = 5417 - 32.86ΔT - 0.844depth;   (3.2)

Correlation coefficient R= 0.86.

where ΔT is sonic transit time for shale, and *depth* is the corresponding depth for the shale interval.

The equation has the form of a general multivariate regression equation:

$$Y = \beta_0 + \beta_1 X_1 + \beta_2 X_2 + ... \beta_n X_n + \varepsilon \qquad (3.3)$$

Where:

> TES = y= the dependent variable
> 5417 = β_0 = intercept
> (-) 32.86 = β_1 = regression model coefficient
> (-) 0.844 = β_2 = regression model coefficient
> ΔT = X_1= an independent variable
> Depth = X_2= an independent variable
> ε = Error Term

This equation was tested on several intervals across the basin (Table 3.3) as well as the Triassic – Jurassic exhumation values as reported by Duddy *et al.* (2006) on the Acacia 1 well in the Barbwire Terrace (Fig 3.4). The observed TES agrees with the measured data from AFTA studies (Table 3.1) and have a good correlation with the calculated exhumation values, using equation 3.2. Also, further validation is carried out on the studied data as well as data across the basin (Table 3.3). However, in the deeper parts of the basin, where the compaction curve/porosity approaches zero, estimation of exhumed sections in that section has a shallow slope and projection of the sonic data on the normal

compaction curve would yield a high, inaccurate erosion estimate. Therefore, in those areas, equation 3.2 can be used to calculate the thickness of exhumed sections (Table 3.3).
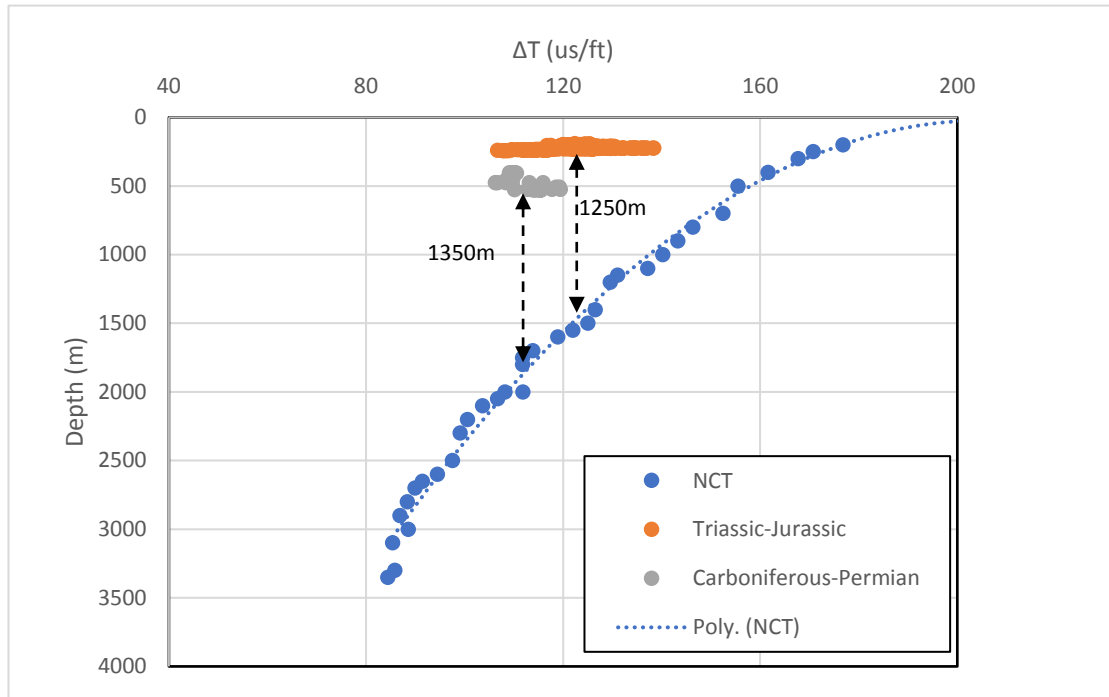
Figure 3.4 A plot showing TES for the Acacia#1. This further validates the equation; at 250m depth for the Triassic-Jurassic sediments, and ΔT of 120 μs/ft.

Calculated TES in this case is 1262m, while the observed displacement value is 1250m. AFTA reports also indicate a value of 1300m.

The dataset in Table 3.3 demonstrates that Net Exhumation shows a good relationship to Depth and ΔT. Net Exhumation can be modelled using Equation 3.2, which has a significant fit to the data (p-value of < 0.05) with calculated erosion values within ±200m of the observed TES.

Table 3.3 Data from different intervals showing the sonic transit time (ΔT) and the corresponding depth, the visual observed displacement (Jankowsky, 1972), and the calculated displacement using equation 3.2.

Well Name	Depth (m)	ΔT (ms/ft)	Observed TES (m)	Calculated TES (m)
Acacia 1	230	120	1250	1279.68
Acacia 1	529	114	1350	1224.48
Hilltop 1	1150	90	1650	1489.00
Edgar Range 1	268	120	1250	1247.60
Edgar Range 1	321	112	1400	1465.75
Edgar Range 1	774	107	1226	1247.72
Kunzea 1	250	125	1150	1098.50
Musca 1	754	107	1050	1264.60
Santalum 1	800	95	1600	1620.10
Sharon Ann 1	479	145	350	248.00

Equation 3.2 has been used to calculate erosion estimates from 4 additional Broome Platform wells (Table 3.4) which can be used for better burial history and maturation modelling. The magnitude of erosion from well to well across the sub-basin is represented in the contour maps shown in Fig 3.5 a,b which indicate general trends that can be integrated with seismic maps to better understand the Broome Platform structural history.

Table 3.4 Estimation of Erosion from 8 Broome Platform wells.

Well Name	Sections	
	Jurassic-Cretaceous	Carboniferous-Permian
Hilltop 1	400-2100 (1600)	500-2000 (1400)
Aquila 1	800-1900 (1400)	500-2200 (1300)
McLarty 1	200-1200 (800)	1000-2000 (1700)
Kunzea 1	400-800 (500)	200-1800 (900)
Musca 1	600-2000 (1200)	300-1500 (1200)
Matches Springs 1	400-1300 (1000)	300-900 (600)
Santalum 1	900-2000 (1800)	*No Records*
Edgar Range 1	300-2100 (1000)	200-1700 (1400)
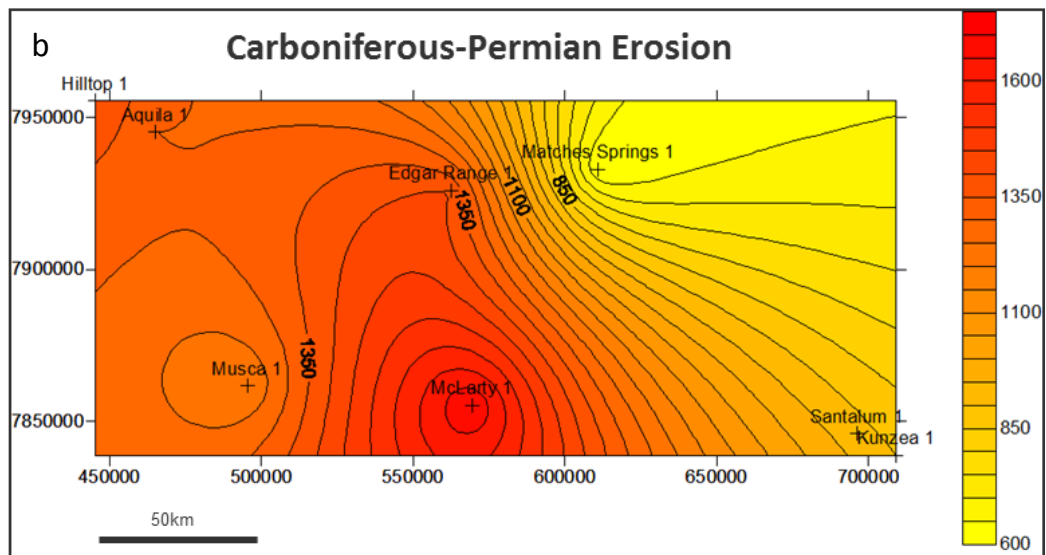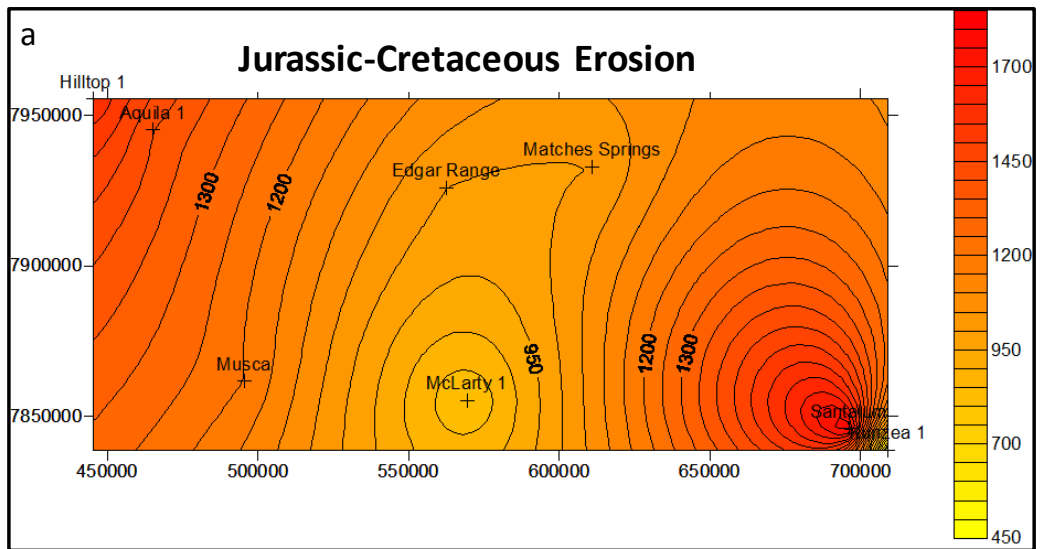
Figure 3.5 Contour maps showing the magnitudes of erosion from the northwest to the south eastern parts of the Broome Platform in the (a) Triassic-Jurassic Period; and (b) Carboniferous-Permian Period. Data from 8 wells.

3.6   Discussion and Conclusion

In sedimentary basins, accurate delineation of the thickness of the exhumed sections is important to establish the basin's subsidence history. This directly impacts the maximum temperatures that a formation has been exposed to over geologic time, and this could have both positive and negative impacts on organic matter maturation, trap timing and formation, and ultimately hydrocarbon prospectivity in the basin.

Several methods have been proposed to estimate thickness of eroded sections in sedimentary basins, and each have their own limitations. While AFTA and vitrinite reflectance methods are routinely used in exploration, the estimated erosion thickness may be inaccurate (Burns *et al.*, 2005). These methods may require assumed values for the basins geothermal gradient and thermal conductivities. This is more significant in basins that have been affected by heating related to fluid flow or volcanic activities. Therefore, a major advantage of the compaction-based method for exhumation estimation is that the estimates are somewhat independent of the basin's thermal history. Also, sonic logs are routinely acquired during drilling, hence sonic logs are available for most wells relative to AFTA and R_o data, without requiring further time or expense.

The exhumation values reported from AFTA (e.g. Duddy *et al.* (2006)) include a range of uncertainty, while calculation of exhumation values from the new approach gives a good approximation. The main limitation to use of organic matter reflectance is the difficulty of applying those techniques for pre-Carboniferous rocks, before the common occurrence of vascular plants, as is the case in the Ordovician Goldwyer Formation.

However, a limitation to the compaction-based method for estimation of exhumation is that the absolute timing of the erosional or cooling event cannot be independently constrained (Tassone, 2014). Also, variation in rock composition can make it difficult to differentiate radiogenic sands from shales.

Since all these methods are commonly prone to significant uncertainties, a combination of different approaches is usually recommended, to accurately constrain the thickness of exhumed sections (Corcoran and Doré, 2005; Tassone *et al.*, 2014).

This study has considered both compaction-based estimates and thermal based estimation of exhumed sections. Gamma ray logs, sonic transit time logs, formation tops and biostratigraphic data have been used for this purpose. The results demonstrate that a good estimate of exhumation can be obtained from the

displacement of a sonic-depth trend in a well from the normal compaction trend. This procedure was repeated for several wells in the Broome Platform, Canning Basin.

Sonic logs are preferred to other porosity logs because they display relatively simple normal compaction trends (Poelchau, 2001; Tassone, 2014). The new derived equation forms an empirical relationship between shale ΔT values, depth and the magnitude of erosion. This equation appears to have a good agreement with both the measured AFTA data and the observed exhumation from several wells in the Canning Basin.

In the studied basin, exhumation data from 8 wells are computed and contoured. These contours show that exhumation has been relatively uneven across the sub-basin and has varied from episode to episode. The results suggest that the western area has undergone substantial uplift and erosion in each tectonic episode. In contrast, the central part of the Broome Platform underwent substantial exhumation in the Carboniferous-Permian Period but much less in the Jurassic-Cretaceous and Tertiary Periods. Uplift and erosion was less intense in the south-east towards the Kidson sub-basin in the Carboniferous-Permian and Tertiary but was substantial in the Jurassic-Cretaceous Period.

CHAPTER 4. Hydrocarbon generation kinetics in the Goldwyer shales

4.1   Introduction

In hydrocarbon exploration, there is an acute need to evaluate the type of petroleum that can be generated from the organic rich rocks. Basic analytical methods such as the Rock Eval pyrolysis (Chapter 2) provide a rapid screening assessment of the quality and thermal maturity of the kerogen within a rock matrix. Other techniques such as optical microscopy have also been routinely used to identify maceral composition and their state of preservation, which in turn can be used to determine the level of maturity by the Spore Colour Index (SCI) or vitrinite reflectance (Ro %), and to predict the hydrocarbon type likely to be generated at peak maturity (Peters and Cassa, 1994).

Structurally, kerogen is known to be a cross-linked macromolecular system with a highly complex structure that undergoes progressive physico-chemical changes with increasing thermal maturation (Behar and Vandenbroucke, 1987) and this governs the amount and composition of hydrocarbon that can be generated from an organic rich interval. Therefore, authors such as Larter (1984), Behar and Vandenbroucke (1987); Horsfield (1989) amongst others, directed efforts towards understanding the molecular composition of kerogens and monitoring its behaviour under thermal stress.

A common approach used to evaluate the molecular composition and kerogen degradation in rocks is the kinetic approach, using combined pyrolysis-gas chromatography (Py-GC). This, simply put, involves further analysis of the S_2 effluent, to separate the S_2 yield into individual components (Pepper and Corvi, 1995).

Jones (1987) introduced the concept of organic facies for predicted petroleum type generation, while Horsfield (1989); Horsfield (1997); Di Primio and Horsfield (2006) proposed the characterisation of organic facies with the

generated portions of the hydrocarbon classes with or without the presence of sulphur in the sediments. These authors defined a ternary diagram in terms of the n-alkyl chain length distributions from the Py-GC pyrograms, showing petroleum-type organofacies. This ternary diagram is defined in terms of the total resolved C_{1-5} hydrocarbons, the sum of the n-alkenes/n-alkanes in the C_{6-14} range, and the sum of the n-alkenes/n-alkanes in the C_{15+} range (Fig. 4.1)
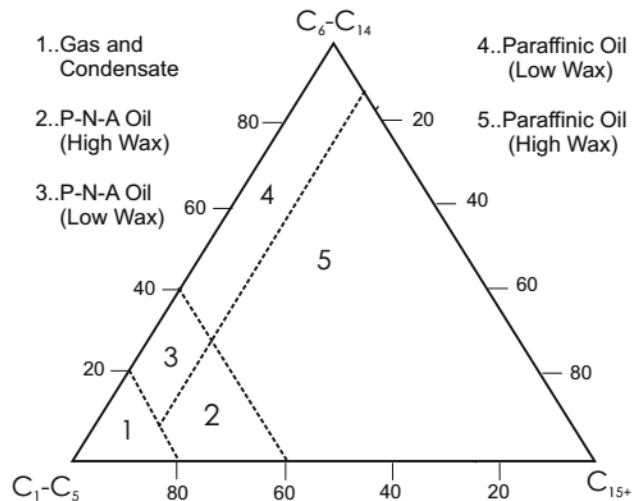
Figure 4.1 Characterization of kerogen by the generated petroleum type: Five organic facies are defined according to the generative potential for three HC classes (C1 – C5, C6 – C14, C15+) (Horsfield, 1997).

In kerogen degradation, it is assumed that a certain number of parallel reactions take place for the conversion of educt (kerogen) to product (petroleum) (Schenk *et al.*, 1997), which is characterised by a reaction order and a rate constant. These reactions are usually temperature dependent and slight variations in temperature will usually yield considerable differences in the rate of the chemical reaction. To quantify this temperature dependence, the Arrhenious theory of thermodynamic equilibrum is employed, which depends on the concept of overcoming an activation energy for products to be formed during a chemical reaction.

The Py-GC configuration allows accurate temperature measurements, which are required to establish valid Arrhenius parameters (Braun *et al.*, 1991). In kerogen

kinetics, the Arrhenius parameters are largely dependent on the kerogen type, heating rates and time. The equation, (Hart *et al.*, 2011; Pepper and Corvi, 1995; Waples and Nowaczewski, 2014; Peters *et al.*, 2015) (equation 4.1) is given as

$$k = A\exp(-Ea/RT) \tag{4.1}$$

where

- k: rate constant (of hydrocarbon generation)
- A: The (collision) frequency factor, which is temperature and reactant property (kerogen) dependent
- E_a: The activation energy, that is – the threshold energy that the reactant(s) must attain before reaching the transition state. (kJ/mol), also temperature and reactant property dependent
- R: The universal gas constant (8.314 J/mol K)
- T: The absolute temperature at which the reaction takes place (in Kelvin (K)).

Detailed discussions of kinetics of kerogen degradation, petroleum generation and the influence of time, temperature, and precursor materials can be found in Behar and Vandenbroucke (1987), Schenk *et al.* (1997), Horsfield (1997), Dieckmann *et al.* (1998), Di Primio and Horsfield (2006), Hantschel and Kauerauf (2009), Welte *et al.* (2012), Waples and Nowaczewski (2014).

In petroleum systems and basin analysis, hydrocarbon generation is most sensitive to temperature, therefore, the degree of accuracy of any prediction of the timing and volumes of petroleum hydrocarbon generation is largely dependent on the accuracy of the thermal history model (Welte and Yalchin, 1987; Poelchau et al., 1997; Yalchin et al., 1997). The petroleum type organofacies and kinetic properties of organic rich intervals is also of crucial importance (Horsfield, 1989; Tegelaar and Noble, 1994) in hydrocarbon generation for both conventional and unconventional systems. This allows adequate quantification and description of the potential of any hydrocarbon

bearing interval, as it takes the molecular composition and thermal stability of the organic matter into account. Although, there is a relationship between Rock Eval (kerogen type and thermal maturity) data and bulk kinetic character, organic facies, heterogeneity, sulphur contents, and thermal stability can lead to variation in hydrocarbon generation rates. Yalcin *et al.* (1997) discussed the concept of heat transfer in sedimentary basins and the importance of kinetic character of sediments in hydrocarbon generation.

Default kinetics in commercially available software packages (e.g. Trinity, PetroMod™) are based on published sets of kinetic parameters defined for specific shale or source rock intervals. Sometimes, the application of these (default) kinetics e.g. Burnham (1989); Pepper and Corvi (1995); Di Primio *et al.* (1998) provide an over-estimation or under-estimation of kerogen stability, as the rate of thermal decomposition of kerogen to petroleum in fact differs for all individual source rocks because they contain different proportions of organic matter types (Smith and Cook, 1980; Waples and Nowaczewski, 2014).

Kinetic data for the Ordovician Goldwyer shales is scarce or non-existent in the literature. This chapter documents the results of bulk kinetic measurements on Ordovician Goldwyer shale samples from wells in the north-western part of the Canning Basin (Fig. 1.1) to assess the type of geochemical organofacies more accurately. The kinetic data have a direct impact on the temperature for the onset (10%TR) and peak (T_{peak}) of petroleum generation in the Goldwyer Formation. The samples were mainly taken from the Goldwyer III and two from the Goldwyer I shale unit (Section 1.3).

4.2   Materials and Methods

4.2.1   Sample set

Core and chip samples for this Formation were collected from the Western Australia Department of Mines core repository and subjected to geochemical analyses.

More than eighty samples were analysed for Rock Eval pyrolysis (Chapter 2, Appendix I). Based on the Rock Eval character, thirteen (13) samples from the Theia 1, Cyrene 1, McLarty 1, and Solanum 1 wells were subjected to pyrolysis-Gas Chromatography experiments in order to assess their kerogen composition. In addition, a kerogen sample for the Santalum 1 well was made available from Geoscience Australia (GA) (Table 4.1).

The samples from Theia 1, Cyrene 1, and McLarty 1 wells are from the Goldwyer III shale unit while samples from Santalum 1 and Solanum 1 wells are from the Goldwyer I unit.

4.2.2 Experimental Methods

4.2.2.1 Rock Eval Pyrolysis

The Rock Eval pyrolysis was carried out using the Vinci Rock Eval 6 equipment. This process involves a two-step-controlled heating of the pulverised sample, i.e., heating in an inert environment of nitrogen followed by combustion in an oxidizing environment. The detailed methodology for this is provided in Chapter 2.

4.2.2.2 Open-System Pyrolysis Gas Chromatography (Py-GC)

Pyrolysis Gas Chromatography (Py-GC) was performed using the Quantum MSSV-2 Thermal Analysis System® interfaced with an Agilent GC-6890A (Horsfield *et al.*, 2014). A HP-Ultra 1 dimethylpolysiloxane capillary column of 50 m length, 0.32 mm internal diameter and 0.52 μm film thickness connected to the Flame Ionization Detector (FID) was employed using helium as carrier gas (Han *et al.*, 2014; Yang *et al.*, 2016). Open-system pyrolysis was performed by loading approximately 10-30 mg of each sample into a small open glass tube and heating it, after isothermally venting off free hydrocarbon compounds for 3 minutes at 300°C, in a flow of helium from 300°C to 600°C at 40°C/min, while the final temperature was maintained for 2 minutes. Generated pyrolysis products were collected in a liquid nitrogen cooled trap and, after 10 minutes, liberated by

removing the cooling agent and heating the trap to 300°C. The GC oven temperature was programmed from 30°C to 320°C at 5°C/min.

Quantification of individual compounds and boiling range splits were conducted by external standardisation with *n*-butane. Prominent hydrocarbon peaks were identified by reference chromatograms and using GC ChemStation© software from Agilent Technologies.

4.2.2.3 Bulk Kinetics

The Source Rock Analyser (SRA-TPH/IR) from Humble Instruments was used for non-isothermal open-system pyrolysis at four different heating rates of 0.7, 2, 5 and 15 K/min (Schaefer *et al.*, 1990) to determine the bulk kinetic parameters. 3-30mg of crushed rock material (depending on the heating rates and the shale/source rock quality) was weighed into small vessels and heated from 250°C to 600°C, with a helium gas flow of 50ml/min. The bulk generated products are detected at the attached FID. The recorded generation rate curves are computed into discrete activation energy distributions with a single variable frequency factor (A) (Burnham *et al.*, 1987) using the Lawrence Livermore National Laboratory KINETICS2015® software. The mathematical routine for the first-order kinetic scheme is based on the Arrhenius law (Schaefer et al., 1990; Pepper and Corvi, 1995; Schenk et al., 1997; Schenk and Dieckmann, 2004).

4.3   Results and Discussion

4.3.1   Shale reservoir quality and petroleum potential

The shale samples used in this study are organic rich, with TOC contents and S_2 values between 1.8 – 6.4 % and 1.7 – 52.9mg/g rock respectively. (Table 4.1). The highest TOC values are recorded for the two Goldwyer I shale samples (S/No. 13-14), with TOC >6% and S2 values > 50mg/g rock suggestive of excellent petroleum potential.

Table 4.1Rock Eval pyrolysis data used for kinetics study. The legend for the studied wells is as follows; S well: Solanum 1, MC well: McLarty 1 well, C well: Cyrene 1 well, T well: Theia 1 well, and So 1 represents the Goldwyer sample from Santalum 1 well, provided by Geoscience Australia (GA).

S/No.		Sample	Depth (m)	S1 - (mg/g)	S2 - (mg/g)	S3 - (mg/g)	TOC (%)	Tmax (°C)	HI (mg/g TOC)	OI mgCO$_2$/g TOC	PI
Goldwyer III Unit											
1	G017691	T18	1473.4	2.12	7.55	0.51	3.2	454	236	16	0.22
2	G017692	T29	1529.9	2.33	5.83	0.49	2.76	448	211	18	0.29
3	G017693	T31	1534.7	2.92	5.57	0.36	3.26	444	171	11	0.34
4	G017694	T22	1506.2	1.78	5.62	0.57	2.6	453	216	22	0.24
5	G017695	T25	1516.58	2.33	5.17	0.59	2.11	445	245	28	0.31
6	G017696	C4	973.9	3.1	12.41	0.16	3.82	442	325	4	0.2
7	G017697	C1	958	2.64	12.78	0.2	3.3	445	387	6	0.17
8	G017698	C5	976.7	1.92	8	0.25	2.74	448	292	9	0.19
9	G017699	C7	994.1	1.47	3.94	0.2	1.86	440	212	11	0.27
10	G017700	MC1	1893.4	2.29	3.02	0.37	3.15	458	96	12	0.43
11	G017701	MC3	2004.1	1.77	1.77	0.5	2.31	461	77	22	0.5
12	G017702	MC4	2002.2	1.45	2.72	0.53	1.94	457	140	27	0.35
Goldwyer I Unit											
13	G017703	S2	315	1.04	50.69	0.35	6.27	450	808	6	0.02
14	G012801K	So 1 (Goldwyer FM from GA)	470.0	0.5	52.9	nd	6.4	433	828	nd	0.01

The TOC values from the selected Goldwyer III shales indicate good to very good organic content (TOC = 1.86 to 3.82 %; S/No. 1-12), with S$_2$ values indicating moderate to good potential to generate hydrocarbons (S$_2$ = 1.77 to 12.78 mg/g; S/No. 1-12).

The thermal maturity of the studied samples derived from the Rock-Eval T$_{max}$ data range between 433 and 460°C, which indicates that the samples are in the early – late mature stages of hydrocarbon generation.

For kerogen typing, hydrogen index (HI) values suggest that the least mature samples from the Goldwyer Sequence I contain Type I (oil-prone) kerogen, and type II and II/III (oil to oil- and gas-prone) kerogen in the case of the Goldwyer III shale unit samples (Fig. 4.2). The HI versus T_{max} plot shows that the samples from the Goldwyer I shale unit are in the early to mid-mature stage of hydrocarbon generation, while the Goldwyer Sequence III samples are in the late -mature stages of hydrocarbon generation (Fig. 4.2).
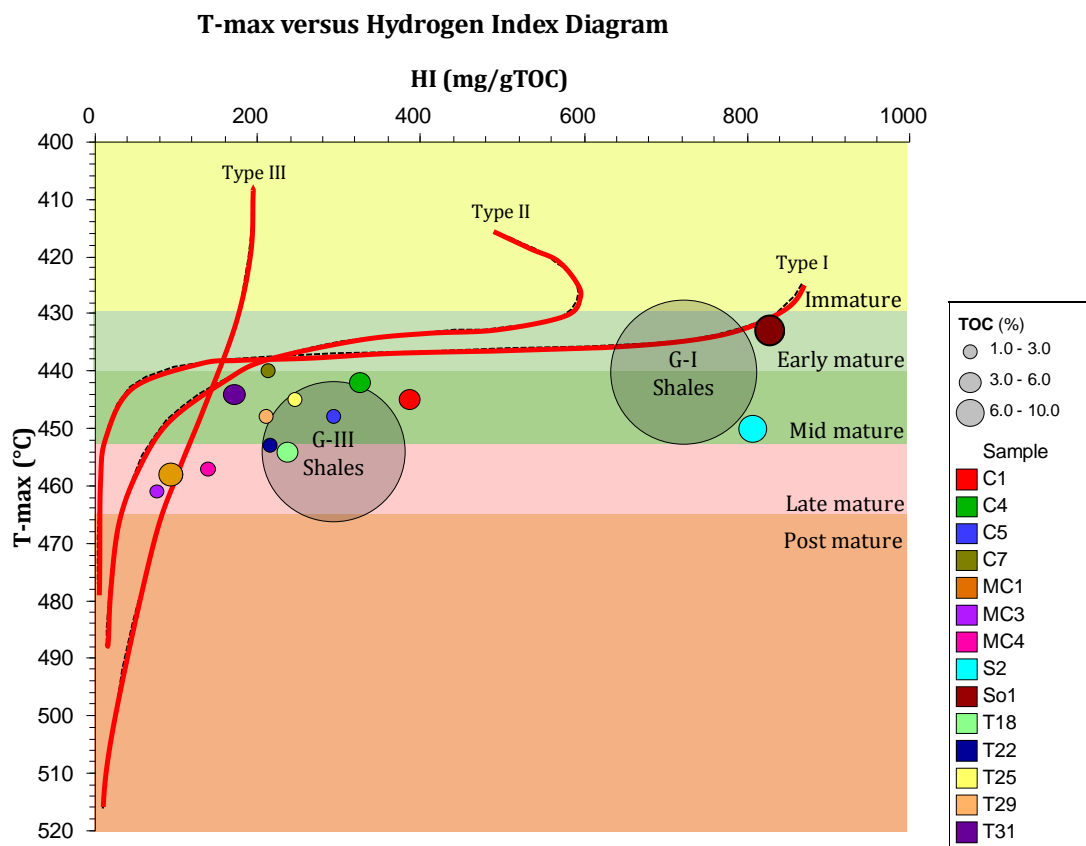
Figure 4.2 Plot of Hydrogen Index versus Tmax showing generalized kerogen type evolution pathways with thermal maturity. G-III = Goldwyer III, G-I = Goldwyer I.

4.3.2 Molecular Composition of Pyrolysates

Pyrolysis-Gas Chromatography (Py-GC) was used to obtain a detailed molecular description of the bulk pyrolysate in order to assess kerogen composition and type of petroleum that can be generated by the source rock during the process of natural maturation.

76

The Py-GC chromatograms of the studied samples are shown in Fig 4.3a for the Goldwyer I shale unit, and for the Goldwyer III shale unit in Fig. 4.3b. The Goldwyer I shale unit pyrogram shows a predominance of the low to intermediate (C_{6-14}) molecular weight straight chain aliphatic hydrocarbons (*n*-alkane/*n*-alkene doublets) with negligible amounts of aromatic compounds (Fig. 4.3a). In contrast, the Goldwyer III shale unit pyrogram is dominated by intermediate to longer chain (C_{15+}) molecular weight aliphatic hydrocarbon besides a significantly higher amount of aromatic compounds (Fig 4.3b). The Goldwyer I unit fingerprint is similar to algal dominated organic matter, deposited in marine settings (Edwards *et al.*, 1997). The homogeneity here (strongly dominated by aliphatic compounds) probably indicates an enrichment of selectively preserved lipid fractions of the micro-organism *G. prisca*, as described by Hoffmann *et al.* (1987) and Spaak et al. (2017), which commonly occurs in Ordovician restricted marine environments. The Py-GC chromatogram of the Goldwyer III unit has a fingerprint that shows toluene being the most abundant of the alkylbenzenes, with trimethylbenzene and alkylnaphthalenes being readily discernible, typically exhibiting higher or similar yields than that of the *n*-alkane/*n*-alkene doublets eluting at similar retention times. The source of the aromatic hydrocarbons within the pyrolysis products is either as aromatic moieties within the kerogen itself or aromatisation products from cross-linked or alicyclic moieties (Hartgers *et al.*, 1994; Muscio and Horsfield, 1996; Behar and Vandenbroucke, 1987). Furthermore, within marine organic matter, aromatic compounds are formed from cyclic structures with only a few condensed nuclei (Behar and Vandenbroucke, 1987). Phenolic compounds are not a major pyrolysis product and are abundant in land-plant-derived organic matter (Horsfield, 1989). Hence, are scarce or absent in the studied samples.
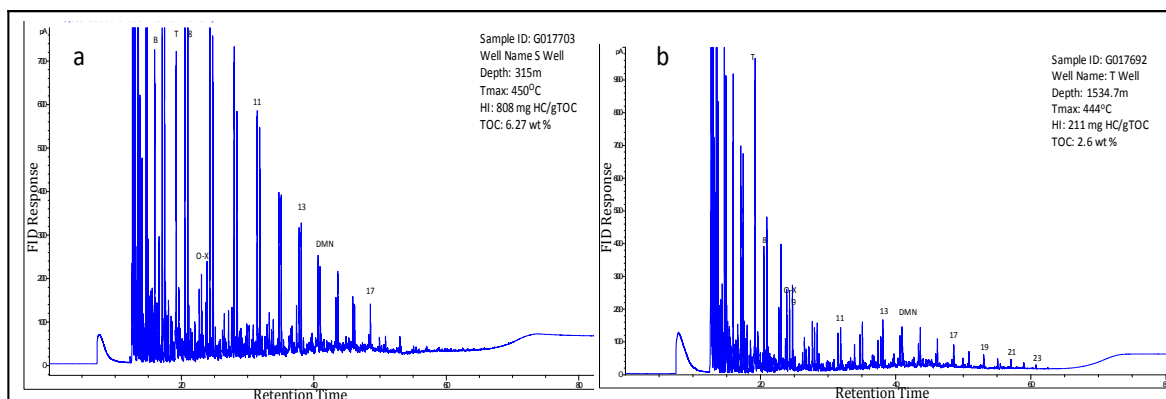
Figure 4.3 Open pyrolysis gas chromatography traces for selected samples from (a) Goldwyer I unit and (b) Goldwyer III unit sampled from Theia 1 well. Numbered peaks represent the number of carbon atoms in the n-alkane/n-alkene doublets. Other peaks labelled include Benzene (B), Toluene (T), Ortho-xylene (O-X) and Dimethylnaphtalene (DMN).

4.3.3 Petroleum type organofacies

A ternary diagram of the n-alkyl chain length distributions derived from the Py-GC experimental results was defined to infer petroleum-type organofacies by Horsfield (1989); Horsfield (1997). Total resolved C_{1-5} hydrocarbons are shown versus the sum of the *n*-alkenes/*n*-alkanes in the C_{6-14} range and the sum of the *n*-alkenes/*n*-alkanes in the C_{15+} range. The studied samples plot in three fields using this approach: the Paraffinic oil low wax, Paraffinic-Naphthenic-Aromatic (P-N-A) low wax, and the Gas and Condensate organofacies (Fig. 4.4).

The Goldwyer I shale unit samples, with low molecular weight - straight chained hydrocarbon predominance, plot in the Paraffinic oil low wax oil organofacies field and, with increasing maturity, on the border of the PNA oil low wax organofacies field. This is in agreement with their previously measured high HI values and are typical for algal (and in this case *G. prisca*-derived) organic matter deposited in an anoxic and restricted marine environment (Spaak *et al.*, 2017). The samples from the Goldwyer III shale unit plot within the P-N-A oil field (low wax), and gradually transition, with increasing maturity, to the gas and condensate field. This is also consistent with their hydrocarbon-generating potential and in good agreement with the reported Type II and Type II/III

kerogen with HI values mostly less than 250 mg/g TOC from the Rock Eval analysis.
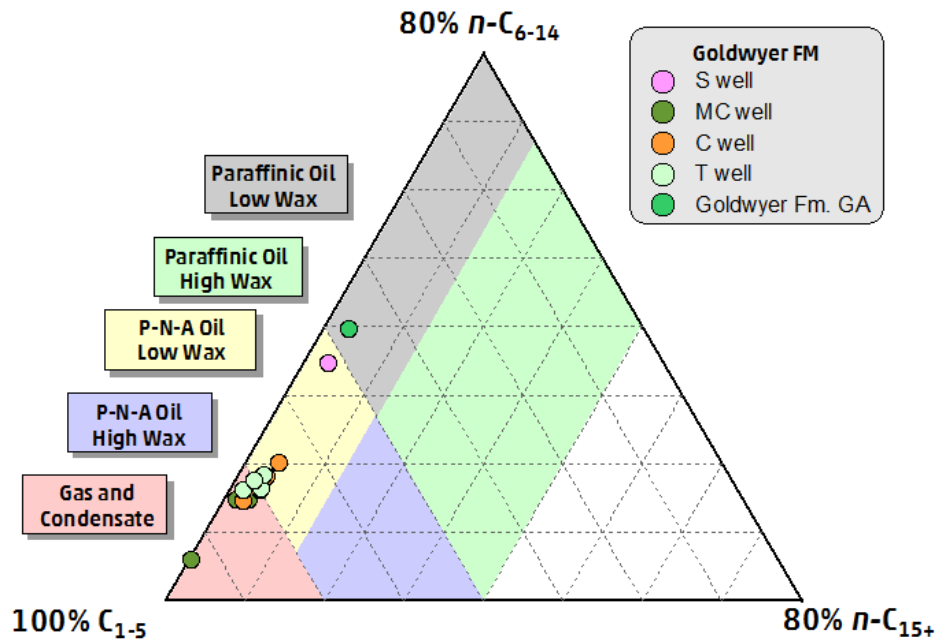
Figure 4.4 Ternary diagram of total C1-5 hydrocarbons, C6-14 n-alkenes plus n-alkanes, and C15+ n-alkenes plus n-alkanes using (Horsfield, 1989) fields, showing the composition of pyrolysates (Py–GC data) for the studied shale intervals.

P–N–A = paraffinic–naphthenic–aromatic. The legend for the studied wells is as follows; S well: Solanum 1, MC well: McLarty 1, C well: Cyrene 1, T well: Theia 1 well, and Goldwyer Fm. GA represents the Goldwyer sample from Santalum 1 well, provided by Geoscience Australia (GA)

Eglinton *et al.* (1990) designed a ternary plot to assess kerogen sulphur-richness by using the relative percentages of three pyrolysate components (2,3-dimethylthiophene, ortho-xylene and *n*-non-1-ene) which represent aliphatic structures, aromatic structures, and organic sulphur within the macromolecular organic matter (Fig. 4.5). The studied samples are sulphur lean and plot between the aliphatic to aromatic fields of the Eglinton *et al.* (1990) ternary plot (Fig. 4.5). The samples from the Goldwyer I unit plot within the aliphatic region, while samples from the Goldwyer III shale plot in the intermediate to the aromatic fields. The samples with higher aromaticities have lower hydrogen index values.
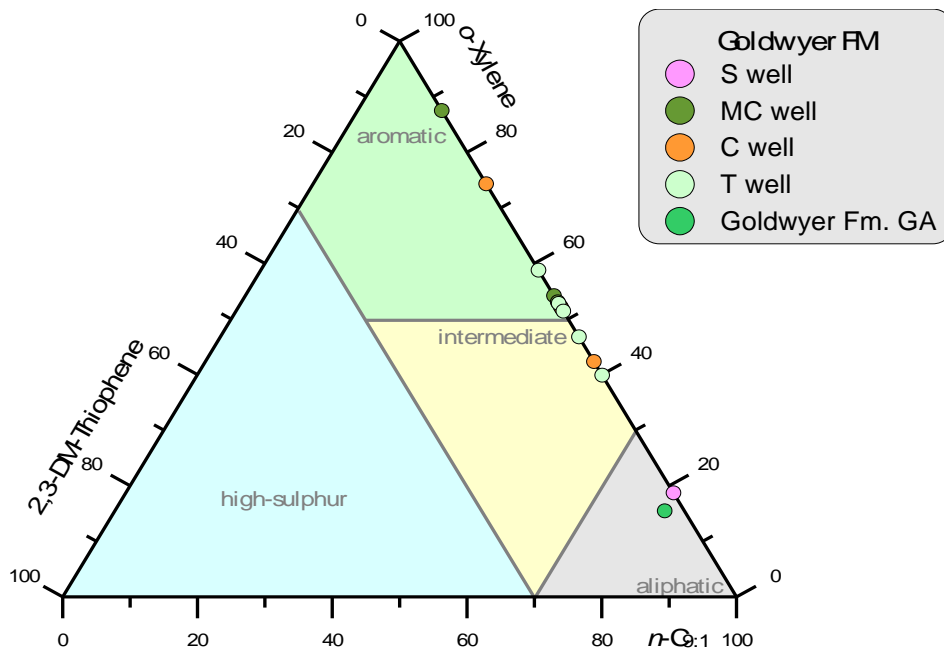
Figure 4.5 The kerogen type characterisation after Eglinton et al. (1990)

Similar to the Eglinton *et al.* (1990) plot, a ternary plot from Larter (1984) is used to assess the kerogen type in terms of relative percentages of its phenolic contents (Fig. 4.6). Low phenol contents for all of the studied Goldwyer samples indicate that they are lean in terrestrial organic matter, although rare land-plant microfossils (cryptospores) have been reported in the upper Goldwyer Formation at Theia 1 well by Spaak et al. (2017).
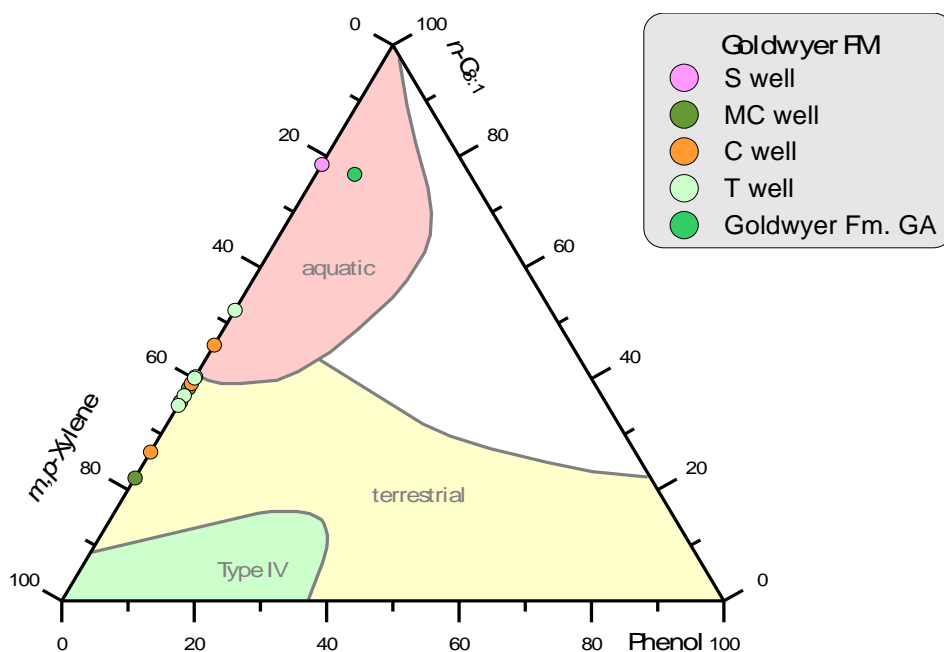
Figure 4.6 Phenol abundance (diagram after Larter, 1984)

4.3.4 Bulk kinetics and activation energy distribution

The sample selection was made to represent different maturities in each of the studied samples and well locations, as well as their potential to generate hydrocarbons. The Goldwyer I and III shale units can be easily distinguished based on their specific activation energy distributions. The Goldwyer I unit samples are characterised by a narrow activation energy (Ea) distribution, with the main activation energy at approximately 56kcal/mol, which accounts for approximately 78-90% of the total bulk reaction (Fig 4.7a and b). The corresponding frequency factor in these samples range between $6.56E^{+14}$ and $8.39E^{+14}$. This distribution is attributed to the limited range of stable chemical bonds, which crack at relatively high thermal stress stages, typical for marine type I alginite-rich shales; or, in this case *G. prisca.* Extrapolating to a geological heating rate of 3°C/Ma (Dieckmann, 2005), the transformation ratio evolution curves reveal the generation kinetics of the Goldwyer I unit samples from Solanum 1 and Santalum 1. The temperature for the onset of hydrocarbon generation (10%TR) and end of generation (90%TR) is 142°C and 169°C, respectively (Fig 4.7c), with the temperature for T_{peak} being ~155°C (Fig 4.7d).

This confirms that upon maturation, hydrocarbon generation in the Goldwyer I unit will take place over a narrow temperature interval of (~25 °C). For the slightly more mature sample from Solanum 1, petroleum generation starts ~5°C later (10%TR at ~146°C) as more labile precursor structures are already lost. Primary kerogen to petroleum conversion is predicted to also end below 170°C indicating presence of a similar kerogen.
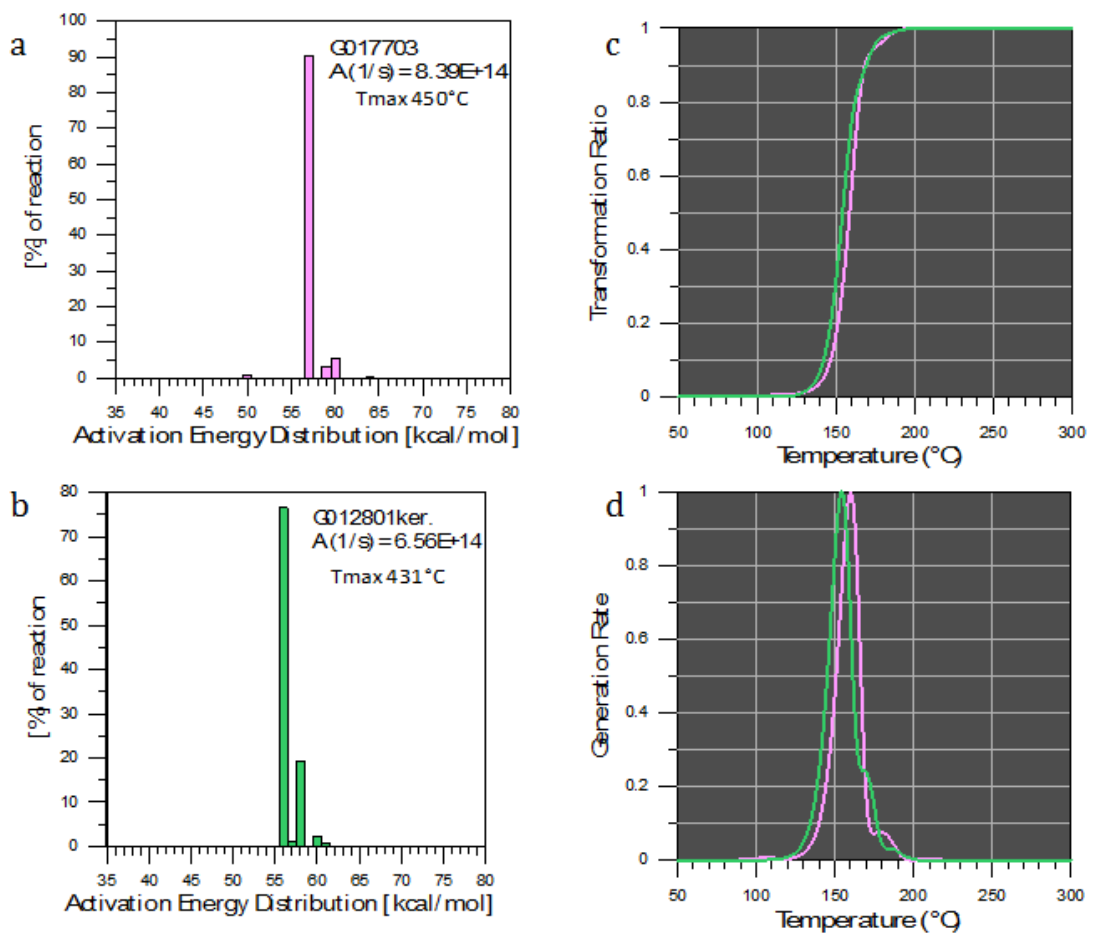
Figure 4.7 a and b. Bulk kinetic parameters in terms of activation energy (Ea) distribution and frequency factors (A) of the studied Goldwyer I unit shales (c) Transformation ratio and (d) generation rate curves for Goldwyer I shales for Santalum 1 and Solanum 1 at a geological heating rate of 3°C/Ma.

In contrast, the Goldwyer III shale samples display broad activation energy distributions (Fig. 4.8 a- d), typical of mixed marine Type II/III kerogen in general (Burnham *et al.*, 1987; Espitalié *et al.*, 1988). The measured Ea for these samples

range from 54 - 63 kcal/mol with associated frequency factors between 4.13E^{+12} in Theia 1 to 5.23E^{+13} in the McLarty 1 wells. The broader activation energy distribution and frequency factors of Goldwyer III unit is shown by the temperatures at which the kerogen conversion takes place assuming a constant heating rate of 3°C/Ma. The organic matter in the Goldwyer III shale unit samples generate hydrocarbons over a broad temperature range of ~50°C, with onset of hydrocarbon generation at >100°C (10%TR) and the end (90%TR) at <160°C (Fig 4.8e). Peak generation temperatures (T_{peak} in Fig. 4.8f) occur over a range between 140 and 145°C.
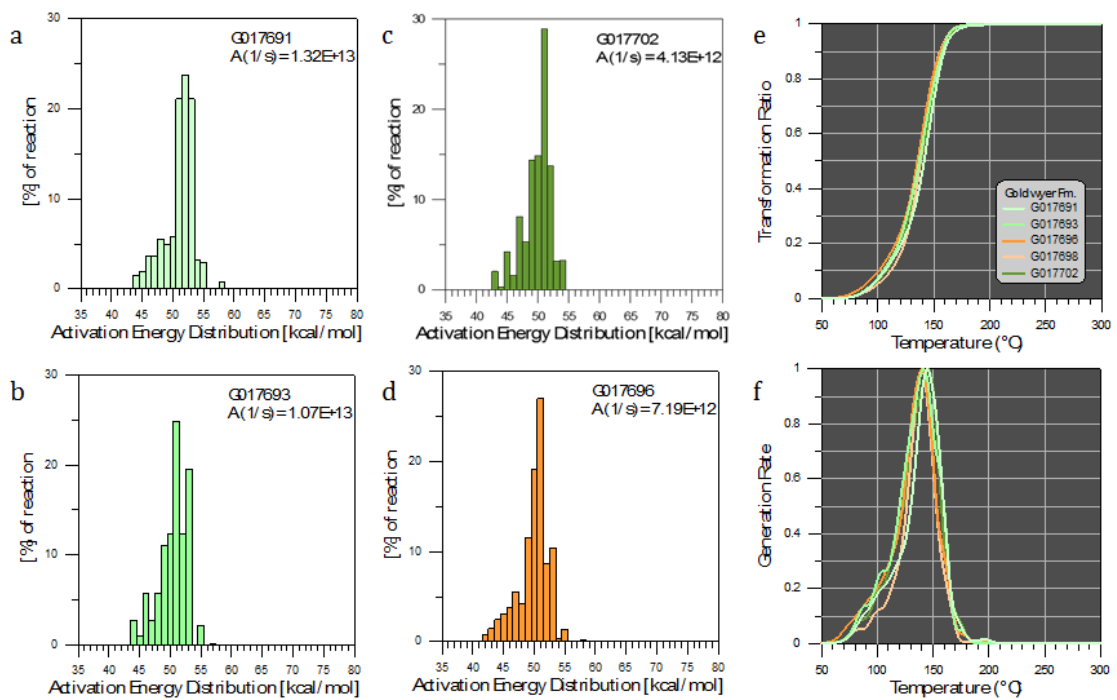
Figure 4.8 a-d. Bulk kinetic parameters in terms of activation energy (Ea) distribution and frequency factors (A) of the studied Goldwyer III unit shales. (e) shows the transformation ratio and (f) generation rate curves for the Goldwyer III shale unit at a geological heating rate of 3°C/Ma.

The higher onset temperature required to crack the kerogen in the Goldwyer I shales is indicative of its relative homogeneity compared to that of the Goldwyer unit III. The low sulphur content in the samples also partly explains their relatively high thermal stabilities.

4.4   Implications on kerogen transformation Theia 1 well.

Burial history plots were conducted for several wells on the Broome Platform and the adjacent Mowla Terrace using the PetroMod™ software (Next Chapter). Results from the Theia 1 well are discussed here.

The Theia 1 well was drilled in the central to south-eastern part of the Broome Platform (see figure 1.4) in 2015 as a wildcat well to test the Middle Ordovician Goldwyer III liquids-rich resource play, validate the company's geological model and de-risk the shale play. The well was drilled to a present-day depth of 1645 m on the Willara Formation. The burial and thermal history for this well were modelled (Fig. 4.9a) using present-day depths, lithology, age and thicknesses for each of the formations encountered, obtained from the well completion and Finder Energy's Theia 1 well database. This well was calibrated using the Horner corrected bottom hole temperature (BHT) value extracted from the well completion report. It should be noted that no measured vitrinite reflectance data is available from this well; however, the modelled vitrinite reflectance trend is shown in Fig 4.9c.

The geothermics used for the modelling are based on transient heat flow at the base of the sediment, with heat flow values projected from Kennard *et al.* (1994) which allowed calibration of the temperature data at this well location. The amounts of Permian and Late Jurassic exhumation events were obtained using the sonic compaction curve method discussed in Chapter 3, which indicate that, paleo burial depths of up to 2400 m were reached in the Carboniferous, with the Goldwyer III shale unit reaching temperatures of 130°C in this Period and temperatures up to 150°C in the late Jurassic. Also, the modelled source rock parameters (TOC and HI) for the Goldwyer III shale unit were obtained from the Rock Eval pyrolysis data discussed in Chapter 2.

The temperature calibration has a good match with the modelled trend (Fig 4.9b) with an average geothermal gradient value of 30°C/km indicated for this well at present day.
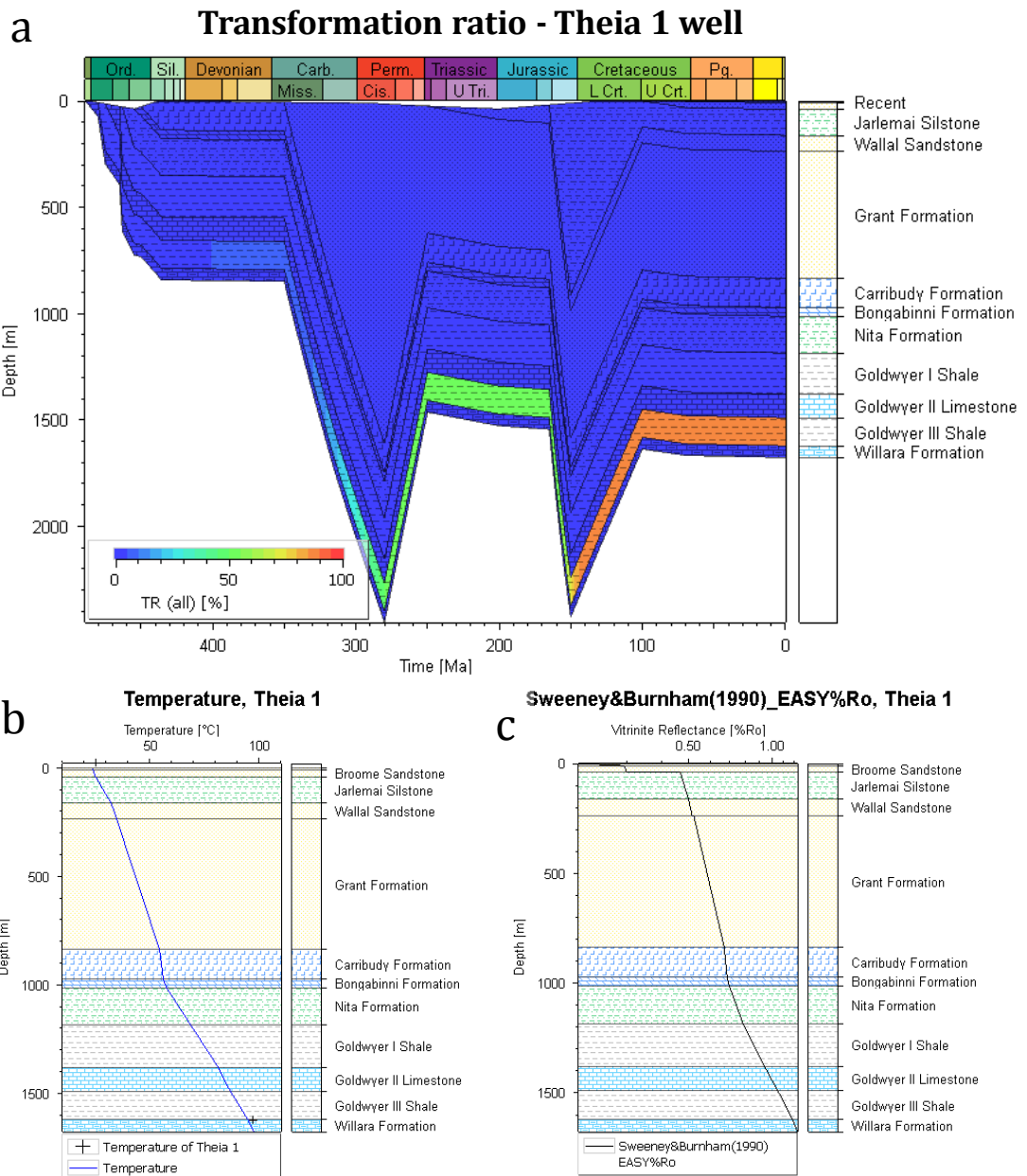
Figure 4.9 (a) Burial history curve for Theia 1 well showing the degree of kerogen transformation for the Goldwyer III shale unit; (b) Horner corrected bottom hole temperature versus depth; (c) plot of modelled vitrinite reflectance versus depth for Theia 1.

The model was initially run with two different kinetic models; the Pepper and Corvi (1995) Type II organofacies B kinetics and the Burnham (1989) Type II kinetics for the Goldwyer III shale unit. These kinetic models are often employed in frontier studies and are specific to Type II kerogen source rocks deposited in marine environments. The outputs from the models of the Goldwyer III shale

were compared to the laboratory generated kinetics from this study. The kinetics results from this study is significantly different to the default kinetics (provided in the utilized software). The laboratory generated kinetics suggest that hydrocarbon generation (10% TR) commenced in the late Carboniferous and rapidly reached 67% TR in the mid Permian until the Jurassic. The subsequent Jurassic tectonics allowed further kerogen maturation and modelled TR% value of 88% is obtained. The Pepper and Corvi (1995) kinetic model on the other hand, suggests earlier onset of hydrocarbon generation (compared to the laboratory generated kinetics), and hydrocarbon generation reached ~ 80% TR in the Permian. With this model, the renewed burial in the early Jurassic allowed further kerogen transformation, with up to 88% present day transformation ratio. The model of Burnham (1989) however suggests that transformation (10%TR) commenced in the Carboniferous and reached a maximum of ~40% in the Permian (Fig. 4.10). This model suggests maximum TR of ~50% was reached in the early Cretaceous.

No transformation reaction was observed for the Goldwyer I shale unit at Theia 1 well in which the organic matter type requires higher temperatures to convert kerogen to hydrocarbon.
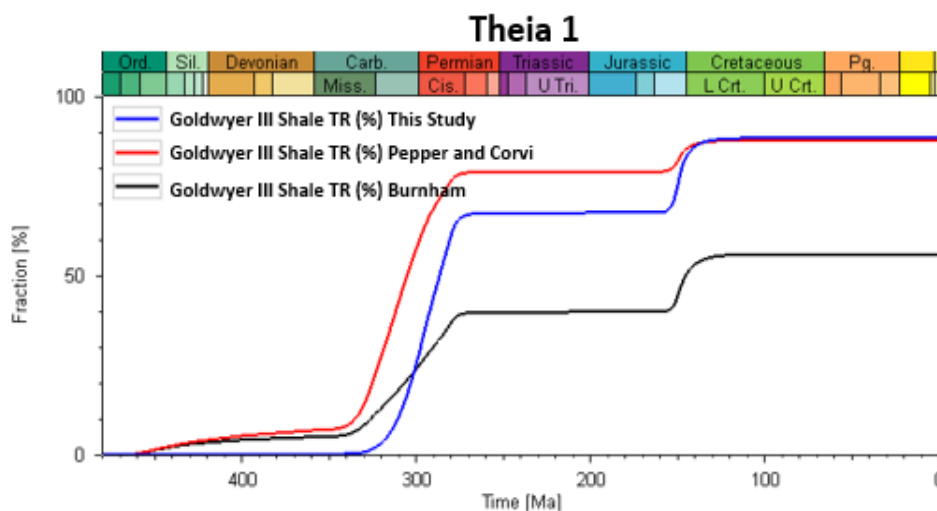
Figure 4.10 Comparison of the transformation ratios (%) from the (Pepper and Corvi, 1995) and (Burnham, 1989) models with the models derived in this study for the Goldwyer III shale unit at Theia 1 well.

4.5   Conclusions.

Organic-rich samples from the Middle (Darriwilian) Ordovician Goldwyer Formation were pyrolysed to contrast the molecular and kinetic parameters between the upper (unit I) and lower (unit III) sections of this formation.

The shale samples studied from the Ordovician Goldwyer Formation have typical characteristics for marine derived organic matter with insignificant input of land plant material. Spaak *et al.* (2017) suggested that terrestrial plant input (crypto-spores) is evident in the Goldwyer I shales, which are locally derived rather than derived from long distance transport from the hinterland, suggesting that perhaps the contribution from early plants was low and localised. Hence, the presence of primitive land plant material is very minor and has no significant effect on the organic matter petroleum generation.

The Goldwyer I shale samples from Solanum 1 and Santalum 1 contain Type I kerogen which upon Py-GC showed a dominance of the aliphatic moieties in their chromatograms and a narrow activation energy distribution, indicating a late onset of hydrocarbon generation. Assuming a geologic heating rate of 3°C/Ma, high temperatures of at least 140°C are required to bring about petroleum formation within this shale unit. Hence, in areas where the Goldwyer 1 unit is buried deeper producing thermal maturation, especially if the burial is recent, it should generate excellent Paraffinic low wax oils.

The pyrolysates of the Goldwyer III shale unit analyzed from Cyrene 1, Theia 1 and McLarty 1 wells are dominated by intermediate to long chained, higher molecular weight aliphatic and aromatic hydrocarbon compounds. This results in broader activation energy distributions and predicted lower starting temperatures for petroleum generation of ~100°C. This unit is predicted to generate Paraffinic-Naphthenic-Aromatic (P-N-A) low wax oils, grading at higher temperatures to condensate and gas.

The kinetic model from this study was tested against the Theia 1 well in the Broome Platform. The outputs show a marked difference in the degree of kerogen transformation between the kinetic models generated in the present study and some of the default kinetic models provided in the PetroMod™ software, which could significantly impact the assessment of oil and gas in-place in conventional and unconventional systems. While the Burnham (1989) kinetic model suggests relatively lower TR (%) values and mid-mature oil generating window for the Goldwyer III shale unit, the kinetic models from Pepper and Corvi (1995) and current study suggest late mature stage of oil generation to early stage of gas generation. See Appendix II for relationship between hydrocarbon generation-defined and common maturity parameters for type II kerogens.

Due to the stable bond and higher temperatures required to break the bonds in the Goldwyer I shale unit, no transformation reaction was observed this well.

CHAPTER 5. Thermal and Burial history reconstruction for selected wells in north-west Canning Basin

5.1   Introduction

Different working petroleum systems have been identified in the various parts of the Canning Basin, with only half of the wells drilled having recorded hydrocarbon shows. The basin contains several small petroleum fields that demonstrate a working Ordovician petroleum system with good source rocks, although no large traps have been discovered to-date (GWA, 2017). Kingsley and Streitberg (2013) noted that less than 5% of drilled wells in the basin have yielded commercial quantities for conventional production. This suggests a better strategy may be to target direct development of the "source rocks" using unconventional production techniques. Several studies, including Brown *et al.* (1984), Haines (2004), Ghori and Haines (2006), Ghori (2013) and GSWA (2014) have identified the Ordovician Goldwyer Formation as one of the main source rocks in the Canning Basin. Few studies such as Kuuskraa *et al.* (2013) and Triche and Bahar (2013) investigated the volumetrics associated with this Formation as a shale reservoir, and Kuuskraa *et al.* (2013) have suggested that this basin has the best potential for unconventional hydrocarbon production in Australia. Ghori (2013), carried out burial and thermal history modelling for some of the Canning Basin wells, using the Lawrence Livermore National Laboratory default kinetics in the BasinMod software.

A good understanding of organic matter character and their maturity evolution through time in shales is important for reconstruction of the timing and amounts of hydrocarbon generation in well locations across a sedimentary basin.

Burial history modelling is an approach that aims to reconstruct the geological processes that have taken place in a sedimentary basin over geologic time. As a prerequisite, a good understanding is required of the basin geology and the processes involved in the generation of hydrocarbons. The model results are

usually verified against measured data like vitrinite reflectance and borehole temperatures in order to accurately calibrate and constrain the simulated burial histories (Grobe *et al.*, 2015). Detailed information on theories and principles behind various aspects of basin modelling are discussed in Yalcin *et al.* (1997), Hantschel and Kauerauf (2009) and Welte *et al.* (2012).

This chapter documents the results of burial and thermal history modelling for 5 wells in the north-western quadrant (around the Broome Platform) of the Canning Basin (Fig. 5.1 a and b), using the 1D module in the PetroMod™ basin modelling software.
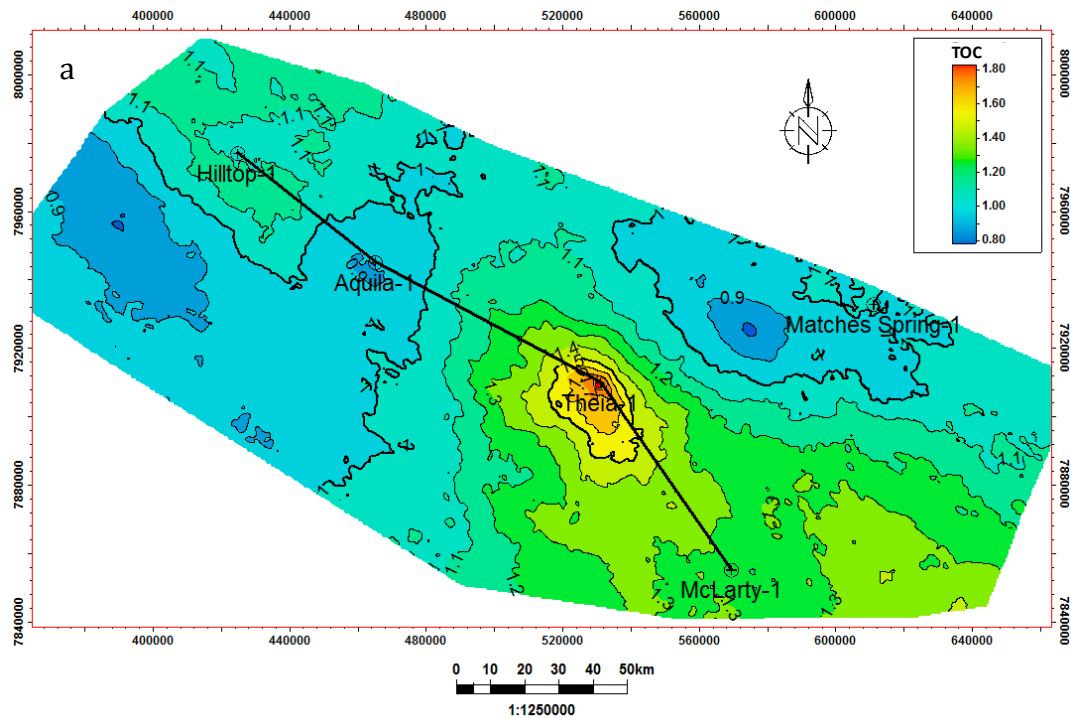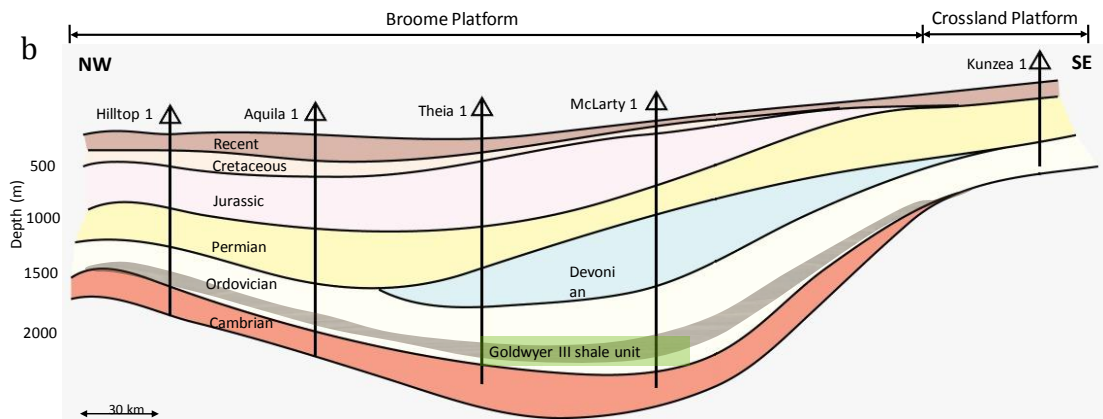
Figure 5.1 (a) Modelled average TOC map of the Broome Platform (chapter 2) showing 5 wells used for burial and thermal history modelling. Bold line shows the transect across 4 wells. (b) A simplified NW-SE cross section across the study area (not to scale). Note that the Goldwyer III shale unit was not penetrated in the Kunzea 1 well.

The details of exploration activities in the Canning Basin are available in Section 1.2 while a summary of the basin evolution and sedimentation history is available in Section 1.3.

5.2   Methodology

5.2.1   Burial history modelling

Burial history modelling usually incorporates a host of geologic data, most of which are available from the well completion, palynological and biostratigraphic reports.

Present-day depths, lithology, age and thicknesses of the formations encountered in each well serve as basic inputs for the model building, while geochemical data such as the TOC, type of kerogen and the kinetics of hydrocarbon generation are further inputs for petroleum systems modelling (Appendix VI). Present-day temperature measurements (bottom hole temperature (BHT), temperature logs & geothermal gradients) and the palaeotemperature indicators like vitrinite reflectance serve as calibration data. Vitrinite reflectance data (where available) is restricted to the post Silurian successions. The Horner corrected borehole temperature data were obtained from well completion reports and well log

headers for each well while all vitrinite reflectance data were obtained from the WAPIMS open file database (Table 5.1).

The range of paleo-heat flow data (Fig. 5.2) were taken from Kennard et. al. (1994a), and (Ghori, 2010). Basement compositions in this study are defined using the basement compositions described in the well completion reports.

Table 5.1 Available vitrinite reflectance data for three of the modelled Canning Basin wells (WAPIMS online database). No vitrinite reflectance data available for the Theia 1, McLarty 1 and Kunzea 1 wells

	MD (m)	Value (Ro)	Min (Ro)	Max (Ro)	Number of readings	Remarks
Hilltop 1	205	0.31	0.25	0.4	17	Vit & Exin sparse; Inert rare
	210	0.31	0.23	0.43	3	Exin & Inert rare to sparse; Vit rare
	215	0.26	0.24	0.28	6	Exin sparse; Vit & Inert rare
	310	0.31	0.21	0.41	25	Vit comm; Exin & Inert rare
	320	0.31	0.22	0.43	25	Vit sparse; Inert & Exin rare
	395	0.34	0.22	0.42	25	Vit sparse; Inert & Exin rare
	770	0.37	0.32	0.46	16	Exin rare to sparse; Inert & Vit rare
	780	0.38	0.29	0.5	12	Vit sparse; Exin rare to sparse; Inert rare
	790	0.34	0.3	0.38	8	Exin & Vit rare to sparse; Inert rare
	810	0.43	0.36	0.51	6	Inert sparse; Exin & Vit rare
Aquila 1	477	0.49	0.44	0.54	34	No Information
	497	0.53	0.47	0.59	17	No Information
	522	0.52	0.47	0.58	18	No Information
	547	0.59	0.53	0.65	19	No Information
	577	0.55	0.48	0.61	10	No Information
	607	0.52	0.46	0.59	25	No Information
	632	0.54	0.45	0.63	11	No Information
Matches Springs 1	393	0.44	0.38	0.51	43	No Information
	529	0.49	0.44	0.53	6	No Information
	802	0.65	0.62	0.69	4	No Information
	1221	0.58	0.53	0.63	No Information	No Information
	1535	0.47	0.42	0.52	No Information	No Information
	1710	0.61	0.56	0.66	No Information	No Information

The paleo-water depth is estimated from the palynological information contained in the well completions reports from the studied wells. Surface temperature (sediment–water interface temperature) values were calculated based on the paleo-latitude of North Australia, the paleo-water depth (PWD) data and using the Wygrala (1989) data compilation integrated in the PetroMod™ software.

The estimation of the removed sections was obtained using the sonic compaction curve methods described in Chapter 3. Thermal maturity was calculated using the Sweeney and Burnham (1990) EASY%Ro model, while the Goldwyer Formation kerogen reaction kinetics described in Chapter 4 were used to calculate kinetics of kerogen transformation.
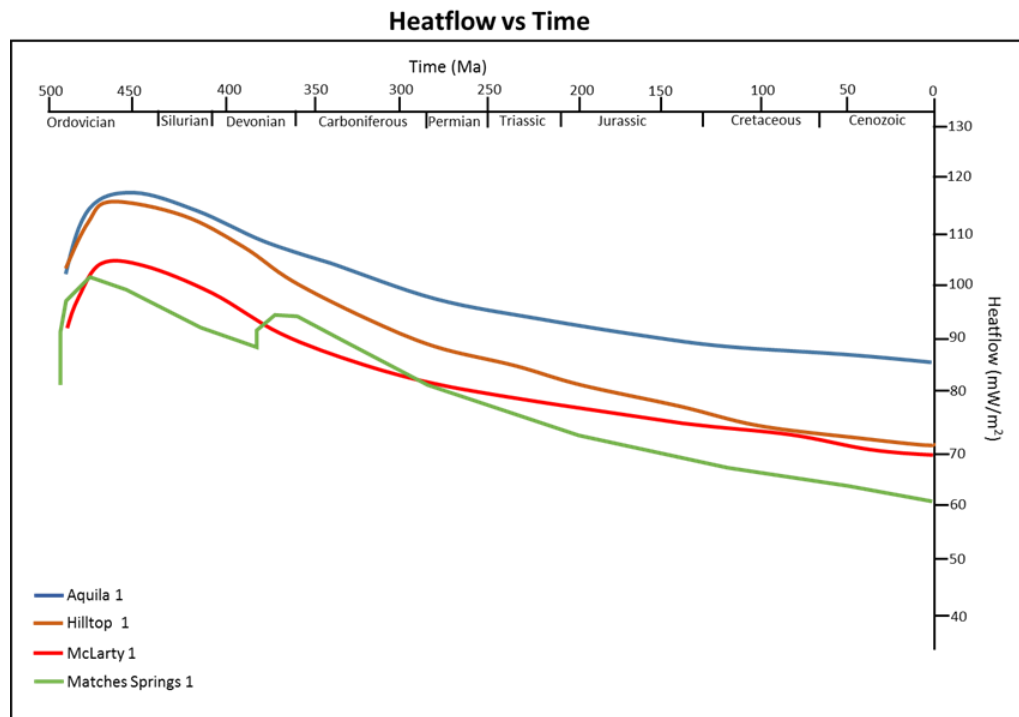
Figure 5.2 Paleo-heat flow variation through time in some Canning Basin wells (modified from Kennard et al., 1994a). The values shown here were used in the basin modelling.

5.3   Results

5.3.1   Burial and thermal history modelling

The present-day depths for the Goldwyer Formation in the study area range from ~1000m, in the shallower wells, to 2300 m depth in the deeper wells, towards the Mowla Terrace (Appendix I). The Kunzea 1 well is situated on the boundary between the Broome and Crossland Platforms, with shallow basement at approximately 500 m, and no penetration of the Goldwyer III shale unit.

5.3.1.1 Hilltop 1 Well

The Hilltop 1 well in the north-western part of the study area has a modelled maximum paleo-burial depth of about 2000 m for the Goldwyer III shale at the end of the Permian subsidence (Fig. 5.3a). A phase of rapid burial occurred during the Late Jurassic to Early Cretaceous rifting event. This was immediately followed by a period of minor uplift and erosion which removed up to 1500 m of sediments.

Figure 5.3 Burial history curve showing (a) temperature evolution for Hilltop 1 well; (b) degree of kerogen transformation for the Goldwyer III shale; (c) modelled and measured (crosses) present day temperature vs depth; (d) modelled vitrinite reflectance vs depth. (crosses with error bars mark measured vitrinite reflectance data).

In this well, the Goldwyer III shale unit has present-day temperature values of up to 72°C (Fig. 5.3a) and about 21% modelled kerogen transformation (Fig 5.3b), using the Goldwyer III shale specific reaction kinetics described in Chapter 4 The modelled and measured present-day temperature profiles are shown in Fig 5.3c. The modelled vitrinite reflectance curve (Fig 5.3d) shows that the Goldwyer III

shale falls within the early to mid-mature oil generating window (0.68-0.77%Ro), consistent the Rock Eval-T_{max} values (Appendix I and II). It is noted that there is an overall poor calibration of measured to modelled vitrinite reflectance data in this well, which is largely attributed to unreliable measured data (See Table 5.1).

The Hilltop 1 well is situated on a paleo-high (Fig. 5.1) where the Goldwyer III shale unit is at a shallow present-day burial depth when compared to other modelled wells in the sub-basin. This explains the lower thermal maturity attained by the Goldwyer III shale unit in this well location.

5.3.1.2 Aquila 1 Well

The Aquila 1 well shows a similar burial history as Hilltop 1 well, with the Goldwyer III shale unit reaching modelled paleo-burial depths of up to 1400 m at the end of the Permian deposition.
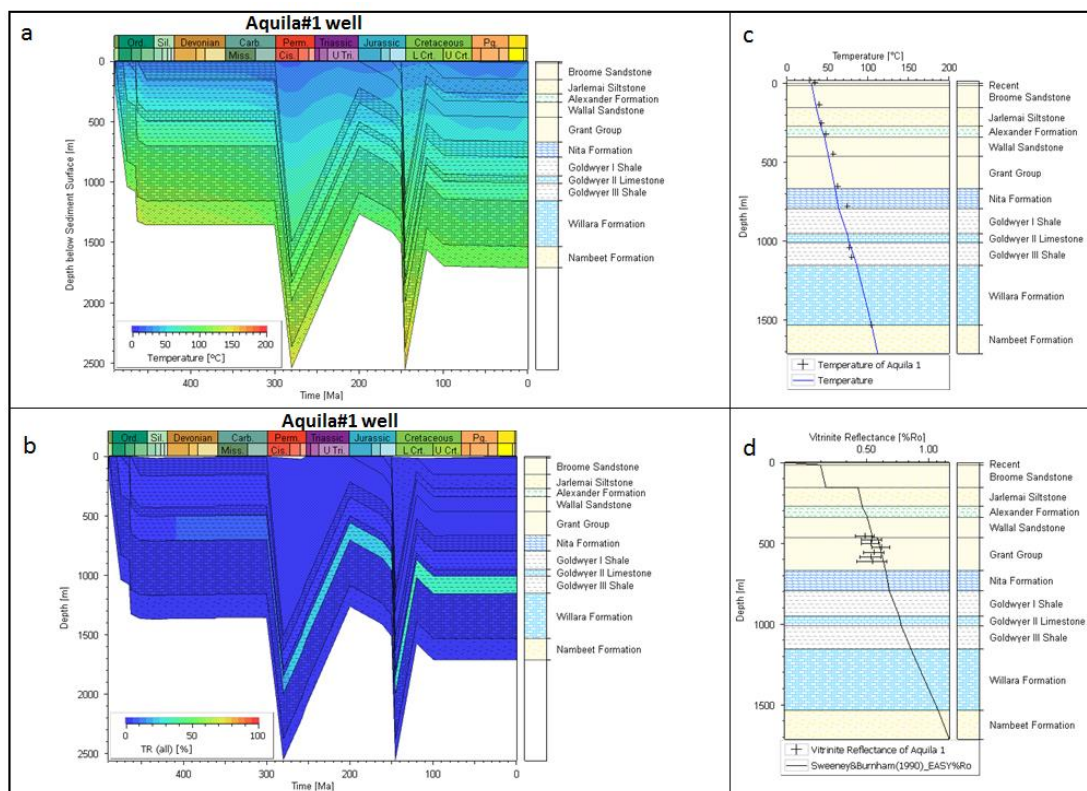
Figure 5.4 Burial history curve showing (a) temperature evolution for Aquila 1 well; (b) degree of kerogen transformation for the Goldwyer III shale; (c) modelled and measured (crosses) present day temperature vs depth; (d) modelled vitrinite reflectance vs depth (crosses with error bars mark measured vitrinite reflectance data).

In this well, the Goldwyer III shale unit has a maximum present-day temperature of 84°C (Fig. 5.4a). The results of 1D modelling of this well also show that the thermal transformation of kerogen in this shale unit continued to increase from 15%, after maximum burial in the Permian, to approximately 26% during the Jurassic subsidence prior the Cretaceous uplift. Present day 30 %TR is modelled in this well (Fig. 5.4b). It should be noted that the measured temperature data show good agreement with the modelled trend in this well (Fig 5.4c). Also, the modelled and measured vitrinite reflectance data in the post Carboniferous Grant Group show a good match, hence this well is assumed to be well calibrated. The modelled vitrinite reflectance values in the Goldwyer III shale unit suggests mostly mid-mature oil window (0.74 – 0.83 %Ro) at the present day (Fig 5.4d), consistent with the Rock Eval-T_{max} values (Appendix I and II).

5.3.1.3 Theia 1 Well

The Theia 1 well is located central part of the Broome Platform, and has a present-day depth of 1645 m. In this well, the modelled maximum paleo-burial depth of for the Goldwyer III shale unit is approximately 2500 m. The Goldwyer III shale unit in this drilled location reached modelled temperatures of 130°C in the Carboniferous and temperatures up to 150°C in the late Jurassic. (Fig. 5.5a). The modelled kerogen transformation in the Theia 1 well suggests that hydrocarbon generation commenced in the Carboniferous (10%TR) with a maximum transformation of approximately 88% TR in the Cretaceous (Fig.5.5b). This well was calibrated using the Horner corrected bottom hole temperature (BHT) value extracted from the well completion report, and a good match was achieved between the measured data and the modelled temperature trend (Fig.5.5c). It should be noted that no measured vitrinite reflectance data is available from this well; however, the modelled vitrinite reflectance values of 1.05 to 1.15 (Fig.5.5d) suggests late mature oil generation window at present day in this well location.
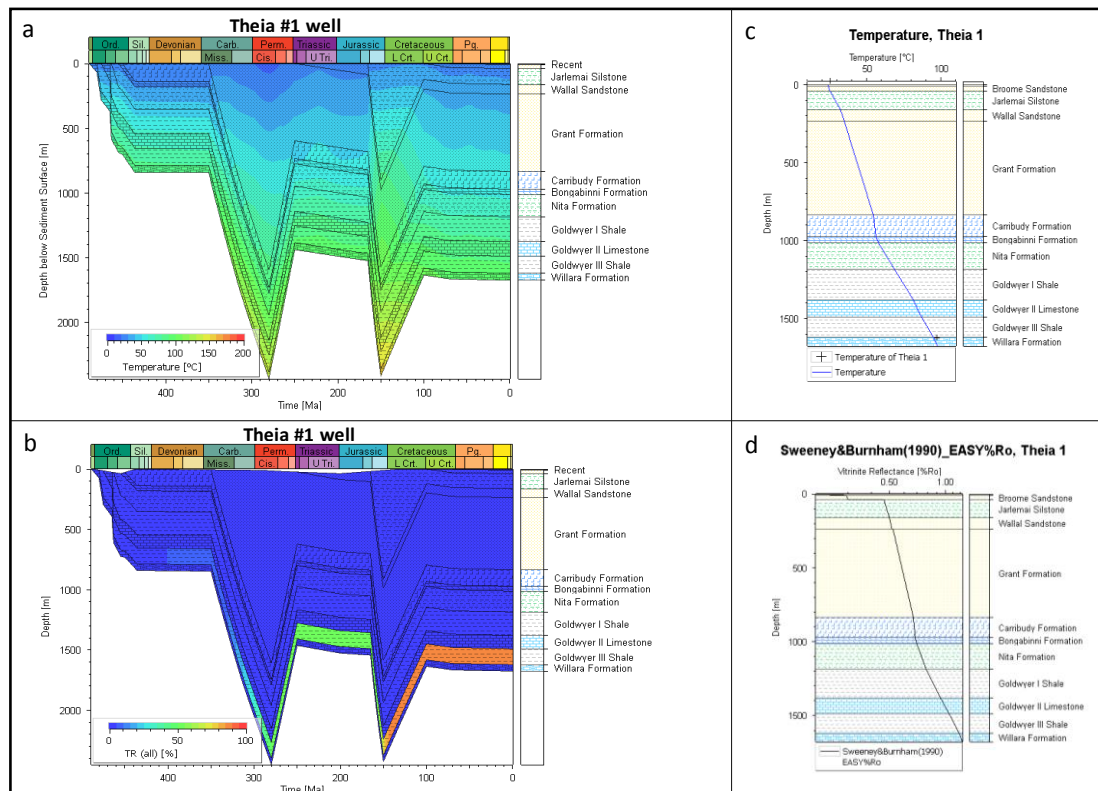
Figure 5.5 Burial history curve showing (a) temperature evolution for Theia 1 well; (b) degree of kerogen transformation for the Goldwyer III shale; (c) modelled and measured present day bottom hole temperature vs depth; (d) modelled vitrinite reflectance vs depth

5.3.1.4 McLarty 1 Well

The McLarty 1 well is situated in the south-central part of the Broome Platform (Fig 5.1a and 5.1b). In this well, the modelled maximum paleo-burial depth for the Goldwyer III shale unit is approximately 3400 m. The Goldwyer III shale unit in this well has modelled present-day temperature of up to 80°C, however, the modelling results suggest that this shale unit had been exposed to approximately 140°C temperatures in the late Carboniferous Period (Fig. 5.6a). Thermal transformation of kerogen gradually increased with 10% TR in the Devonian. Deeper burial prior the Permian uplift exposed this shale to higher temperatures and approximately 68% kerogen transformation (Fig 5.6b) and the maximum Goldwyer III shale transformation has not significantly increased since the end of the Jurassic.
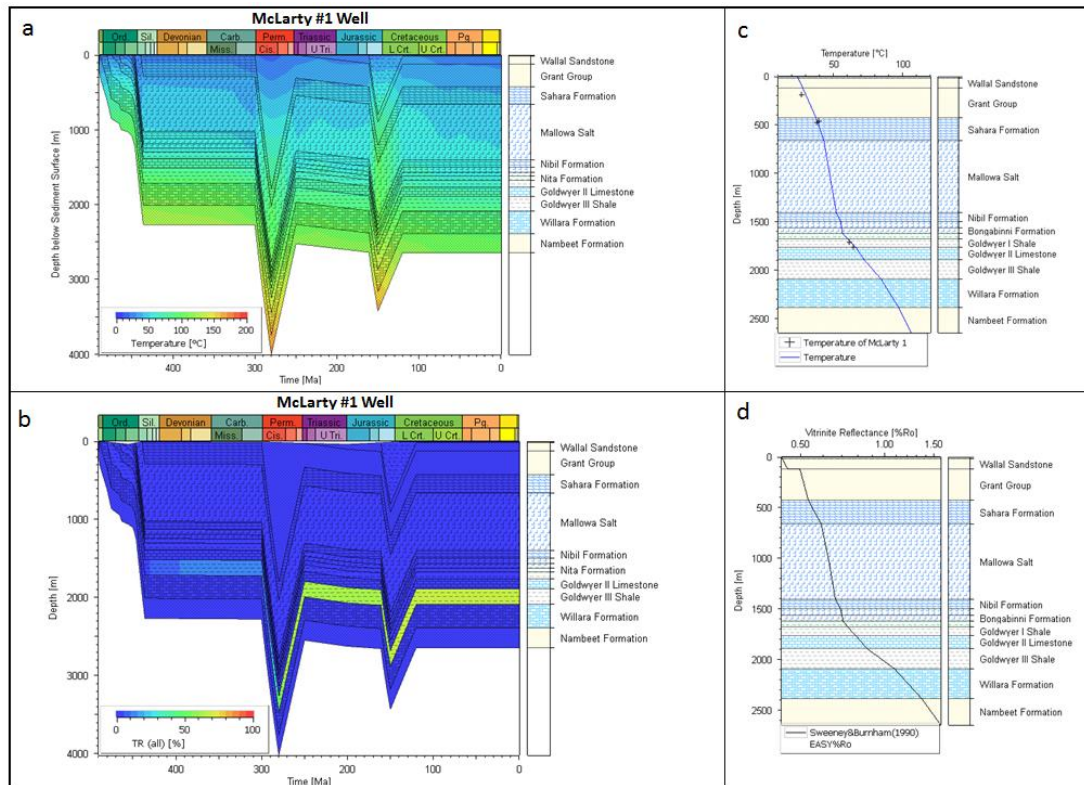
Figure 5.6 Burial history curve showing (a) temperature evolution for McLarty 1 well; (b) degree of kerogen transformation for the Goldwyer III shale; (c) modelled and measured (crosses) present day temperature vs depth; (d) modelled vitrinite reflectance vs depth

A good calibration to the measured temperature data is obtained in the McLarty 1 well, similar to other modelled wells discussed previously (Fig. 5.6c). The modelled vitrinite reflectance values for the Goldwyer III shale are between 0.85 to 1.08 % Ro (Fig. 5.6d), which indicate a mid to late-mature oil maturity at present day. It is noted that the modelled vitrinite reflectance values for the Goldwyer III shale in this well suggest a higher maturity than indicated by Rock-Eval T_{max} data (Appendix I and II).

The simplified cross section across the Broome Platform (Fig 5.1a and b) shows that the McLarty 1 and Theia 1 wells are located in a deeper portion of the Broome Platform, where the Carribuddy Group – salt deposits are well developed, and sediments have reached higher maturities at deeper burial depths. However, the Carribuddy Group was either not deposited or has been

removed by the pre-Permian erosion in the north-western portion of the Broome Platform, as well as along the basin margins (Haines, 2010).

The McLarty 1 well has higher paleo and present-day burial depths compared to the Theia 1 well. However, the relatively lower-modelled TR (%) estimates in the McLarty 1 is due to the "salt chimney" effect (Magri *et al.*, 2008; Zhuo *et al.*, 2016) from the presence of thick evaporite deposits (>1000 m) in this well location. This suppressed the geothermal gradient and the maximum temperature the Goldwyer shales were exposed to, thereby, delaying the onset and peak time of hydrocarbon generation.

5.3.1.5 Matches Springs 1 Well

The Matches Springs 1 well is located on the Mowla Terrace, a down-stepping faulted block, adjacent to the Broome Platform. Present-day sediment thickness in this well is approximately 3000 m, with a well-developed Devonian section with different facies compared to other wells on the Broome Platform.

In this well, the model for the Goldwyer III shale unit shows it attained a maximum paleo-burial depth of approximately 3600 m before the Late Permian uplift, exposing the shale unit to temperatures greater than 160°C (Fig. 5.7a). Hence the kerogen transformation of the Goldwyer III shale unit in the Matches Spring 1 well was 90% completed prior to the Late Permian uplift (Fig. 5.7b). There is a good fit between modelled and measured temperature for the Matches Springs 1 well (Fig. 5.7c), with an average geothermal gradient of 35°C/km.

The modelled vitrinite reflectance values of 1.31 – 1.47% R_o indicate that this shale unit is within the mid-mature gas window at present day in this well location (Fig. 5.7d).
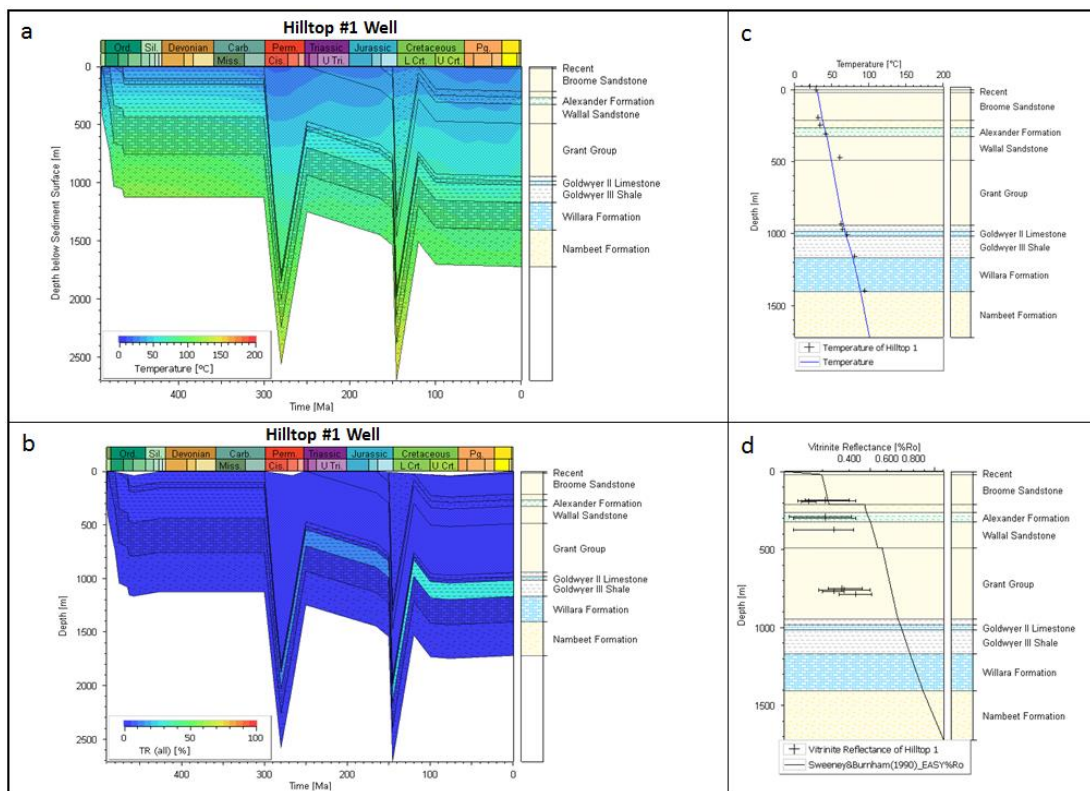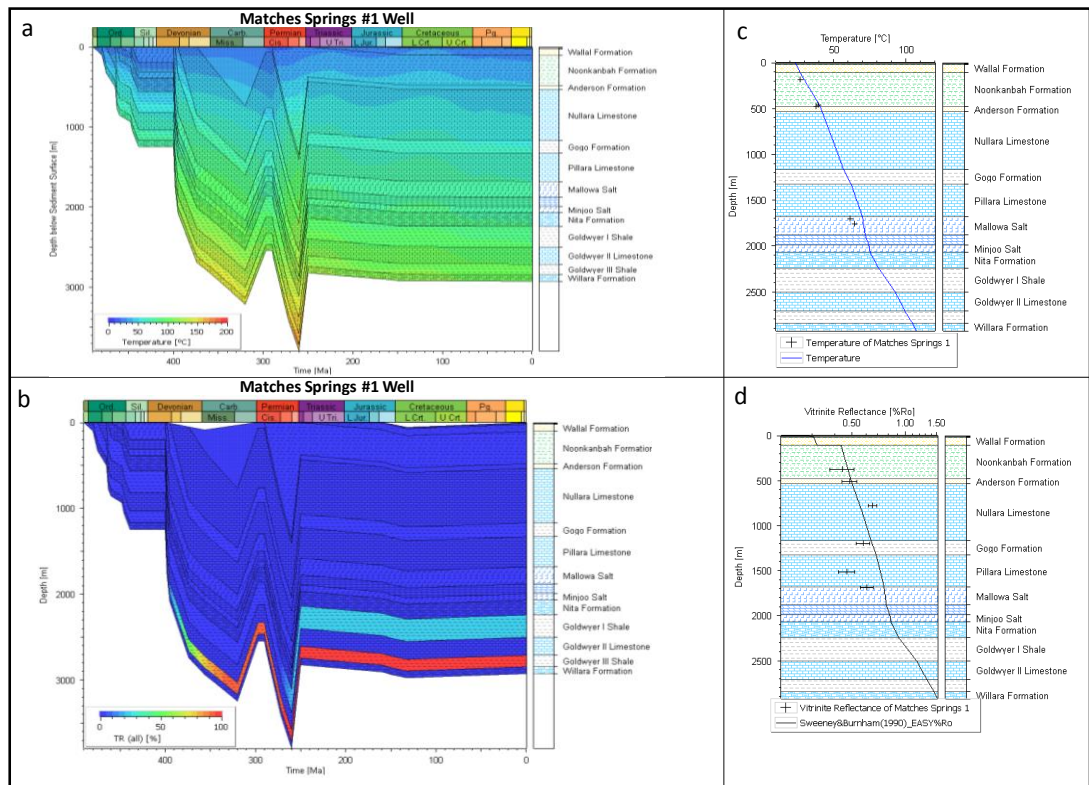
Figure 5.7 Burial history curve showing (a) temperature evolution for Matches Spring 1; (b) degree of kerogen transformation for the Goldwyer shales; (c) modelled and measured (crosses) present day temperature vs depth; (d) modelled vitrinite reflectance vs depth

In Matches Springs 1 there is a good fit between modelled and measured temperature with an average geothermal gradient of 35°C/km (Fig. 5.7c). Also, the modelled vitrinite reflectance curve shows reasonable agreement with measured data for the post-Silurian sequences (Fig. 5.7d). The Goldwyer III shale transformation ratio is estimated to be up to 98% TR.

Furthermore, using the Goldwyer I shale reaction kinetics described in Chapter 4, up to 24% kerogen transformation is predicted to occur in the Goldwyer I shale in this well (Fig. 5.7a). This is probably attributed to the higher temperatures of up to 140°C that the Goldwyer I shale was exposed to in the Permian. This is not unexpected as the more stable organic bonds in the Goldwyer I shale need exposure to higher thermal stress to break the bonds (Chapter 4).

5.3.1.6 Kunzea 1 well

The Kunzea 1 well is situated on the boundary between the Broome and Crossland Platforms. This part of the basin has a shallower basement (Scibiorski, 1984) when compared to other areas, and has experienced a lower subsidence in the Ordovician, containing less than 200 m preserved thickness of Ordovician – Silurian sediments. However, the Permian Grant Group is well developed in this well with over 200m thickness. Estimated maximum paleo-burial depths of approximately 800 m and temperatures up to 54°C were attained by the Goldwyer II limestone unit in this well during the Permian (Fig. 5.8a). Although, the Goldwyer III shale unit was not penetrated in this well, it is assumed that if present, this shale unit would likely be in the immature oil window, with no significant transformation (Fig. 5.8b) given the shallow burial depths of the sediments on this platform.

It should be noted that while the modelled temperature profile shows a good agreement with measured temperature data in this well (Fig. 5.8c), and there is no vitrinite reflectance data available for the model calibration (Fig. 5.8d).
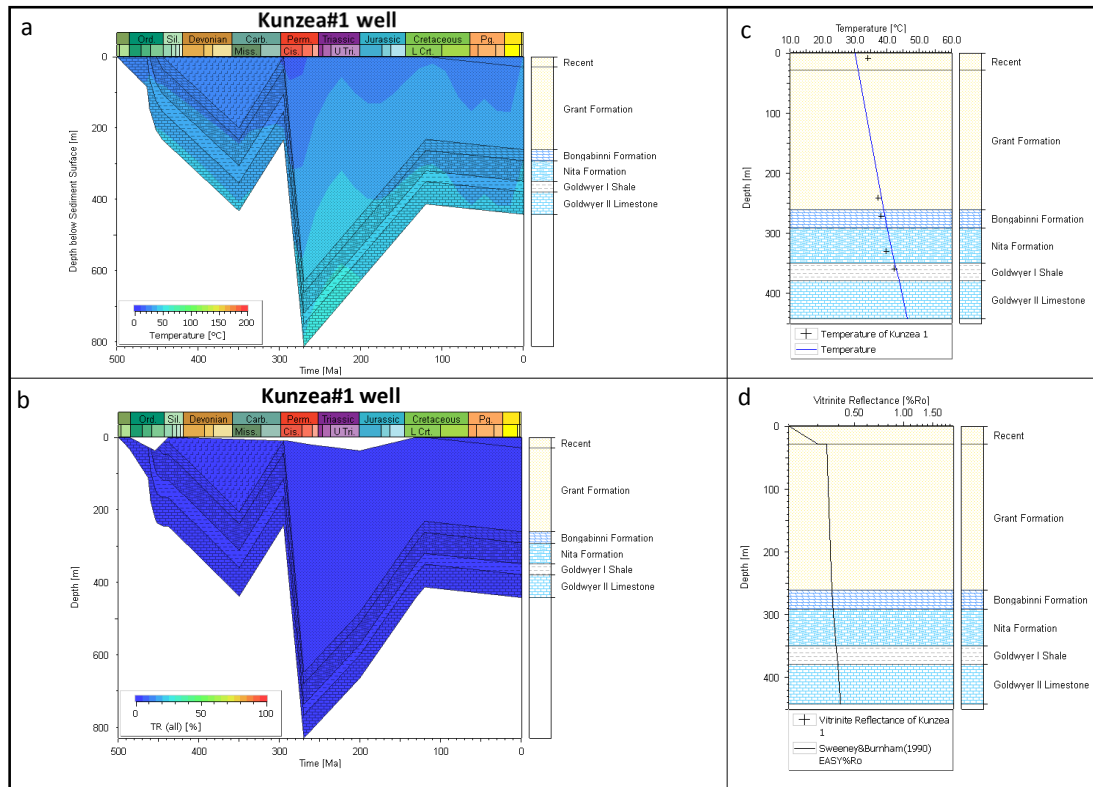
Figure 5.8 Burial history curve showing (a) temperature evolution for Kunzea 1 well; (b) burial history curve with TR overlay; (c) modelled and measured (crosses) present day temperature vs depth; (d) modelled vitrinite reflectance profile vs depth.

5.4   Discussion and Conclusion

The 1-D models constructed for the five selected wells show the sedimentation and tectonic histories in different portions of the Broome-Crossland Platform. Five wells lie along an approximate northeast-southwest transect across the Broome Platform to the Crossland Terrace, with one well offset to the NE from the adjacent Mowla Terrace (Figure 5.1a and 5b). The burial histories for Hilltop 1, Aquila 1 and McLarty 1 have similar geohistory profiles typical of the Broome Platform with three major depositional and burial phases and three uplift phases. Matches Springs 1 located on the Mowla Terrace, and Kunzea 1 to the SE on the border with the Crossland Platform, had a significantly different geohistories.

The first phase of sedimentation and burial occurred from the Ordovician to Silurian, with sediments being rapidly buried in all wells, but decreasing from the NW to SE. A phase of uplift and erosion in the early Devonian is recorded in Matches Springs 1, this probably had a more pronounced effect in wells to the NE, whereas furthest to the SE Kunzea 1 shows that slow sedimentation and burial continued until the Carboniferous.

A second phase of sedimentation and burial from the mid Devonian to early Carboniferous is also recorded in Matches Spring 1 and Kunzea 1. This section is missing in the other wells on the Broome Platform probably due to continued non-deposition and erosion. This burial phase ended with uplift and widespread erosion over the study area in the late Carboniferous that affected all wells.

A third phase of rapid sedimentation and substantial subsidence to maximum depths of burial followed in the Permian which ended with a major and basinwide period of uplift and erosion. Minor sedimentation and burial renewed during the Triassic followed by another period of rapid and substantial burial in the Jurassic to the NW on the Broome Platform which did not affect the Matches Springs 1 or the SE at Kunzea 1.

A final phase of major basinwide uplift and erosion occurred by the end of the Jurassic associated with the Fitzroy Transpression (Kennard et al., 1994). Since then, the last phase of the basin development has been relatively uniform with only minor sedimentation and burial from the Cretaceous to the present in the Canning Basin.

The best-fit models that are presented here are based on synthesis of the burial and thermal models for the wells, including measured vitrinite reflectance and temperature data, different scenarios for paleo-thickness of eroded sections, and sensitivity analysis of heat flow data. The erosional values used in the modelling are within +/- 200m of the range reported in Chapter 3, while the final heat flow values used in this study are within +/- 5mW/m^2 of the range reported by Kennard *et al.* (1994). Duddy *et al.* (2006) suggested that geothermal gradient in

the Canning Basin has been consistent with the present-day heat flow with no sign of elevated basal heat flow during the exhumation periods. The maximum burial was reached mostly in the Permian over the Broome Platform and the adjacent sub-basins.

The kerogen transformation for the Goldwyer III shale unit in the studied wells across the Broome Platform gradually increases from the north-western part of the Broome Platform (Hilltop 1 well, ~21% TR; Aquila 1 well, ~30% TR) to the highest degree of transformation towards the basin centre (Theia 1 well, ~88% TR, McLarty 1 well ~68% TR) (Fig. 5.9). In these wells, modelled vitrinite reflectance values of 0.64 to 1.08 %Ro indicate that the Goldwyer III shale unit is within the main oil to early mature gas generating window at present day. In contrast, the Matches Springs 1 well (Section 5.3.1.5) located on the Mowla Terrace has modelled vitrinite reflectance values of 1.31 – 1.47 % Ro that suggest that the Goldwyer III shale unit lies within the early to mid-mature gas window. Also, in the Matches Springs 1 well, up to 24% kerogen transformation is predicted to occur in the Goldwyer I shale unit (Fig. 5.7b). This indicates the Goldwyer I shale unit should have experienced higher kerogen transformation in possibly deeper portions of the Mowla Terrace, where the stable bonds in the Goldwyer I shale unit would have been exposed to higher degree of higher thermal stress.
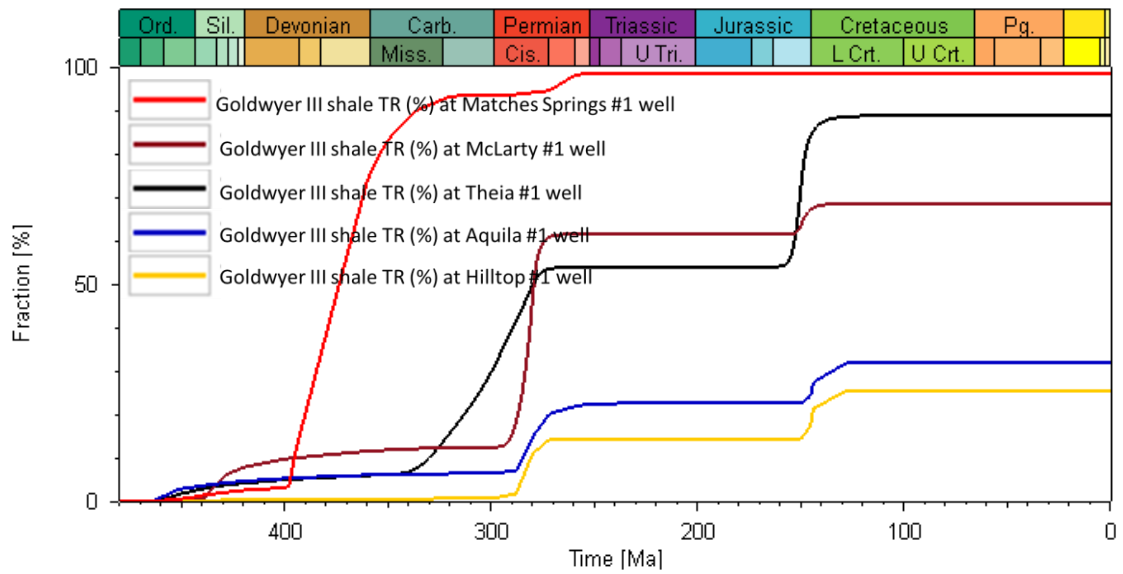
Figure 5.9 Plots showing the transformation ratio (%) of the Goldwyer III shale unit through geological time in the studied wells.

In summary, the results of thermal and burial history modelling for the studied wells suggest that areas towards the central part of the Broome Platform (around the McLarty 1 and Theia 1 wells) have the best potential for shale oil exploration in terms of thermal maturity and kerogen transformation ratios.

CHAPTER 6.0   Discussion and Conclusions.

"Source-rock reservoirs are fine-grained petroleum source rocks from which liquid and gaseous hydrocarbons may be produced following fracture stimulation. A major factor that allows such a source rock to function well as a reservoir is its organic matter – specifically the quantity, quality and thermal maturity of that organic matter as it occurs within the source-rock reservoir" (Curiale and Curtis, 2016)

The Canning Basin contains several small petroleum fields that demonstrate a working petroleum system with good source rocks. However, several episodes of uplift in the basin history are not ideal for timing of migration and entrapment and no large traps have been discovered to-date. This suggests an alternative strategy may be to target direct development of organic rich rocks, using unconventional production techniques. The Ordovician Goldwyer Formation represents one of the best intervals for the application of such techniques in this basin (Kuuskraa *et al.*, 2013). This study assessed the petroleum potential of the Goldwyer Formation over and around the Broome Platform, in terms of: the organic geochemical shale reservoir quality; their lateral and vertical distribution; the thermal evolution and the burial history. The results provide answers to many of the questions with respect to the organic matter richness, and hydrocarbon maturation and generation, including timing and preservation within the formation.

Sedimentological, petrophysical, and sequence stratigraphic assessments of the Ordovician Goldwyer Formation show that it can be subdivided into three main units known as the Goldwyer I, II and III (Triche and Bahar, 2013; Haines, 2004). Some authors have subdivided it into four units by splitting the lowest unit into two (Foster *et al.*, 1986; Winchester-Seeto *et al.*, 2000). The 3-unit nomenclature has been adopted here because analysis of the log signatures, particularly the gamma ray and sonic logs, indicate this is most appropriate for log-based interpolation of the wells over the Broome Platform. This practice is also

followed in well completion reports for several wells drilled recently on the Broome Platform.

The Goldwyer Formation was deposited in the Canning Basin during the middle Ordovician when rising sea levels and waning subsidence produced a major deepening and transgression from SE to NW over most of the study area. Overall, the Goldwyer Formation comprises two main sequences with mudstones toward the base shallowing upwards to carbonate shoals at the top (the upper carbonates are assigned to the Nita Formation). The basal Goldwyer III shale unit consists of open to restricted marine mudstones passing upwards into the limestone reef shoals that comprise the Goldwyer II unit. Deposition of the Goldwyer I shale unit followed representing a return to restricted to open marine sedimentation. The restricted marine Goldwyer shales are the most organic-rich units but their precise areal mapping is hindered by the sparse well occurrence over the Broome Platform and surrounding areas.

The main activities performed in this study, and their conclusions, are summarised in the following sections.

1. Shale reservoir evaluation and geochemical property modelling

Core logging was carried out to identify trends, sequences and cycles in some of the drill cores. The facies established from core logging were tied to the corresponding lithology log by tying the stratigraphy from the cores to the petrophysical well logs. Samples were collected from the shale units (mostly Goldwyer III) and subjected to geochemical analysis. The existing pyrolysis data collated from the WAPIMS open file database was combined with additional pyrolysis data from Rock-Eval experiments carried out in the Curtin University Department of Petroleum Engineering Laboratory.

The data demonstrate that the Goldwyer III shales have organic richness values ranging between 0.1-4.6 wt% TOC, with hydrocarbon generative potential (S_2) mostly ranging from poor to moderate/good potential. A plot of log S_2 versus log

TOC shows the highest potential in the samples from the Aquila 1, McLarty 1 and Theia 1 wells. The Van Krevelen Plot shows that the Goldwyer III shales are mostly Type II oil prone kerogen and Type III gas prone kerogen. The graph of Rock-Eval T_{max} versus HI shows that the shales have reached thermal maturities in the early to peak stages of oil generation.

In addition to the Goldwyer III shales, a few samples were investigated from the Goldwyer I shale unit. The results suggest limited potential for hydrocarbon generation in the Goldwyer I shale on the Broome Platform, mainly attributed to the shallow burial depths and temperatures (T_{peak}), that these shales have experienced at the sampled locations. However, the HI values from deeper areas suggest that they contain mainly Type I (oil prone) kerogen, with the HI versus T_{max} plot showing that the shales are in the early to mid-mature stage of hydrocarbon generation.

Continuous geochemical logs were generated using supervised training of artificial neural networks (ANN). This was carried out in order to establish both quantitative and qualitative organic geochemical character distribution of the Goldwyer III shale unit along the well bore. The aim of this process was to obtain a good relationship with detailed resolution between laboratory measured geochemical data points. Then, the ANN was used to predict organic geochemical values in wells with no laboratory measured data and in wells with limited geochemical laboratory data. Data from the Goldwyer Formation, collected from other sub-basins in the Canning Basin, were included to provide a more robust training dataset, starting with 96 data points. The dataset covers the range from low to moderate to high TOC shales as well as calcareous shales. Well logs used in this study include gamma ray, resistivity, sonic and density logs. The geochemical outputs included hydrogen index (HI), total organic content (TOC), free oil yield (S_1) and source potential (S_2).

The accuracy of the predicted logs was validated against the laboratory measured values for the training set. These logs display good correlation coefficients (R^2) with the laboratory data, especially with the TOC and S_2 logs. The accuracy of the

standard laboratory measured S_1 values is probably reduced, because the S_1 represents the free thermally extractible hydrocarbons that vaporize at temperatures of approximately 300°C, whereas heavier free hydrocarbons that vaporize at higher temperatures are included in the S_2 peak. Nonetheless, in the example well, only a few laboratory-measured data points fall short of the neural network predicted logs. A low correlation was obtained for the HI logs between the measured and the modelled value as expected, which meant the input logs did not generate a good neural network model for HI.

The large area of the Broome Platform and the sparse well spacing mean sophisticated geostatistical techniques, conditioned by seismic data, are required to predict the lateral property distribution into areas with little or no well control. The Krigged models identify the potential sweetspots in 3D. Many realizations from Gaussian simulations measured the uncertainty for each property. The average realization maps for each property show that in the Goldwyer III shale unit, kerogen type distribution (HI), organic content (TOC), higher free oil yield (S_1) and source potential (S_2) are higher in the central to south-eastern part of the Broome Platform and relatively lower in the north-west. This may result from better organic matter preservation in deeper (distal) parts of the basin compared to the proximal parts of the sub-basin.

The maps and 3D geological modelling provide a detailed understanding of the geochemical property distribution and can be related to the basins geological settings and depositional environment. They have identified areas with potential for unconventional hydrocarbon accumulation, additional laboratory studies and further exploration drilling.

2. Thermal and burial history reconstruction

The burial histories for the wells on the Broome Platform have similar profiles in response to the subsidence, sedimentation, uplift, erosion and non-deposition. Together they show that there were three major depositional and burial phases separated by three uplift phases. In contrast, Matches Springs 1 in the Mowla

Terrace, and Kunzea 1 to the SE on the border with the Crossland Platform, had significantly different geohistories. The Matches Springs 1 has a well-developed (> 1000 m thick) Devonian sequence while Kunzea 1 has less than 200 m preserved thickness of Ordovician – Silurian sediments, with no Devonian sequence present. However, the Permian Grant Group is well developed in this well with over 200m thickness.

The amount of exhumed section in the basin is a key process for definition of kerogen maturation, hydrocarbon generation potential and burial history for potential source rocks or shale reservoirs. However, in-spite of the significance of exhumation to unconventional hydrocarbon recovery, only a few papers have discussed this in detail for the Canning Basin. The most relevant publication is Duddy *et al.* (2006), who obtained estimates of removed sediments in the Triassic-Jurassic and Eocene-present day erosional events, using Apatite Fission Track Analysis (AFTA), that were consistent with results in this study (as discussed in Chapter 3).

Here, the sonic transit time logs, formation tops and biostratigraphic data have been employed to estimate the amounts of exhumed sections based on the method of Jankowsky (1962), Magara (1976) and Heasler and Kharitonova (1996). The method obtains a theoretical transit time curve for the Canning Basin, using a polynomial function of the sonic transit time with depth. A new equation was derived for the Canning Basin, providing an empirical relationship between shale ΔT values, depth and the magnitude of erosion. This new equation appears to be in good agreement with both the measured AFTA data and the observed exhumation for several wells in the Canning Basin.

Exhumation of up to 1700m was estimated in the Silurian-Carboniferous Period, while the Triassic-Jurassic Period has estimated exhumation of up to 1800m. The exhumation data from eight wells over and around the Broome Platform were computed and contoured. These contour maps show that exhumation has been relatively uneven across the basin. The results suggest that for each tectonic episode, deformation and erosion are less intense towards the SE in the Kidson

sub-basin and progressively increase in the NW direction. The uplift and erosion results serve as a critical input for the thermal and burial history model.

Pyrolysis-Gas Chromatography (Py-GC) and Bulk Kinetics experiments were carried out on the Goldwyer shales as inputs to the thermal history models. The results provide data on the molecular composition and organic facies to help predict petroleum type and the kinetics of hydrocarbon generation in these shales. Although, a relationship exists between bulk kinetic character and Rock-Eval estimates of kerogen type and thermal maturity, variation in hydrocarbon generation rates can result from variation in organic facies, maceral content heterogeneity, sulphur contents and thermal stability.

The studied shale samples from the Ordovician Goldwyer Formation have characteristics typical of marine derived organic matter with low input of land plant material. The terrestrial plant input (mainly pollen and spores) in the Goldwyer I shales is minor and has no significant effect on petroleum generation behaviour. The Type I – Goldwyer I shales show dominance of aliphatic moieties in their Py-GC pyrolysates which produces a narrow activation energy distribution and late onset of hydrocarbon generation. High temperatures of at least 135°C are required to bring about kerogen transformation within this shale unit assuming a geologic heating rate of 3°C/Ma. The pyrolysates of the Goldwyer III shales, in contrast, are dominated by intermediate to long-chain, higher molecular weight aliphatic and aromatic hydrocarbon compounds. This leads to broader activation energy distributions and lower predicted temperatures of 100°C for onset of petroleum generation. Generally, upon thermal maturation, the Goldwyer I shale unit is predicted to generate Paraffinic low wax oils while the Goldwyer III shale has the ability to generate Paraffinic-Naphthenic-Aromatic (P-N-A) low wax oils, or gas and condensates, dependent on the level of maturation.

The basin-specific kinetics obtained for the Goldwyer shales have proved important for the assessment of in-place oil and gas for both conventional and unconventional hydrocarbon systems. For example, the model based on

measured kinetic parameters of samples from a well analysed in this study, suggests that hydrocarbon generation commenced in the late Carboniferous (10%TR), but rapidly reached 67 % TR in the Permian and 88% TR in the Jurassic, with a maximum transformation of approximately 88% in the Cretaceous. On the other hand, the default kinetics model of Pepper and Corvi (1995) suggest that hydrocarbon generation commenced earlier in the Devonian (10%TR) but rapidly reached 85 % TR in the Permian and 88% TR in the Jurassic. In contrast, the Burnham (1989) TR (%) model shows transformation (10%TR) in the late Carboniferous and reached TR of 40% in the Permian and ~50% in the early Cretaceous. These different kinetic estimates lead to significant differences in estimation of the timing of hydrocarbon generation, migration and entrapment and hence consequent hydrocarbons in place for these shale reservoirs.

In Matches Springs 1 drilled on the down-thrown Mowla Terrace, the measured kinetics gave a TR of 24% for the Goldwyer I shales. The default kinetics from Burnham (1989) and the Pepper and Corvi (1995) gave no transformation reaction, because these default kinetics require relatively higher temperatures for kerogen transformation, being derived on specific datasets from different study areas. In this study, the stable bonds in the Goldwyer I shale organic matter need exposure to high thermal stress to break the bonds. Thus, the Goldwyer I shale interval might have begun kerogen transformation in deeper portions of the Mowla Terrace and areas adjacent to the Broome Platform, where the stable bonds in this shale could have been exposed to higher temperatures.

The kerogen transformation in the Goldwyer III shale interval, studied across the Broome Platform, gradually increases from the north-western part of the sub-basin (Hilltop #1 and Aquila 1 wells) with the highest degree of transformation towards the basin centre in the Theia 1 and the McLarty 1 wells. Rock- Eval data of a few Goldwyer III shale samples from McLarty 1, show T_{max} values between 435-440°C, indicative of early oil window maturity. The low maturation level in the Goldwyer shales in the McLarty 1 results from the thick layer of salt (>1km) in the overburden above the (Goldwyer) Formation. The analytical data input to

the 1-D burial and thermal history modelling for the McLarty 1 well estimate the maturity of the Goldwyer shales within the main oil maturity window at present day, with modelled vitrinite reflectance values between 0.85 to 1.08 % Ro and up to 68% kerogen transformation.

Similarly, Kennard *et al.* (1994) also reported lower than expected maturation in the Acacia 1 well from the Barbwire Terrace. The Acacia 1 well also has thick salt units (~320m) above the Goldwyer Formation.

6.1 Summary and Petroleum Potential

This thesis has provided a number of new insights into the occurrence, burial and maturation history of the Goldwyer Formation and its contained organic matter. Some new methods such as machine learning and 3D modelling have been used to overcome the sparse well data and old seismic data. Some traditional modelling methods have been tested with analytical data which show that they require calibration for accurate prediction.

6.1.1 Summary

- Data from 16 wells in the Broome Platform and adjacent sub-basins in the Canning Basin have been carefully studied and interpreted in terms of their organic geochemical character and thermal history to assess the Ordovician Goldwyer shales for its potential as a reservoir for unconventional hydrocarbon exploration. The paucity of well data normally would impact the confidence level and quality of the property distribution models. Hence, new methods such as machine learning and 3D modelling have been used to overcome the sparse well data and old seismic data. The uncertainties in the models can be further improved by updating the models as more wells are drilled.
- The amounts of removed sections from well locations were estimated using the sonic compaction method. This yielded similar values to the amounts estimated from previous studies that used AFTA methods. The

advantage of the sonic compaction method is that it is significantly cheaper as sonic logs are routinely acquired during drilling. Furthermore, an empirical equation was generated, which related sonic ΔT values, depth and the magnitude of erosion. This new equation appears to be in good agreement with both the measured AFTA data and the observed exhumation for several Canning Basin wells and provides well constrained values for estimation of removed sections in burial history models.

- Kerogen kinetics experiments provided new insights into the temperatures required to bring about kerogen transformation in the different shale units of the Goldwyer Formation. The experimental bulk kinetic results were compared to some of the PetroMod™ software-default values and significant differences were observed in the modelled kerogen transformation ratios. This highlights the significance of obtaining specific kinetics data on samples from a specific shales and basins rather than using "global" average kinetics.

6.1.2 Petroleum Potential

The results from the evaluation of shale reservoir properties and thermal and burial history modelling for the study area indicate that the potential for unconventional shale oil exploration in the Goldwyer III shale, may be higher in the central to south-western part of the Broome Platform. This region has the best combination of laboratory measured source parameters for the Goldwyer III shale (up to 4.0 wt% TOC, 13 mg/g S_2 and 419 mg HC/g rock HI). It is predicted to lie within the main oil maturity window at the present day (modelled VR of 0.74-1.15 %R_o), which is within the range defined for prospective shale oil plays (Jarvie, 2012; Passey *et al.*, 2012; Peters *et al.*, 2016).

On the Mowla Terrace the potential for an additional shale gas play may exist - with higher transformation ratios and thermal maturities (modelled VR = 1.31–1.47 %R_o) predicted for the Goldwyer III shale.

The measured kinetics indicate that the activation energy distributions in the Goldwyer III shales require temperatures of 100°C for petroleum generation to start. In the central to south-eastern part of the Broome Platform, the maximum temperatures estimated from the burial history curves were 127°C in Aquila 1, 151°C in Theia 1 and 150°C in McLarty 1, indicating this area is in the mid to late mature window for petroleum generation.

6.2   Limitations and recommendations

- The quality and sparse line separation of the available 2D seismic data in the Canning Basin is generally poor. This reduces the precision of the main horizons (top of the Goldwyer III shale unit and top of the Willara Formation) that were used to construct and tie the wells for input to the 3-D geochemical property models. Higher resolution seismic data would be beneficial in mapping other key surfaces, which could also be used as input to the 3-D burial history models. Nevertheless, the constructed 3D and 1-D models adequately show the burial histories across the study area.

- The geochemical property simulation models were generated for the entire Goldwyer III shale interval and averaged. Further subdivision of this shale interval could be carried out for more detailed, higher resolution evaluation of the organic matter and geochemical property distribution within the upscaled layers in the formation.

- The kinetic results were very promising and useful. Further kerogen kinetic analyses should be obtained on more samples from the Goldwyer I shale unit in the study area to more confidently ascertain the activation energy distribution and petroleum type organofacies for this shale. Also, additional kinetics experiments are recommended for the Goldwyer I and III shales in other sub-basins across the Canning, to further understand the controlling factors for organofacies development within these shales.

- The constructed burial and thermal history models were calibrated with the hole temperatures and measured vitrinite reflectance in the post

Silurian sediments in three of the modelled wells. While these provided a relatively good match with the modelled data, it would be beneficial to obtain vitrinite reflectance data from all modelled wells. The absence of higher plant vitrinite in the Ordovician sediments is a limitation. However, graptolite reflectance together with conversion of other thermal indicators such as T_{max} to vitrinite reflectance equivalent may provide better insight into the thermal maturity.

Organic geochemistry and burial history modelling are key to hydrocarbon generation for unconventional exploration and production and have been used to identify the potential shale reservoir sweet spots. Now, an understanding of the distribution of key petrophysical properties, such as mineralogy, clay content, brittleness index, porosity, permeability and gas content, should also be pursued in those sweet spots, given they are key properties for shale oil and gas exploitation.

References

Alizadeh, B.; Najjari, S. & Kadkhodaie-Ilkhchi, A. 2012. Artificial neural network modeling and cluster analysis for organic facies and burial history estimation using well log data: A case study of the South Pars Gas Field, Persian Gulf, Iran. *Computers & Geosciences,* 45**,** 9,

Andrews, I. 2014. The Jurassic shales of the Weald Basin: geology and shale oil and shale gas resource estimation. British Geological Survey for Department of Energy and Climate Change. London, UK.

Athy, L. F. 1930. Density, Porosity, and Compaction of Sedimentary Rocks. *American Association of Petroleum Geologists (AAPG) Bulletin,* 14**,** 1-24,

Behar, F.; Beaumont, V. & Penteado, H. D. B. 2001. Rock-Eval 6 technology: performances and developments. *Oil & Gas Science and Technology,* 56**,** 111-134,

Behar, F. & Vandenbroucke, M. 1987. Chemical modelling of kerogens. *Organic Geochemistry,* 11**,** 15-24.10.1016/0146-6380(87)90047-7

Bissada, K. 1982. Geochemical constraints on petroleum generation and migration—a review. *Proceedings ASCOPE,* 81**,** 69-87,

Blackbourn, G. A. 2009. *Cores and Core Logging for Geoscientists*, Whittles Publishing.

Boadu, F. K. 1997. Rock Properties and Seismic Attenuation: Neural Network Analysis. *Pure and Applied Geophysics,* 149**,** 507-524.10.1007/s000240050038

Bohacs, K. M.; Grabowski, G. J. J.; Carroll, A. R.; Mankiewicz, P. J.; Miskell-Gerhardt, K. J.; Schwalbach, J. R.; Wegner, M. B. & Simo, J. A. 2005. Production, destruction, dilution, and accommodation—the many paths to source-rock development. *In:* Harris N. (ed.) *The Deposition of Organic Carbon-Rich Sediments: Mechanisms, Models, and Consequences.* SEPM, Special Publication

Braun, R. L.; Burnham, A. K.; Reynolds, J. G. & Clarkson, J. E. 1991. Pyrolysis kinetics for lacustrine and marine source rocks by programmed micropyrolysis. *Energy & Fuels,* 5**,** 192-204.10.1021/ef00025a033

Brown, S.; Boserio, I.; Jackson, K. & Spence, K. (1984) The geological evolution of the Canning Basin—implications for petroleum exploration. *In* The Canning Basin, WA (ed.) PG Purcell: Geological Society of Australia and

Petroleum Exploration Society of Australia; Canning Basin Symposium, Perth, Western Australia, p. 85-96,

Burnham, A. K. 1989. A simple kinetic model of petroleum formation and cracking. Intern. Publ. UCID-21665, Lawrence Livermore National Lab., CA (USA), p. 11

Burnham, A. K.; Braun, R. L.; Gregg, H. R. & Samoun, A. M. 1987. Comparison of Methods for Measuring Kerogen Pyrolysis Rates and Fitting Kinetic Parameters†. *Energy and Fuels,* 1**,** 452-458.10.1021/ef00006a001

Burns, W. M.; Hayba, D. O.; Rowan, E. L. & Houseknecht, D. W. 2005. Estimating the amount of eroded section in a partially exhumed basin from geophysical well logs: an example from the North Slope. *Studies by the US Geological Survey in Alaska: US Geological Survey, Special Paper***,** 1-18

Cannon, S. 2018. *Reservoir Modelling: A Practical Guide*, John Wiley & Sons.

Carlsen, G. & Ghori, K. 2005. Canning Basin and global Palaeozoic petroleum systems - A review. *APPEA Journal,* 45**,** 349–364,

Clementz, D. M.; Demaison, G. J. & Daly, A. R. 1979. Well Site Geochemistry By Programmed Pyrolysis. Offshore Technology Conference.10.4043/3410-MS

Copp, I. 2015. Theia 1: lithofacies and organofacies review. Good Earth Consulting,

Corcoran, D. & Doré, A. 2005. A review of techniques for the estimation of magnitude and timing of exhumation in offshore basins. *Earth-Science Reviews,* 72**,** 129-168,

Curiale, J. A. & Curtis, J. B. 2016. Organic geochemical applications to the exploration for source-rock reservoirs – A review. *Journal of Unconventional Oil and Gas Resources,* 13**,** 1-31. http://dx.doi.org/10.1016/j.juogr.2015.10.001

Di Primio, R.; Dieckmann, V. & Mills, N. 1998. PVT and phase behaviour analysis in petroleum exploration. *Organic Geochemistry,* 29**,** 207-222. https://doi.org/10.1016/S0146-6380(98)00102-8

Di Primio, R. & Horsfield, B. 2006. From petroleum-type organofacies to hydrocarbon phase prediction. *American Association of Petroleum Geologists (AAPG) Bulletin,* 90**,** 1031-1058,

Dieckmann, V. 2005. Modelling petroleum formation from heterogeneous source rocks: the influence of frequency factors on activation energy distribution

and geological prediction. *Marine and Petroleum Geology,* 22**,** 375-390. http://dx.doi.org/10.1016/j.marpetgeo.2004.11.002

Dieckmann, V.; Schenk, H. J.; Horsfield, B. & Welte, D. H. 1998. Kinetics of petroleum generation and cracking by programmed-temperature closed-system pyrolysis of Toarcian Shales. *Fuel,* 77**,** 23-31. https://doi.org/10.1016/S0016-2361(97)00165-8

DMP 2014. Western Australia's Petroleum and Geothermal Explorer's Guide. Perth Australia: Government of Western Australia,

Dow, W. G. 1977. Kerogen studies and geological interpretations. *Journal of Geochemical Exploration,* 7**,** 79-99,

Dowd, P. & Sarac, C. 1994. A neural network approach to geostatistical simulation. *Mathematical Geology,* 26**,** 491-503,

Duddy, I. R.; Moore, M. E. & O'Brien, C. 2006. Thermal History Reconstruction in Five Canning Basin Wells: Acacia-1 &-2, Kidson-1, Willara-1 & Yulleroo-1 Based on Apatite Fission Track Analysis (AFTA®) and Vitrinite Reflectance Data. *Geotrack Report.* Victoria, Australia

Edwards, D.; Summons, R.; Kennard, J.; Nicoll, R.; Bradshaw, J.; Bradshaw, M.; Foster, C.; O'Brien, G. & Zumberge, J. 1997. Geochemical characteristics of Palaeozoic petroleum systems in northwestern Australia. *The APPEA Journal,* 37**,** 351-379,

Eglinton, T. I.; Damsté, J. S. S.; Kohnen, M. E. & de Leeuw, J. W. 1990. Rapid estimation of the organic sulphur content of kerogens, coals and asphaltenes by pyrolysis-gas chromatography. *Fuel,* 69**,** 1394-1404,

Espitalie, J.; Deroo, G. & Marquis, F. 1985. Rock Eval pyrolysis and its applications. *Revue De L Institut Francais Du Petrole,* 40**,** 563,

Espitalie, J.; Madec, M.; Tissot, B.; Mennig, J. J. & Leplat, P. 1977. Source Rock Characterization Method for Petroleum Exploration. *Offshore Technology Conference.*10.4043/2935-MS

Espitalié, J.; Ungerer, P.; Irwin, I. & Marquis, F. 1988. Primary cracking of kerogens. Experimenting and modelling C1, C2–C5, C6–C15 and C15+ classes of hydrocarbons formed. *Organic Geochemistry,* 13**,** 893-899. https://doi.org/10.1016/0146-6380(88)90243-4

Eyles, N.; Eyles, C. H.; Apak, S. N. & Carlsen, G. M. 2001. Permian-Carboniferous tectono-stratigraphic evolution and petroleum potential of the northern Canning Basin, Western Australia. *American Association of Petroleum*

Geologists (AAPG) Bulletin, 85, 989-1006, http://www.geoscienceworld.org/cgi/georef/2001060294

Forman, D. J. & Wales, D. W. 1982. Geological Evolution of the Canning Basin, Western Australia. (ed.) Bureau of Mineral Resources Australia. Bull. 210,

Foster, C. B.; O'Brien, G. W. & Watson, S. T. 1986. Hydrocarbon source potential of the Goldwyer Formation, Barbwire Terrace, Canning Basin, Western Australia. *The APPEA Journal,* 26, 142-155. https://doi.org/10.1071/AJ85015

Ghori, A. 2010. New heat flow data aids exploration in the Canning Basin, Western Australia. *The APPEA Journal,* 50, 411-424. https://doi.org/10.1071/AJ09025

Ghori, K. 2013. Petroleum geochemistry and petroleum systems modelling of the Canning Basin, Western Australia. (ed.). Geological Survey of Western Australia

Ghori, K. A. R. & Haines, P. W. 2006. Paleozoic Petroleum Systems of the Canning Basin, Western Australia: A review. *American Association of Petroleum Geologists (AAPG).* Perth, Australia: Search and Discovery Article,

Gonzalez, J.; Lewis, R.; Hemingway, J.; Grau, J.; Rylander, E. & Pirie, I. 2013. Determination of Formation Organic Carbon Content Using a New Neutron-Induced Gamma Ray Spectroscopy Service that Directly Measures Carbon *Unconventional Resources Technology Conference (URTeC).* Denver, Colorado. USA: SPE,

Grobe, A.; Littke, R.; Sachse, V. & Leythaeuser, D. 2015. Burial history and thermal maturity of Mesozoic rocks of the Dolomites, Northern Italy. *Swiss Journal of Geosciences,* 108, 253-271,

GSWA 2014. Petroleum prospectivity of State Acreage Release Area L14-2, Canning Basin, Western Australia. Perth, WA: Geological Survey of Western Australia,

Guzman, J. (2003) Formation characterization in a different perspective: drill cuttings analysis revisited. AADE-03-NTCE-25, Proc. AADE 2003 National Tech. Conf."Practical Solutions for Drilling Challenges," Texas.

GWA 2014. Canning Basin *In:* Western Australia's Petroleum and Geothermal Explorer's Guide DMP (ed.). Government of Western Austrailia, Perth. WA

GWA 2017. Summary of petroleum prospectivity: Canning Basin. Department of Mines and Petroleum. Government of Western Australia, Perth, W.A

Haines, P. 2010. The Carribuddy Group and Worral Formation, Canning Basin, Western Australia: reassessment of stratigraphy and petroleum potential. *The APPEA Journal,* 50**,** 425-444,

Haines, P. W. 2004. Depositional facies and regional correlations of the Ordovician Goldwyer and Nita Formations, Canning Basin, Western Australia, with implications for petroleum exploration. Perth: Geological Survey of Western Australia,

Han, S.; Horsfield, B.; Zhang, J.; Chen, Q.; Mahlstedt, N.; di Primio, R. & Xiao, G. 2014. Hydrocarbon Generation Kinetics of Lacustrine Yanchang Shale in Southeast Ordos Basin, North China. *Energy & Fuels,* 28**,** 5632-5639.10.1021/ef501011b

Hantschel, T. & Kauerauf, A. I. 2009. *Fundamentals of basin and petroleum systems modeling*, Springer Science & Business Media. Heidelberg, Berlin

Hart, H.; Hadad, C.; Craine, L. & Hart, D. 2011. *Organic Chemistry: A Short Course*, Cengage Learning.

Hartgers, W. A.; Sinninghe Damsté, J. S.; Requejo, A. G.; Allan, J.; Hayes, J. M.; Ling, Y.; Xie, T.-M.; Primack, J. & de Leeuw, J. W. 1994. A molecular and carbon isotopic study towards the origin and diagenetic fate of diaromatic carotenoids. *Organic Geochemistry,* 22**,** 703-725. https://doi.org/10.1016/0146-6380(94)90134-1

Heasler, H. P. & Kharitonova, N. A. 1996. Analysis of sonic well logs applied to erosion estimates in the Bighorn Basin, Wyoming. *American Association of Petroleum Geologists (AAPG) Bulletin,* 80**,** 630-646,

Hillis, R. R.; Thomson, K. & Underhill, J. R. 1994. Quantification of Tertiary erosion in the Inner Moray Firth using sonic velocity data from the Chalk and the Kimmeridge Clay. *Marine and Petroleum Geology,* 11**,** 283-293.http://dx.doi.org/10.1016/0264-8172(94)90050-7

Hoffmann, C.; Foster, C.; Powell, T. & Summons, R. 1987. Hydrocarbon biomarkers from Ordovician sediments and the fossil alga Gloeocapsomorpha prisca Zalessky 1917. *Geochimica et Cosmochimica Acta,* 51**,** 2681-2697,

Hood, A.; Gutjahr, C. & Heacock, R. 1975. Organic metamorphism and the generation of petroleum. *American Association of Petroleum Geologists (AAPG) Bulletin,* 59**,** 986-996,

Horsfield, B. 1989. Practical criteria for classifying kerogens: some observations from pyrolysis-gas chromatography. *Geochimica et Cosmochimica Acta,* 53**,** 891-901,

Horsfield, B. 1997. The Bulk Composition of First-Formed Petroleum in Source Rocks. *In:* Welte D. H., Horsfield B. & Baker D. R. (eds.) *Petroleum and Basin Evolution: Insights from Petroleum Geochemistry, Geology and Basin Modeling.* Berlin, Heidelberg: Springer Berlin Heidelberg.

Horsfield, B.; Leistner, F. & Hall, K. 2014. Microscale Sealed Vessel Pyrolysis. *In* Grice K. (ed.). *Principles and Practice of Analytical Techniques in Geosciences.* Cambridge : Royal Society of Chemistry, pp. 209—250.

Huang, Z. & Williamson, M. A. 1996. Artificial neural network modelling as an aid to source rock characterization. *Marine and Petroleum Geology,* 13**,** 277-290. http://dx.doi.org/10.1016/0264-8172(95)00062-3

Jankowsky, W. 1962. Diagenese und Ölinhalt als Hilfsmittel für die strukturgeschichtliche Analyse des Nordwestdeutschen Beckens. *Zeitschrift der Deutschen Geologischen Gesellschaft***,** 452-460

Japsen, P.; Mukerji, T. & Mavko, G. 2007. Constraints on velocity-depth trends from rock physics models. *Geophysical Prospecting,* 55**,** 135-154.10.1111/j.1365-2478.2007.00607.x

Jarvie, D. 2015. Geochemical Assessment of Unconventional Shale Gas Resource Systems. *In:* Rezaee R. (ed.) *Fundamentals of Gas Shale Reservoirs.* USA: Wiley.

Jarvie, D. & Tobey, M. 1999. TOC, Rock-Eval and SR Analyzer Interpretive Guidelines. *Application Note 99-4.* Humble Instruments and Services, Inc. Geochemical services Division Texas.

Jarvie, D. M. 1991. Total Organic Carbon (TOC) Analysis. *In:* Merrill R. K. (ed.) *Source and migration processes and evaluation techniques.* American Association of Petroleum Geologists (AAPG).

Jarvie, D. M. 2012. Shale resource systems for oil and gas: Part 2—Shale-oil resource systems. *In:* Breyer J. A. (ed.) *Shale reservoirs—Giant resources for the 21st century.* Memoir 97, American Association of Petroleum Geologists (AAPG)

Jarvie, D. M.; Claxton, B. L.; Henk, F. & Breyer, J. T. 2001. Oil and shale gas from the Barnett Shale, Ft. Worth Basin, Texas *American Association of Petroleum Geologists (AAPG) Annual Meeting Program,* 10**,** A100,

Jarvie, D. M.; Hill, R. J.; Ruble, T. E. & Pollastro, R. M. 2007. Unconventional shale-gas systems: The Mississippian Barnett Shale of north-central Texas as one model for thermogenic shale-gas assessment. *American Association of Petroleum Geologists (AAPG) Bulletin,* 91**,** 475-499,

Jiang, Z.; Zhang, W.; Liang, C.; Wang, Y.; Liu, H. & Chen, X. 2016. Basic characteristics and evaluation of shale oil reservoirs. *Petroleum Research,* 1**,** 149-163.https://doi.org/10.1016/S2096-2495(17)30039-X

Johnson, L. M.; Rezaee, R.; Kadkhodaie, A.; Smith, G. & Yu, H. 2017. A new approach for estimating the amount of eroded sediments, a case study from the Canning Basin, Western Australia. *Journal of Petroleum Science and Engineering,* 156**,** 19-28,

Jones, R. 1987. Organic facies. *In:* Brooks J. & Welte D. H. (eds.) *Advances in Petroleum Geochemistry* London: Academic Press.

Kadkhodaie-Ilkhchi, A.; Rahimpour-Bonab, H. & Rezaee, M. R. 2009a. A committee machine with intelligent systems for estimation of total organic carbon content from petrophysical data: An example from Kangan and Dalan reservoirs in South Pars Gas Field, Iran. *Computers & Geosciences,* 35**,** 459-474,

Kadkhodaie-Ilkhchi, A.; Rezaee, M. R. & Rahimpour-Bonab, H. 2009b. A committee neural network for prediction of normalized oil content from well log data: An example from South Pars Gas Field, Persian Gulf. *Journal of Petroleum Science and Engineering,* 65**,** 23-32. http://dx.doi.org/10.1016/j.petrol.2008.12.012

Kamali, M. R. & Allah Mirshady, A. 2004. Total organic carbon content determined from well logs using ΔLogR and Neuro Fuzzy techniques. *Journal of Petroleum Science and Engineering,* 45**,** 141-148. http://dx.doi.org/10.1016/j.petrol.2004.08.005

Karajas, J. & Kernick, C. 1984. A prospective Nita Formation reservoir trend on the Broome Platform, *in* The Canning Basin, WA *edited by* PG Purcell: Geological Society of Australia and Petroleum Exploration Society of Australia; Canning Basin Symposium, Perth, Western Australia. Proceedings, p. 169–177

Kaye, M. 2006. Training Guides in Petroleum Geochemistry Reference Manual. Aberdeen,

Kennard, J.; Jackson, M.; KK, R. & PN, S. 1994. *Canning Basin Project Stage II-Geohistory Modelling*, Australian Geological Survey Organisation (AGSO).

King, M. R. 1998. The Palaeozoic Play in the South Canning Basin - Results of Looma 1. *In:* Purcell P. & Purcell R. (eds.) *The Sedimentary Basins of Western Austraila 2.* Perth: Proceedings of Petroleum Exploration Society of Australia.

Kingsley, D. & Streitberg, E. 2013. The exploration history of the Laurel Basin-Centred Gas System Canning Basin, Western Australia. *In:* Keep M. & Moss S. (eds.) *The Sedimentary Basins of Western Australia.* Perth, WA: Petroleum Exploration Society of Australia Symposium.

Kuuskraa, V.; Stevens, S. H. & Moodhe, K. D. 2013. Technically recoverable shale oil and shale gas resources: an assessment of 137 shale formations in 41 countries outside the United States. US Energy Information Administration, US Department of Energy,

Larter, S. 1984. Application of analytical pyrolysis techniques to kerogen characterization and fossil fuel exploration/exploitation. *In* K.J. Voorhes (ed.) *Analytical pyrolysis. Techniques and Applications.* Butterworths, London (1984), pp. 212-275 Elsevier.

Magara, K. 1976. Thickness of removed sedimentary rocks, paleopore pressure, and paleotemperature, southwestern part of Western Canada Basin. *American Association of Petroleum Geologists (AAPG) Bulletin,* 60**,** 554-565,

Magri, F.; Littke, R.; Rodon, S.; Bayer, U. & Urai, J. 2008. Temperature fields, petroleum maturation and fluid flow in the vicinity of salt domes. *In* R. Littke et al (ed.). *Dynamics of Complex Intracontinental Basins–The Central European Basin System.* Springer Verlag**,** 519-540

Mastalerz, M.; Schimmelmann, A.; Drobniak, A. & Chen, Y. 2013. Porosity of Devonian and Mississippian New Albany Shale across a maturation gradient: Insights from organic petrology, gas adsorption, and mercury intrusion. *American Association of Petroleum Geologists (AAPG) Bulletin,* 97**,** 1621-1643,

McCarthy, K.; Rojas, K.; Niemann, M.; Palmowski, D.; Peters, K. & Stankiewicz, A. 2011. Basic petroleum geochemistry for source rock evaluation. *Oilfield Review,* 23**,** 32-43,

Meyer, B. & Nederlof, M. 1984. Identification of source rocks on wireline logs by density/resistivity and sonic transit time/resistivity crossplots. *American Association of Petroleum Geologists (AAPG) Bulletin,* 68**,** 121-129,

Mory, A. & Hocking, R. 2011. Permian, Carboniferous and Upper Devonian geology of the northern Canning Basin, Western Australia — a field guide. Geology Survey of Western Australia, Department of Mines and Petroleum,

Muscio, G. P. & Horsfield, B. 1996. Neoformation of inert carbon during the natural maturation of a marine source rock: Bakken Shale, Williston Basin. *Energy & Fuels,* 10**,** 10-18,

Orr, W. L. 1986. Kerogen/asphaltene/sulfur relationships in sulfur-rich Monterey oils. *Organic geochemistry,* 10**,** 499-516,

Parra-Garcia, M.; Sanchez, G.; Dentith, M. & George, A. 2014. Regional structural and stratigraphic study of the Canning Basin, Western Australia. *In:* Department of Mines and Petroleum. (ed.) Geological Survey of Western Australia.

Passey, Q. R.; Bohacs, K. M.; Esch, W.; Klimentidis, R. & Sinha, S. 2012. My source rock is now my reservoir-Geologic and petrophysical characterization of shale-gas reservoirs. *American Association of Petroleum Geologists (AAPG) Search and Discovery Article,* 90124,

Passey, Q. R.; Creaney, S.; Kulla, J. B.; Moretti, F. J. & Stroud, J. D. 1990. Practical model for organic richness from porosity and resistivity logs. *American Association of Petroleum Geologists Bulletin (AAPG),* 74**,** 1777-1794, http://www.scopus.com/inward/record.url?eid=2-s2.0-0025570519&partnerID=40&md5=914afe78a548c8dae35f18be5e56c670

Pedersen, T. & Calvert, S. 1990. Anoxia vs. productivity: what controls the formation of organic-carbon-rich sediments and sedimentary Rocks?(1). *American Association of Petroleum Geologists (AAPG) Bulletin,* 74**,** 454-466,

Pepper, A. S. & Corvi, P. J. 1995. Simple kinetic models of petroleum formation. Part I: oil and gas generation from kerogen. *Marine and Petroleum Geology,* 12**,** 291-319. http://dx.doi.org/10.1016/0264-8172(95)98381-E

Peters, K.; Xia, X.; Pomerantz, A. & Mullins, O. 2016. Geochemistry applied to evaluation of unconventional resources. *Unconventional oil and gas resources handbook.* Elsevier.

Peters, K. E.; Burnham, A. K. & Walters, C. C. 2015. Petroleum generation kinetics: Single versus multiple heating ramp open-system pyrolysis. *American Association of Petroleum Geologists (AAPG) Bulletin,* 99**,** 26,

Peters, K. E. & Cassa, M. R. 1994. Applied source rock geochemistry: Chapter 5: Part II. Essential elements. *The petroleum system—from source to trap,* American Association of Petroleum Geologists (AAPG) Memoir 60,

Pettijohn, F. 1975. *Sedimentary Rocks,* Harper & Row Publishers. *New York,*

Poelchau, H. S. 2001. Modeling an Exhumed Basin: A Method for Estimating Eroded Overburden. *Natural Resources Research,* 10**,** 73-84.10.1023/a:1011537632624

Poelchau, H. S.; Baker, D. R.; Hantschel, T.; Horsfield, B. & Wygrala, B. 1997. Basin Simulation and the Design of the Conceptual Basin Model. *In:* Welte D. H., Horsfield B. & Baker D. R. (eds.) *Petroleum and Basin Evolution: Insights from Petroleum Geochemistry, Geology and Basin Modeling.* Berlin, Heidelberg: Springer Berlin Heidelberg.

Raji, M.; Gröcke, D. R.; Greenwell, H. C.; Gluyas, J. G. & Cornford, C. 2015. The effect of interbedding on shale reservoir properties. *Marine and Petroleum Geology,* 67**,** 154-169. http://dx.doi.org/10.1016/j.marpetgeo.2015.04.015

Rezaee, M. R.; Slatt, R. M. & Sigal, R. F. 2007. Shale gas rock properties prediction using artificial neural network technique and multi regression analysis, an example from a North American shale gas reservoir. *ASEG Extended Abstracts,* 2007**,** 1-4,

Ringrose, P. & Bentley, M. 2015. The Property Model. *Reservoir Model Design: A Practitioner's Guide.* Dordrecht: Springer Netherlands.

Romine, K. K.; Southgate, P. N.; Kennard, J. M. & Jackson, M. J. 1994. The Ordovician to Silurian Phase of the Canning Basin, WA: Structure and Sequence Evolution. *In:* Purcell P. G. & Purcell R. R. (eds.) *The Sedimentary Basins of Western Australia.* Perth: Petroleum Exploration Society of Australia.

Rubinstein, C. V.; Gerrienne, P.; de la Puente, G. S.; Astini, R. A. & Steemans, P. 2010. Early Middle Ordovician evidence for land plants in Argentina (eastern Gondwana). *New Phytologist,* 188**,** 365-369.doi:10.1111/j.1469-8137.2010.03433.x

Schaefer, R. G.; Schenk, H. J.; Hardelauf, H. & Harms, R. 1990. Determination of gross kinetic parameters for petroleum formation from Jurassic source rocks of different maturity levels by means of laboratory experiments. *Organic Geochemistry,* 16**,** 115-120.10.1016/0146-6380(90)90031-T

Schenk, H. J. & Dieckmann, V. 2004. Prediction of petroleum formation: The influence of laboratory heating rates on kinetic parameters and geological extrapolations. *Marine and Petroleum Geology,* 21**,** 79-95.10.1016/j.marpetgeo.2003.11.004

Schenk, H. J.; Horsfield, B.; Kroos, B.; Schaefer, R. G. & Schwochau, K. 1997. Kinetics of petroleum formation and cracking. *In* D. H. Welte, B. Horsfield and D. R. Baker (Eds.). *Petroleum and Basin evolution*, Springer, Berlin (1997), pp. 233-269

Schmoker, J. W. 1983. Determination of organic content of Appalachian Devonian shales from formation-density logs. *American Association of Petroleum Geologists (AAPG) Bulletin,* 63**,** 1504-1509,

Schmoker, J. W. & Hester, T. C. 1983. Organic carbon in Bakken formation, United States portion of Williston basin. *American Association of Petroleum Geologists (AAPG) Bulletin,* 67**,** 2165-2174,

Schreier, C. G.; Walker, W. J.; Burns, J. & Wilkenfeld, R. 1999. Total organic carbon as a screening method for petroleum hydrocarbons. *Chemosphere,* 39**,** 503-510.https://doi.org/10.1016/S0045-6535(98)00598-0

Scibiorski, J. P. 1984. Kunzea No. 1 Well Completions Report, Canning Basin. E.P. 225.

Seymour, M. D. 1972. Canning Basin Regional Report. *In:* Department of Mines and Petroleum (ed.). Perth, Australia

Smith, G. C. & Cook, A. C. 1980. Coalification paths of exinite, vitrinite and inertite. *Fuel,* 59**,** 641-646.https://doi.org/10.1016/0016-2361(80)90127-1

Spaak, G.; Edwards, D. S.; Foster, C. B.; Pagès, A.; Summons, R. E.; Sherwood, N. & Grice, K. 2017. Environmental conditions and microbial community structure during the Great Ordovician Biodiversification Event; a multi-disciplinary study from the Canning Basin, Western Australia. *Global and Planetary Change,* 159**,** 93-112. https://doi.org/10.1016/j.gloplacha.2017.10.010

Sweeney, J. J. & Burnham, A. K. 1990. Evaluation of a simple model of vitrinite reflectance based on chemical kinetics (1). *American Association of Petroleum Geologists (AAPG) Bulletin,* 74**,** 1559-1570,

Tassone, D. R.; Holford, S. P.; Stoker, M. S.; Green, P.; Johnson, H.; Underhill, J. R. & Hillis, R. R. 2014. Constraining Cenozoic exhumation in the Faroe-Shetland region using sonic transit time data. *Basin Research,* 26**,** 38-72.10.1111/bre.12052

Tassone, D. R., Holford, S. P., Duddy, I. R., Green, P. F., & Hillis, R. R. 2014. Quantifying Cretaceous–Cenozoic exhumation in the Otway Basin, southeastern Australia, using sonic transit time data: Implications for conventional and unconventional hydrocarbon prospectivity. *American Association of Petroleum Geologists (AAPG) Bulletin,* 98**,** 67-117,

Tegelaar, E. W. & Noble, R. A. 1994. Kinetics of hydrocarbon generation as a function of the molecular structure of kerogen as revealed by pyrolysis-gas chromatography. *Organic Geochemistry,* 22**,** 543-574. https://doi.org/10.1016/0146-6380(94)90125-2

Tissot, B. P. & Welte, D. H. 1978. *Petroleum formation and occurrence.*, New York, Springer-Verlag.

Tissot, B. P. & Welte, D. H. 1984. *Diagenesis, catagenesis and metagenesis of organic matter. Petroleum Formation and Occurrence.* New York, Springer-Verlag.

Triche, N. E. & Bahar, M. 2013. Shale Gas Volumetrics of Unconventional Resource Plays in the Canning Basin, Western Australia. *SPE.* Brisbane, Australia: SPE,

Tucker, M. E. 2009. *Sedimentary petrology: an introduction to the origin of sedimentary rocks*, John Wiley & Sons.

Walker, R. G. 1992. Facies, facies models, and modern stratigraphic concepts. *In* R. G. Walker, and N. P. James (ed.) *Facies models: response to sea level change.* Geological Association of Canada.**,** 1-14

Waples, D. W. & Nowaczewski, V. S. 2014. Source-rock kinetics. *Encyclopedia of Petroleum Geoscience.* New York Springer, https://siriusdummy.files.wordpress.com/2013/11/perspective-on-sr-kinetics-ss.pdf

Ware, P. D. & Turner, J. P. 2002. Sonic velocity analysis of the Tertiary denudation of the Irish Sea basin. *Geological Society, London, Special Publications,* 196**,** 355-370,

Welte, D. H.; Horsfield, B. & Baker, D. R. 2012. *Petroleum and basin evolution: insights from petroleum geochemistry, geology and basin modeling*, Springer Science & Business Media.

Winchester-Seeto, T.; Foster, C. & O'Leary, T. 2000. Chitinozoans from the Middle Ordovician [Darriwilian] Goldwyer and Nita formations, Canning Basin [Western Australia]. *Acta Palaeontologica Polonica,* 45**,** 271-300,

Wygrala, B. 1989. Integrated study of an oil field in the southern Po basin, northern Italy. *Ber. Kernforschungsanlage Jülich, 2313,* pp. 1-217

Yalcin, M.; Littke, R. & Sachsenhofer, R. 1997. Thermal history of sedimentary basins. *Petroleum and basin evolution.* Springer.

Yang, S.; Horsfield, B.; Mahlstedt, N.; Stephenson, M. & Konitzer, S. 2016. On the primary and secondary petroleum generating characteristics of the Bowland Shale, northern England. *Journal of the Geological Society,* 173**,** 292-305.10.1144/jgs2015-056

Yeates, A.; Gibson, D.; Towner, R. & Crowe, R. Regional geology of the onshore Canning Basin, WA. *In:* Purcell P. (ed.) The Canning Basin, WA: Proceedings of the Geological Society of Australia and Petroleum Society of Australia Symposium: Petroleum Exploration Society of Australia, 1984 Perth, Western Australia PESA, 23-55,

Yu, H.; Rezaee, R.; Wang, Z.; Han, T.; Zhang, Y.; Arif, M. & Johnson, L. 2017. A new method for TOC estimation in tight shale gas reservoirs. *International Journal of Coal Geology,* 179**,** 269-277,

Zhuo, Q. G.; Meng, F. W.; Zhao, M. J.; Li, Y.; Lu, X. S. & Ni, P. 2016. The salt chimney effect: delay of thermal evolution of deep hydrocarbon source rocks due to high thermal conductivity of evaporites. *Geofluids,* 16**,** 440-451.10.1111/gfl.12162

Appendices

Appendix I: Pyrolysis data used for this study

	Well	Top-Depth	TOC	S1	S2	S1+S2	T-max	HI	OI	PI
		m	%	mg HC/g rock	mg HC/g rock	mg HC/g rock	°C	mg/g TOC	mg/g TOC	a/(a+b)
1	*Cyrene 1	958	3.3	2.64	12.78	15.42	445	387	6	0.17
2	*Cyrene 1	966.6	2.4	2.13	6.25	8.38	443	260	10	0.25
3	*Cyrene 1	971.3	2.47	2.04	8.09	10.13	447	328	6	0.2
4	*Cyrene 1	973.9	3.82	3.1	12.41	15.51	442	325	4	0.2
5	*Cyrene 1	976.7	2.74	1.92	8	9.92	448	292	9	0.19
6	*Cyrene 1	988.8	2.92	2.36	7.7	10.06	445	264	8	0.23
7	*Cyrene 1	994.1	1.86	1.47	3.94	5.41	440	212	11	0.27
8	*Cyrene 1	998.7	1.27	0.84	1.83	2.67	445	144	22	0.31
9	*Cyrene 1	1003.2	0.66	0.19	0.58	0.77	444	88	24	0.25
10	*Cyrene 1	1006.5	1.31	0.91	2.08	2.99	444	159	21	0.3
11	*Cyrene 1	1007.1	1.34	0.96	1.96	2.92	441	146	14	0.33
12	*Cyrene 1	1012.5	1.31	0.71	1.56	2.27	443	119	22	0.31
13	*Cyrene 1	1013.8	1.44	0.86	1.58	2.44	446	110	14	0.35
14	*Cyrene 1	1014.6	1.47	0.96	2.19	3.15	443	149	18	0.3
15	*Cyrene 1	1016.8	1.25	0.73	1.63	2.36	444	130	12	0.31

16	*Theia 1	977.2	1.22	0.87	2.85	3.72	448	234	18	0.23
17	*Theia 1	1201	0.28	0.04	1.1	1.14	442	393	175	0.03
18	*Theia 1	1217.3	0.3	0.06	2.36	2.42	475	787	57	0.03
19	*Theia 1	1257.4	0.15	0.05	0.9	0.95	437	600	107	0.05
20	*Theia 1	1258.7	0.13	0.03	0.8	0.83	559	615	146	0.04
21	*Theia 1	1307.7	0.09	0.04	0.19	0.23	608	211	133	0.16
22	*Theia 1	1325.9	0.22	0.05	0.32	0.37	445	145	73	0.13
23	*Theia 1	1345.6	0.21	0.03	0.32	0.35	454	152	67	0.1
24	*Theia 1	1358.9	0.33	0.06	0.4	0.46	453	121	61	0.12
25	*Theia 1	1371.3	0.52	0.22	0.9	1.12	453	173	81	0.2
26	*Theia 1	1390.8	1.26	0.63	2.43	3.06	454	193	22	0.21
27	*Theia 1	1397.8	4.28	2.78	14.25	17.03	453	333	8	0.16
28	*Theia 1	1433.9	0.07	0.02	0.11	0.13	373	157	257	0.18
29	*Theia 1	1443.5	0.18	0.09	0.36	0.45	408	200	200	0.21
30	*Theia 1	1453.8	0.09	0.1	0.1	0.2	302	111	611	0.52
31	*Theia 1	1469.6	0.69	0.37	0.7	1.07	458	101	68	0.35
32	*Theia 1	1472.1	3.91	3.18	9.95	13.13	454	254	7	0.24
33	*Theia 1	1473.4	3.2	2.12	7.55	9.67	454	236	16	0.22
34	*Theia 1	1478.3	2.82	1.57	4.66	6.23	456	165	15	0.25
35	*Theia 1	1490.3	0.16	0.12	0.14	0.26	305	88	300	0.47
36	*Theia 1	1491.6	0.11	0.13	0.2	0.33	312	182	527	0.39
37	*Theia 1	1506.2	2.6	1.78	5.62	7.4	453	216	22	0.24
38	*Theia 1	1512.7	2.87	3.95	6.82	10.77	442	238	10	0.37
39	*Theia 1	1516.5	1.53	1.74	3.41	5.15	441	223	23	0.34
40	*Theia 1	1516.5	2.11	2.33	5.17	7.5	445	245	28	0.31

41	*Theia 1	1518.1	1.47	1.64	2.08	3.72	450	141	39	0.44
42	*Theia 1	1520.42	1.24	1.43	3.23	4.66	453	260	32	0.31
43	*Theia 1	1526.7	0.13	0.17	0.18	0.35	302	138	323	0.48
44	*Theia 1	1529.9	2.76	2.33	5.83	8.16	448	211	18	0.29
45	*Theia 1	1531.5	0.75	0.51	0.85	1.36	458	113	55	0.37
46	*Theia 1	1534.7	3.26	2.92	5.57	8.49	444	171	11	0.34
47	*Theia 1	1540.34	0.83	1.24	1.9	3.14	456	229	18	0.4
48	*Theia 1	1557.25	2.68	3.73	7.18	10.91	446	268	12	0.34
49	*Theia 1	1585.97	0.93	1.1	0.96	2.06	456	103	29	0.53
50	*Theia 1	1587.4	1.54	1.15	1.48	2.63	461	96	27	0.44
51	*Theia 1	1593.7	1.01	0.54	0.61	1.15	468	60	38	0.47
52	**Edgar Range 1	841	0.15	0.02	0.03	0.05	427	20	526.7	0.4
53	**Edgar Range 1	925.1	0.3	1.04	1.02	2.06	371	340	220	0.5
54	*Edgar Range 1	947.928	0.15	0.08	0.32	0.4	446	213	220	0.2
55	**Edgar Range 1	948.6	0.15	0.03	0.09	0.12	432	60	40	0.25
56	**Edgar Range 1	978.4	0.24	0.27	0.25	0.52	404	104.2	295.8	0.52
57	**Edgar Range 1	1039	0.19	0.06	0.13	0.19	377	68.42	210.5	0.32
58	*Edgar Range 1	1042.4	0.27	0.09	0.35	0.44	448	130	141	0.21
59	**Edgar Range 1	1048.5	0.32	0.12	0.18	0.3	432	56.25	37.5	0.4
60	**Edgar Range 1	1080.5	0.23	0.11	0.15	0.26	433	65.22	8.7	0.42
61	**Edgar Range 1	1136	0.27	0.07	0.28	0.35	438	103.7	148.2	0.2
62	**Edgar Range 1	1144.5	0.33	0.41	0.39	0.8	426	118.2	78.79	0.51
63	**Edgar Range 1	1188.72	0.12	0.03	0.09	0.12	461	75	250	0.25
64	**Edgar Range 1	1188.9	0.12	0.04	0.06	0.1	380	50	166.7	0.4
65	**Edgar Range 1	1214.6	0.34	0.12	0.29	0.41	435	85.29	14.71	0.29

66	**Edgar Range 1	1271	1.68	1.19	2.2	3.39	435	131	40.48	0.35
67	**Edgar Range 1	1306.1	1.17	0.93	1.15	2.08	435	98.29	70.94	0.45
68	**Edgar Range 1	1348.8	0.65	0.49	0.49	0.98	425	75.38	126.2	0.5
69	**Edgar Range 1	1350	0.16	0.03	0.07	0.1	367	43.75	387.5	0.3
70	**Edgar Range 1	1676	0.19	0.04	0.04	0.08	375	21.05	115.8	0.5
71	**Edgar Range 1	1683.8	0.22	0.03	0.03	0.06	274	13.64	31.82	0.5
72	**Edgar Range 1	1773	0.44	0.03	0.08	0.11	275	18.18	72.73	0.27
73	**Edgar Range 1	1779.1	1.32	0.23	0.19	0.42	481	14.39	6.06	0.55
74	**Edgar Range 1	1780.8	1.48	0.19	0.23	0.42	486	15.54	0.68	0.45
75	**Edgar Range 1	1785.2	1.52	0.28	0.25	0.53	481	16.45	0.66	0.53
76	**Edgar Range 1	1935	2.39	0.09	1.69	1.78	434	70.71	12.13	0.05
77	**Matches Springs 1	2732.6	1.38	1.09	2.35	3.44	441	170.3	49.28	
78	**Matches Springs 1	2750	0.16	0.04	0.06	0.1	347	37.5	181	0.12
79	**Matches Springs 1	2753	0.14	0.16	0.07	0.23	369	50	42	0.73
80	**Matches Springs 1	2754.8	0.62	0.78	0.91	1.69	430	146.8	64.52	0.66
81	**Matches Springs 1	2764.6	1.48	0.96	2.43	3.39	439	164.2	40.54	0.62
82	**Matches Springs 1	2769.1	2.11	1.3	3.21	4.51	441	152.1	39.34	0.61
83	**Matches Springs 1	2801.2	0.82	0.56	0.93	1.49	445	113.4	87.8	0.44
84	**Matches Springs 1	2811.8	0.34	0.18	0.18	0.36	443	52.94	55.88	0.49
85	**Pictor 1	1430	0.83	0.58	0.51	1.09	429	61.45	67.47	0.53
86	**Pictor 1	1445	1.54	1.15	1.31	2.46	434	85.06	19.48	0.47
87	**Pictor 1	1460	0.92	0.52	0.54	1.06	435	58.7	26.09	0.49
88	**Pictor 1	1940	0.52	0.07	0.06	0.13	345	11.54	55.77	0.54
89	**Pictor 1	1955	0.84	0.07	0.06	0.13	358	7.14	44.05	0.54
90	**Pictor 1	1970	0.65	0.07	0.03	0.1	439	4.62	163.1	0.7
91	**Pictor 1	1985	0.65	0.09	0.07	0.16	305	10.77	49.23	0.56

92	**Hilltop 1	1052.5	2.1	1.68	4.74	6.42	433	225.7	11.9	0.26
93	**Hilltop 1	1079.1	1.45	1.1	2.37	3.47	438	163.5	21.38	0.32
94	**Hilltop 1	1098	2.5	2.29	4.51	6.8	432	180.4	13.6	0.34
95	**Hilltop 1	1128.1	1.3	0.92	1.42	2.34	438	109.2	21.54	0.39
96	**Hilltop 1	1170	0.8	0.42	0.54	0.96	447	67.5	38.75	0.44
97	**Hilltop 1	1286.1	0.06	0.03	0.02	0.05	399	33.33	666.7	0.6
98	**Hilltop 1	1353.1	0.32	0.1	0.15	0.25	424	46.88	156.3	0.4
99	**Hilltop 1	1420.7	0.64	0.19	0.18	0.37	433	28.13	65.63	0.51
100	**Hilltop 1	1436	0.73	0.24	0.17	0.41	462	23.29	52.05	0.59
101	**Hilltop 1	1483.5	0.59	0.07	0.05	0.12	395	8.47	55.93	0.58
102	**Hilltop 1	1505	0.43	0.04	0.07	0.11	330	16.28	97.67	0.36
103	**Hilltop 1	1538	0.6	0.02	0.04	0.06	335	6.67	66.67	0.33
104	**Hilltop 1	1605	0.47	0.01	0.02	0.03	345	4.26	108.5	0.33
105	**Hilltop 1	1630	0.72	0.06	0.05	0.11	331	6.94	98.61	0.55
106	**Hedonia 1	915	1.53	1.19	4.07	5.26	433	266	22.88	0.23
107	**Hedonia 1	930	0.64	0.26	0.96	1.22	439	150	42.19	0.21
108	*Hedonia 1	935.4	0.6	0.3	0.69	0.99	430	115	55	0.3
109	**Hedonia 1	945	1.19	0.84	2.09	2.93	430	175.6	35.29	0.29
110	**Hedonia 1	960	2.07	1.72	4.28	6	435	206.8	19.81	0.29
111	**Hedonia 1	975	1.48	1.3	2.69	3.99	427	181.8	41.89	0.33
112	**Hedonia 1	990	1.19	0.91	1.93	2.84	435	162.2	21.85	0.32
113	**Hedonia 1	1005	1.19	0.95	1.69	2.64	427	142	31.09	0.36
114	**Hedonia 1	1020	0.84	0.49	0.95	1.44	430	113.1	35.71	0.34
115	**Hedonia 1	1022.5	1	0.84	1.14	1.98	432	114	14	0.42
116	*Hedonia 1	1046	0.99	0.58	0.86	1.44	428	86.87	62.63	0.4

117	**Looma 1	2046.6	0.82	0.33	0.13	0.46	411			
118	**Looma 1	1977.1	0.62	0.38	0.38	0.76	415	61.29	85.48	0.50
119	**Looma 1	1987.1	2.2	0.85	1.08	1.93	455	49.09	33.18	0.44
120	**Looma 1	2003.7	0.69	0.25	0.21	0.46	371	30.43	#####	0.54
121	**Looma 1	2046.5	0.74	0.58	0.51	1.09	419	68.92	71.62	0.53
122	**Aquila 1	942	0.56	0.11	0.68	0.79	434	121.4	46.43	0.14
123	**Aquila 1	1050	0.81	0.39	1.24	1.63	436	153.1	40.74	0.24
124	**Aquila 1	1060	1.11	0.7	2.17	2.87	437	195.5	29.73	0.24
125	**Aquila 1	1069.5	1.91	1.25	4.42	5.67	436	231.4	29.32	0.22
126	**Aquila 1	1070	0.95	0.72	2.2	2.92	435	231.6	42.11	0.25
127	**Aquila 1	1080	0.74	0.44	1.23	1.67	435	166.2	48.65	0.26
128	**Aquila 1	1087.5	0.89	0.41	0.81	1.22	430	91.01	65.17	0.34
129	**Aquila 1	1090	0.83	0.55	1.5	2.05	435	180.7	54.22	0.27
130	**Aquila 1	1100	0.85	0.52	1.39	1.91	435	163.5	58.82	0.27
131	**Aquila 1	1110	1.23	1.02	2.55	3.57	436	207.3	30.89	0.29
132	**Aquila 1	1118.5	3.2	2.71	7.02	9.73	436	219.4	25.63	0.28
133	**Aquila 1	1120	1.46	1.51	3.1	4.61	431	212.3	34.93	0.33
134	**Aquila 1	1130	1.04	0.9	1.65	2.55	430	158.7	45.19	0.35
135	**Aquila 1	1140	1.16	1.21	2.38	3.59	426	205.2	48.28	0.34
136	**Aquila 1	1141	2.22	1.12	2.75	3.87	433	123.9	29.28	0.29
137	**Aquila 1	1150	1.18	1.09	1.92	3.01	429	162.7	60.17	0.36
138	**Aquila 1	1160	0.87	0.71	1.24	1.95	426	142.5	66.67	0.36
139	**Aquila 1	1164	0.77	0.31	0.67	0.98	432	87.01	54.55	0.32
140	**Canopus 1	1420	0.42	0.21	0.49	0.7	435	116.7	109.5	0.3
141	**Canopus 1	1430	0.37	0.18	0.41	0.59	421	110.8	124.3	0.31

142	**Canopus 1	1440	0.3	0.12	0.21	0.33	339	70	260	0.36
143	**Canopus 1	1460	0.3	0.14	0.29	0.43	413	96.67	276.7	0.33
144	**Canopus 1	1470	0.32	0.14	0.29	0.43	348	90.62	131.3	0.33
145	**Canopus 1	1475	0.31	0.13	0.23	0.36	340	74.19	151.6	0.36
146	**Canopus 1	1490	0.31	0.11	0.32	0.43	428	103.2	245.2	0.26
147	**Canopus 1	1540	0.3	0.11	0.24	0.35	406	80	146.7	0.31
148	**Canopus 1	1550	0.35	0.12	0.35	0.47	433	100	211.4	0.26
149	**Canopus 1	1560	0.32	0.08	0.27	0.35	413	84.37	346.9	0.23
150	**Canopus 1	1570	0.43	0.13	0.36	0.49	426	83.72	144.2	0.27
151	**Canopus 1	1580	0.32	0.11	0.28	0.39	405	87.5	178.1	0.28
152	**Canopus 1	1590	0.4	0.17	0.54	0.71	430	135	215	0.24
153	**Canopus 1	1600	0.34	0.12	0.31	0.43	404	91.18	97.06	0.28
154	**Canopus 1	1610	0.36	0.11	0.23	0.34	368	63.89	77.78	0.32
155	**Canopus 1	1620	0.39	0.12	0.28	0.4	386	71.79	187.2	0.3
156	**Canopus 1	1695	1.4	0.6	1.09	1.69	430	77.86	20.71	0.36
157	**Crystal Creek 1	2166.5	1.08	0.51	1.34	1.85	432	124.1	27.78	0.28
158	**Crystal Creek 1	2181	3.37	1.51	2.61	4.12	453	77.45	1.48	0.37
159	**Crystal Creek 1	2202.5	0.58	0.24	0.52	0.76	418	89.66	8.62	0.32
160	**Crystal Creek 1	2230.5	0.69	0.29	0.46	0.75	417	66.67	33.33	0.39
161	**Crystal Creek 1	2246.5	0.94	0.34	0.55	0.89	429	58.51	27.66	0.38
162	***McLarty 1	1891.3	0.88	0.68	3.69	4.37	436	419	136	0.16
163	***McLarty 1	1900.4	0.71	0.58	3.04	3.62	398	432	146	0.16
164	***McLarty 1	1903.5	1.36	1.2	3.43	4.63	439	252	120	0.26
165	***McLarty 1	1941.6	0.85	0.45	2.67	3.12	438	314	161	0.14
166	***McLarty 1	1969.0	1.21	0.46	2.73	3.19	435	226	153	0.14

*Rock eval pyrolysis data obtained from the Rock Eval IV equipment by Author

**Pyrolysis data obtained from Western Australia Department of Mines and Petroleum (WAPIMS) online database available at (https://wapims.dmp.wa.gov.au/WAPIMS/)
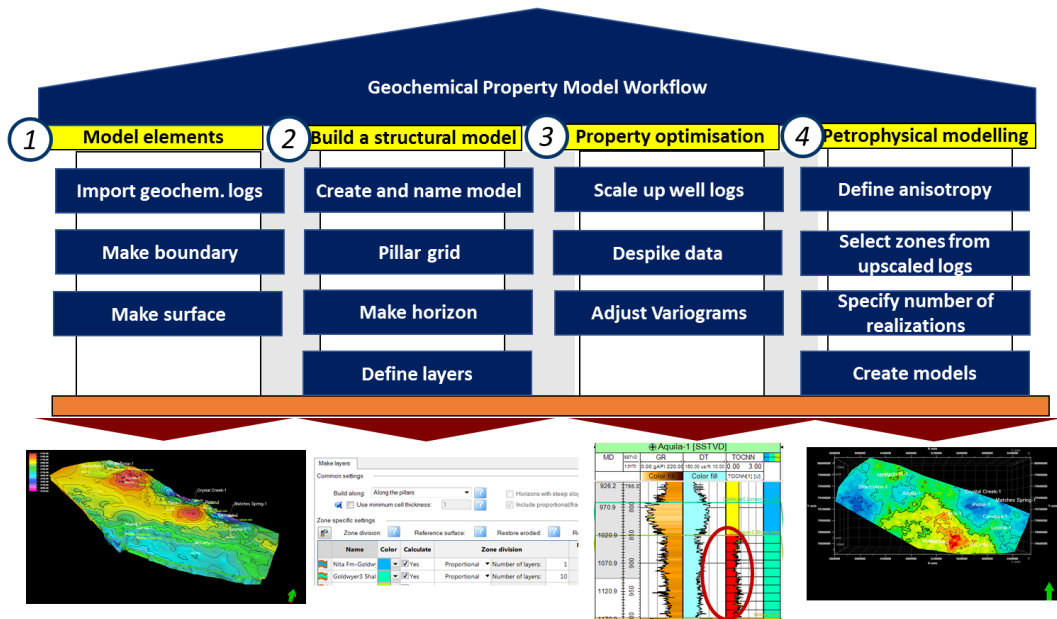
***Pyrolysis data obtained from Kennard *et al.* (1994)

Appendix II: Relationship between common maturity parameters for hydrocarbon generation defined and for type II kerogens. Compiled from Tissot and Welte (1984), Peters and Cassa (1994) and Killops and Killops (2005)
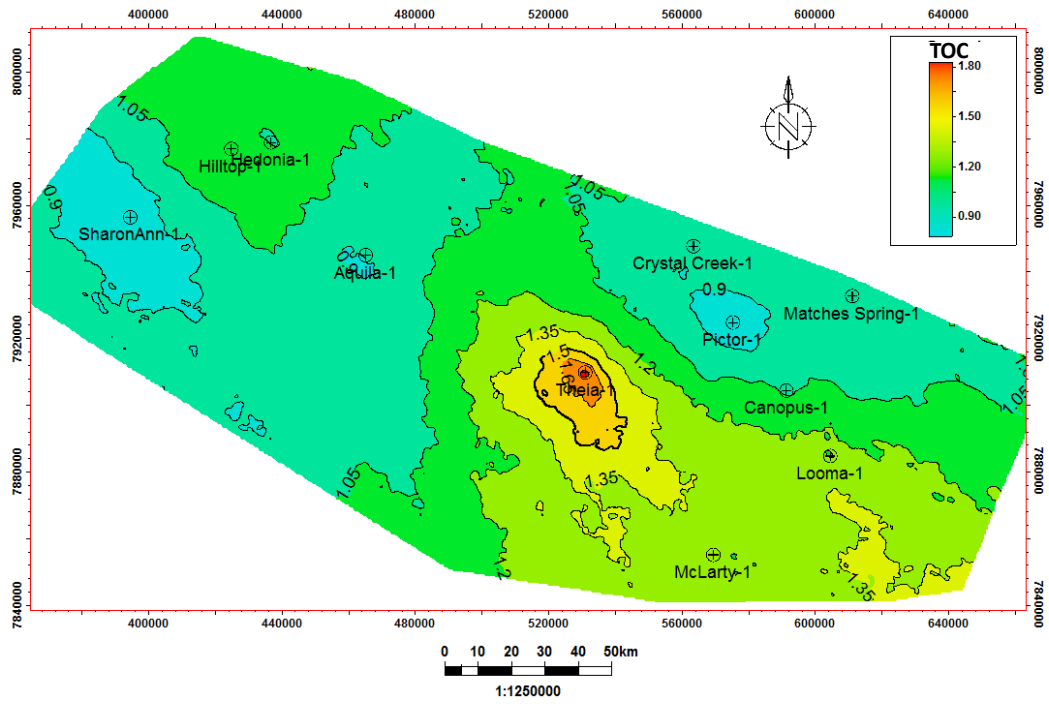
Parameters	Temperature (°C)	Transformation Ratio (%)	Vitrinite Reflectance (%)	Rock Eval T-max (°C)
Early mature	80 – 115	5 – 15	0.5 – 0.7	432 – 442
Mid mature	115 – 145	15 – 65	0.7 – 1.0	442 – 455
Late mature	145 – 165	65 – 95	1.0 – 1.3	455 – 465
Post Mature	>165	>95	>1.3	>465

Tmax = Temperature at maximum hydrocarbon yield during the S_2 cycle as measured by the pyrolysis experiment

Appendix III: Workflow for geochemical property model

Geochemical Property Model Workflow

1 Model elements	2 Build a structural model	3 Property optimisation	4 Petrophysical modelling
Import geochem. logs	Create and name model	Scale up well logs	Define anisotropy
Make boundary	Pillar grid	Despike data	Select zones from upscaled logs
Make surface	Make horizon	Adjust Variograms	Specify number of realizations
	Define layers		Create models

Appendix IV: Average TOC distribution map in the study area

Appendix V. Computed sonic (ΔT) and observed displacement values used to derive the multivariate equation

Input Values		
Depth (m)	Δt (us/ft)	Displacement (m)
1200	91	1400
300	122	1200
1100	112	600
1500	91	1000
600	109	1400
500	122	1000
200	122	1300
600	91	1800
2200	91	500
1150	91	1200
600	122	600
600	106	1100

* Depth = Depth (m)

* Δt = Sonic Transit Time

* Displacement = Exhumation (m) (Using Corresponding Historical Data)

Appendix VI: Burial history modelling inputs. Example from the Aquila 1 well.

Age (Ma)	Formation/Unit	Depth (m)	Thickness (m)	Event type	Paleodeposition/Erosion	Lithology	PSE	Kinetic	TOC (%)	HI (mgHC/gTOC)
0	Recent	0	4	Deposition		Sandstone (typical)	Overburden Rock			
120	Erosion Lower Cretaceous	4	0	Erosion	-1000					
150	Alexander Formation	4	19	Deposition	1000	Siltstone (organic lean)				
161	Wallal Sandstone	23	103	Deposition		Sandstone (typical)				
250	Erosion Lower Triassic	126	0	Erosion	-1200					
280	Grant Group	126	312	Deposition	1200	Sandstone (typical)	Reservoir Rock			
419	Hiatus L.Dev	438	0	Hiatus						
436	Sahara Formation	438	237	Deposition		Dolomite (organic lean, sandy)				
439	Mallowa Salt	675	740	Deposition		Halite				
446	Nibil Formation	1415	97	Deposition		Dolomite (organic lean, sandy)				
448	Minjoo Salt	1512	65	Deposition		Salt (light)				
450	Bongabinni Formation	1577	54	Deposition		Salt (light)	Seal Rock			
455	Nita Formation	1631	57	Deposition		Siltstone (organic lean)	Reservoir Rock			
463	Goldwyer I Shale	1688	77	Deposition		Shale (organic rich, 3% TOC)	Source Rock	G017703_Bulk Kin	4	700
465	Goldwyer II Limestone	1765	122	Deposition		Limestone (organic rich - 1-2% TOC)				
475	Goldwyer III Shale	1887	173	Deposition		Shale (organic rich, typical)	Source Rock	G017691_BulkKin	2	250
480	Willara Formation	2060	281	Deposition		Limestone (shaly)				
489	Nambeet Formation	2341	249	Deposition		Sandstone (typical)				

Appendix VII Copyright Clearance 1

Copyright Clearance Center

RightsLink®

Home | Create Account | Help | LIVE CHAT

COMPUTERS & GEOSCIENCES

Title: Geochemical property modelling of a potential shale reservoir in the Canning Basin (Western Australia), using Artificial Neural Networks and geostatistical tools

Author: Lukman Mobolaji Johnson,Reza Rezaee,Ali Kadkhodaie,Gregory Smith,Hongyan Yu

Publication: Computers & Geosciences

Publisher: Elsevier

Date: November 2018

© 2018 Elsevier Ltd. All rights reserved.

BACK | CLOSE WINDOW

Appendix VIII Copyright Clearance 2

Copyright Clearance Center

RightsLink®

Home | Create Account | Help | LIVE CHAT

LOGIN

If you're a copyright.com user, you can login to RightsLink using your copyright.com credentials.

Already **a RightsLink user** or want to learn more?

BACK | CLOSE WINDOW

Geochemical property modelling of a potential shale reservoir in the Canning Basin (Western Australia), using Artificial Neural Networks and geostatistical tools. *Computers and Geosciences.* 120, 73-81
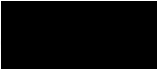
Coauthors

[1]Reza Rezaee, [2]Ali Kadkhodaie, [3]Gregory Smith, [4]Hongyan Yu

[1] Department of Petroleum Engineering, Curtin University, Perth, Australia
[2] Earth Science Department, Faculty of Natural Science, University of Tabriz, Iran
[3] Department Applied Geology, West Australian School of Mines, Curtin University, Perth, Australia
[4] State Key Laboratory of Continental Dynamics, Xi'an, PR China

Name	conception and design	Acquisition of data & method	Data conditioning & manipulation	Analysis & statistical method	Interpretation & discussion	Final approval
Reza Rezaee	✓		✓	✓	✓	✓
I acknowledge that these represent my contribution to the above research output.						
Gregory Smith			✓		✓	
I acknowledge that these represent my contribution to the above research output. G. C. SMITH						
Ali Kadkhodaie	✓			✓	✓	
I acknowledge that these represent my contribution to the above research output.						
Hongyan Yu		✓				
I acknowledge that these represent my contribution to the above research output.						

Paper "title"

A new approach for estimating the amount of eroded sediments, a case study from the Canning Basin, Western Australia. *Journal of Petroleum Science and Engineering,* 156, 19-28.
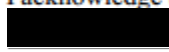
Coauthors

[1]Reza Rezaee, [2]Ali Kadkhodaie, [3]Gregory Smith, [4]Hongyan Yu

[1] Department of Petroleum Engineering, Curtin University, Perth, Australia
[2] Earth Science Department, Faculty of Natural Science, University of Tabriz, Iran
[3] Department Applied Geology, West Australian School of Mines, Curtin University, Perth, Australia
[4] State Key Laboratory of Continental Dynamics, Xi'an, PR China

Name	conception and design	Acquisition of data & method	Data conditioning & manipulation	Analysis & statistical method	Interpretation & discussion	Final approval
Reza Rezaee	✓		✓	✓	✓	✓
I acknowledge that these represent my contribution to the above research output.						
Gregory Smith			✓		✓	
I acknowledge that these represent my contribution to the above research output. G. C. SMITH						
Ali Kadkhodaie	✓			✓		
I acknowledge that these represent my contribution to the above research output.						
Hongyan Yu		✓				
I acknowledge that these represent my contribution to the above research output.						